# CTIPS

Center for Transformative Infrastructure Preservation and Sustainability

**USDOT Region 8 University Transportation Center**

## CTIPS-26-004

R. Dhimal
K. Neupane
Y. Song
M. Zlatkovic

# ASSESSMENT OF SAFETY AND OPERATION PERFORMANCES OF CFIs AND DDIs IN UTAH

A University Transportation Center sponsored by the U.S. Department of Transportation serving the Center for Transformative Infrastructure Preservation and Sustainability members:

Colorado State University
Fort Lewis College
North Dakota State University
South Dakota State University
United Tribes Technical College
University of Colorado Denver
University of Denver
University of North Dakota
University of Utah
University of Wyoming
Utah State University

# Technical Report Documentation Page

| 1. Report No. | 2. Government Accession No. | 3. Recipient's Catalog No. |
|---|---|---|
| CTIPS-26-004 | | |

| 4. Title and Subtitle | 5. Report Date |
|---|---|
| Assessment of Safety and Operation Performances of CFIs and DDIs in Utah | July 2026 |
| | 6. Performing Organization Code<br>CTIPS |

| 7. Author(s) | 8. Performing Organization Report No. |
|---|---|
| ▪ Ramesh Dhimal https://orcid.org/0009-0007-7779-2412<br>▪ Kiran Neupane https://orcid.org/0009-0005-9442-7914<br>▪ Yu (Fred) Song https://orcid.org/0000-0003-2309-716X<br>▪ Milan Zlatkovic https://orcid.org/0000-0002-6777-230X | CTIPS-26-004 |

| 9. Performing Organization Name and Address | 10. Work Unit No. |
|---|---|
| Center for Transformative Infrastructure Preservation and Sustainability<br>North Dakota State University<br>PO Box 6050<br>Fargo, ND 58108 | |
| | 11. Contract or Grant No.<br>69A3552348308 |

| 12. Sponsoring Agency Name and Address | 13. Type of Report and Period Covered |
|---|---|
| Department of Transportation<br>Research and Innovative Technology Administration<br>400 7th Street, SW<br>Washington, DC 20590 | Final Report |
| | 14. Sponsoring Agency Code |

15. Supplementary Notes

Conducted in cooperation with the U.S. Department of Transportation, Federal Highway Administration.

16. Abstract

The Diverging Diamond Interchange (DDI) and the Continuous Flow Intersection (CFI) represent significant innovations in roadway design, offering superior operational performance and enhanced safety compared to conventional signalized ramp terminals and intersections. This study conducts a comprehensive evaluation of these two designs, focusing on both traffic flow and safety outcomes. The research begins by establishing a safety-integrated calibration and validation framework for microscopic traffic simulation models using PTV VISSIM. Unlike traditional approaches, this framework incorporates surrogate safety analysis by embedding bivariate Peak Over Threshold (POT) modeling from Extreme Value Theory (EVT) to jointly capture conflict severity using Time to Collision (TTC) and Maximum Deceleration (MaxD). This dual-purpose modeling approach allows for the estimation of crash frequency directly from simulated conflicts while maintaining operational fidelity. The calibration achieved high accuracy, with GEH values below 5 for all movements and minimal speed errors, and simulation-based crash estimates for CFIs differed from observed frequencies by only 0.07 crashes per year. Validation using 2019 data further confirmed the predictive capability and generalizability of the models.

Complementing the simulation framework, the study utilizes an Empirical Bayes (EB) methodology with crash and traffic data from 2006 to 2021 to evaluate six DDI and eight CFI sites in Utah against matched conventional signalized locations. The research developed state-specific Crash Modification Factors (CMFs) and locally calibrated Safety Performance Functions (SPFs), revealing substantial safety benefits for both designs. DDIs demonstrated a 47.8% reduction in Fatal and Injury (FI) crashes (CMF = 0.522) and a 28.07% reduction in Property Damage Only (PDO) crashes (CMF = 0.719). Similarly, CFI sites showed a 30.7% decrease in FI crashes (CMF = 0.69), a 21.8% decrease in PDO crashes (CMF = 0.78), and a 24.5% decrease in total crashes (CMF = 0.76), preventing an estimated 378 FI and 629 PDO crashes over the analysis period. Collectively, these findings validate that when properly designed and operated, both DDIs and CFIs deliver meaningful improvements in safety performance and offer a robust, transferable framework for evaluating both the operational efficiency and safety of innovative intersection designs at regional and national levels.

| 17. Key Words | 18. Distribution Statement |
|---|---|
| Diverging Diamond Interchange, Continuous Flow Intersection, Empirical Bayes, Crash Modification Factor, Surrogate Safety, Extreme Value Theory | No restrictions. This document is available through the National Technical Information Service, Springfield, VA 22161. |

| 19. Security Classif. (of this report) | 20. Security Classif. (of this page) | 21. No. of Pages | 22. Price |
|---|---|---|---|
| Unclassified | Unclassified | 122 | n/a |

**Form DOT F 1700.7 (8-72)** Reproduction of completed page authorized

CTIPS Center for Transformative Infrastructure Preservation and Sustainability

USDOT Region 8 University Transportation Center

# Assessment of Safety and Operation Performances of CFIs and DDIs in Utah


**Principal Investigators:**

Yu (Fred) Song

Milan Zlatkovic

**Authors**

Ramesh Dhimal, Kiran Neupane,

Yu (Fred) Song, Milan Zlatkovic

**A report from**

University of Wyoming

Department of Civil and Architectural Engineering
and Construction Management

Laramie

Wyoming 82071, USA

Phone: (307) 766-2390

Website: https://www.uwyo.edu/civil/index.html


July 2026

## About the Center for Transformative Infrastructure Preservation and Sustainability

The Center for Transformative Infrastructure Preservation and Sustainability (CTIPS) is the US DOT Region 8 University Transportation Center (UTC) located at North Dakota State University. CTIPS will focus on "Preserving the Existing Transportation System," along with consortium members Colorado State University, Fort Lewis College, South Dakota State University, United Tribes Technical College, University of Colorado Denver, University of Denver, University of North Dakota, University of Utah, University of Wyoming and Utah State University.

## Acknowledgements

The authors gratefully acknowledge the Utah Department of Transportation (UDOT) for providing access to critical traffic and crash data, as well as for its valuable technical input and collaboration. This study was supported by the Center for Transformative Infrastructure Preservation and Sustainability (CTIPS), whose funding made this research possible. The authors also extend their appreciation to partner institutions within the CTIPS consortium and affiliated researchers for their insights and feedback. Finally, the contributions of colleagues, reviewers, and all individuals who provided support and constructive suggestions are sincerely appreciated, as they helped strengthen the quality and impact of this report.

## U.S. Department of Transportation (US DOT) Disclaimer

# ABSTRACT

The diverging diamond interchange (DDI) and the continuous flow intersection (CFI) represent significant innovations in roadway design, offering superior operational performance and enhanced safety compared with conventional signalized ramp terminals and intersections. This study conducts a comprehensive evaluation of these two designs, focusing on both traffic flow and safety outcomes. The research begins by establishing a safety-integrated calibration and validation framework for microscopic traffic simulation models using PTV VISSIM, a leading microscopic traffic flow simulation software developed by the PTV Group Unlike traditional approaches, this framework incorporates surrogate safety analysis by embedding bivariate peak over threshold (POT) modeling from extreme value theory (EVT) to jointly capture conflict severity using time to collision (TTC) and maximum deceleration (MaxD). This dual-purpose modeling approach allows for the estimation of crash frequency directly from simulated conflicts while maintaining operational fidelity. The calibration achieved high accuracy, with GEH values below 5 for all movements and minimal speed errors, and simulation-based crash estimates for CFIs differing from observed frequencies by only 0.07 crashes per year. Validation using 2019 data further confirmed the predictive capability and generalizability of the models.

Complementing the simulation framework, the study utilizes an empirical Bayes (EB) methodology with crash and traffic data from 2006 to 2021 to evaluate six DDI and eight CFI sites in Utah against matched conventional signalized locations. The research developed state-specific crash modification factors (CMFs) and locally calibrated safety performance functions (SPFs), revealing substantial safety benefits for both designs. DDIs demonstrated a 47.8% reduction in fatal and injury (FI) crashes (CMF = 0.522) and a 28.07% reduction in property damage only (PDO) crashes (CMF = 0.719). Similarly, CFI sites showed a 30.7% decrease in FI crashes (CMF = 0.69), a 21.8% decrease in PDO crashes (CMF = 0.78), and a 24.5% decrease in total crashes (CMF = 0.76), preventing an estimated 378 FI and 629 PDO crashes over the analysis period. Collectively, these findings validate that when properly designed and operated, both DDIs and CFIs deliver meaningful improvements in safety performance and offer a robust, transferable framework for evaluating both the operational efficiency and safety of innovative intersection designs at regional and national levels.

## LIST OF FIGURES

## LIST OF TABLES

## LIST OF KEY TERMS

| | |
|---|---|
| AADT | Annual Average Daily Traffic |
| ATSPM | Automated Traffic Signal Performance Measures |
| CFI | Continuous Flow Intersection |
| CMF | Crash Modification Factor |
| CTIPS | Center for Transformative Infrastructure Preservation and Sustainability |
| DCD | Double Crossover Diamond |
| DDI | Diverging Diamond Interchange |
| DLT | Displaced Left Turn |
| EB | Empirical Bayes |
| EVT | Extreme Value Theory |
| FI | Fatal and Injury (crashes) |
| FHWA | Federal Highway Administration |
| GEH | Geoffrey E. Havers (traffic volume goodness of fit statistic) |
| HCM | Highway Capacity Manual |
| HGV | Heavy Goods Vehicle |
| HSM | Highway Safety Manual |
| ISAT | Interchange Safety Analysis Tool |
| MAPE | Mean Absolute Percentage Error |
| MaxD | Maximum Deceleration |
| MOE | Measure of Effectiveness |
| NB | Negative Binomial (regression model) |
| PDO | Property Damage Only (crashes) |
| PET | Post Encroachment Time |
| POT | Peaks Over Threshold |
| SPDI | Single Point Diamond Interchange |
| SPF | Safety Performance Function |
| SSAM | Surrogate Safety Assessment Model |
| TTC | Time to Collision |
| UDOT | Utah Department of Transportation |
| US DOT | United States Department of Transportation |
| UTC | University Transportation Center |

# EXECUTIVE SUMMARY

Innovative intersection and interchange designs have become essential tools for addressing increasing traffic demand, congestion, and safety challenges on urban and suburban roadways. Among these alternatives, diverging diamond interchanges (DDIs) and continuous flow intersections (CFIs) have gained widespread attention for their operational efficiency and potential safety benefits. Despite their growing implementation, transportation agencies continue to seek robust, locally relevant evidence that simultaneously evaluates both operational and safety performance and supports data-driven design and policy decisions.

This technical report presents a comprehensive evaluation of DDIs and CFIs in Utah through an integrated framework that combines microscopic traffic simulation, surrogate safety analysis, and crash-based empirical evaluation. The research leverages long-term traffic and crash data spanning 2006 to 2021 and applies statistically rigorous methods to assess operational effectiveness, crash frequency, and crash severity under local conditions.

The operational component of the study develops and validates safety-integrated microscopic simulation models for selected DDI and CFI sites using PTV VISSIM. Unlike traditional simulation calibration approaches that focus solely on traffic volumes and speeds, this research embeds surrogate safety analysis directly into the calibration process. Conflict-based safety measures derived from time to collision and maximum deceleration are incorporated using extreme value theory to estimate crash frequency from simulated interactions. The calibrated models demonstrate strong agreement with observed field conditions, achieving acceptable volume and speed accuracy and closely matching observed crash frequencies. Validation using independent data confirms the predictive capability and transferability of the proposed framework, enabling proactive assessment of both operational efficiency and safety performance.

Complementing the simulation-based analysis, the report presents crash-based safety evaluations of DDIs and CFIs using the empirical Bayes (EB) before–after methodology. For DDIs, a comparison of six treatment sites and six matched conventional sites show substantial and statistically significant safety improvements following implementation. Results indicate large reductions in both fatal-and-injury and property-damage-only crashes, highlighting the effectiveness of DDIs in reducing crash severity at signalized ramp terminals. Locally developed crash modification factors provide reliable, Utah-specific estimates that can support future planning and design decisions.

Similarly, the safety evaluation of CFIs is based on eight treatment sites and five conventional four-leg signalized intersections. Locally calibrated safety performance functions are developed to account for Utah-specific traffic, geometric, and operational characteristics. The EB analysis indicates meaningful reductions in total crashes, as well as in both fatal-and-injury and property-damage-only crashes. These findings confirm that CFIs, when properly designed and operated, can deliver measurable safety benefits in addition to their well-documented operational and environmental advantages.

Overall, the findings presented in this report demonstrate that both DDIs and CFIs provide significant improvements in operational performance and roadway safety under Utah conditions. The integrated use of simulation-based surrogate safety analysis and crash-based empirical evaluation offers a robust and transferable framework for assessing innovative roadway designs. The results support the continued and expanded application of DDIs and CFIs on high-volume corridors and provide transportation agencies with defensible tools for evidence-based decision-making, safety planning, and design evaluation.

# 1. INTRODUCTION AND BACKGROUND

## 1.1 Overview of Innovative Intersection and Interchange Concepts

Innovative intersections and interchanges, sometimes called unconventional or alternative designs, have emerged because today's transportation professionals must serve growing travel demand with limited funding and right-of-way, while congestion and safety risks at junctions continue to intensify. Conventional solutions such as adding lanes, rebuilding at-grade intersections with more signal phases, or constructing full grade separation are often expensive, disruptive to adjacent land uses, and not always justified by the operational gains they deliver. In response, agencies and designers have been investigating geometric and operational treatments that can achieve better performance with the existing infrastructure. Broadly, innovative designs are at-grade concepts (and a related set of innovative interchange forms) that deliberately reshape or restrict how movements occur so that the main intersection operates with fewer conflict points and fewer signal phases—especially by managing left turns, which typically drive delay, crash exposure, and signal complexity. Many of these designs reroute left turns to occur upstream of the primary junction, separate movements in space or time, or replace direct left turns with combinations of right turns and U-turns. In doing so, they aim to (1) reduce and/or separate conflicts to improve safety, (2) restrict and/or reroute movements to disperse queues and reduce congestion, (3) simplify signal phasing to reduce overall delay and improve progression on the arterial, and (4) provide enough capacity for existing and future volumes to avoid major, costly grade-separated construction. Importantly, these treatments are not "one-size-fits-all" standards; they are a portfolio of options meant to expand the alternatives analysis toolbox when conventional designs are insufficient, helping practitioners weigh mobility, safety, multimodal access, land use constraints, environmental impacts, and economic considerations in a more context-sensitive way.

Among the best-known innovative interchange and intersection treatments are the diverging diamond interchange (DDI), and the continuous flow intersection (CFI), each illustrating how geometry can be used to trade unfamiliar movements for measurable operational and safety benefits. The DDI reconfigures traffic on the cross street to temporarily switch sides between ramp terminals, allowing left turns onto freeway ramps to occur with fewer signal phases and fewer severe crossing conflicts—an approach that can improve flow and reduce congestion at highway junctions without the footprint and cost of many traditional interchange expansions. Early adoption and implementation experiences in states like Utah helped demonstrate its viability, with one of the first U.S. DDIs opening at American Fork and I-15 in August 2010. The CFI relocates left-turn crossings to signalized crossover intersections upstream from the main junction, enabling the main intersection to run fewer phases and serve heavy through volumes more continuously—often yielding capacity and delay benefits where traditional widening provides diminishing returns. A recurring challenge across all innovative designs is driver expectancy: because these layouts can feel "unusual," agencies must pair good geometric design with clear signing/markings, public outreach, and early-period guidance to reduce confusion during initial operation. The broader impact of these designs extends beyond vehicle delay and congestion reduction, affecting safety, pedestrian and cyclist accommodations, transit operations, access management, land use, and environmental considerations. As such, evaluating their effectiveness requires a comprehensive approach, incorporating a range of performance measures. This method enables stakeholders to assess and compare alternatives across various dimensions, such as safety, efficiency, and environmental impact, rather than relying solely on traditional metrics like level of service. The goal of this study is to provide a holistic understanding of these innovative designs and their potential to address the growing demands of transportation systems while considering broader societal impacts.

## 1.2 Diverging Diamond Interchange (DDI)

**Geometric Design**

The DDI (Figure 1), also referred to as the double crossover diamond (DCD), represents a transformative innovation in interchange design, particularly in its ability to improve traffic operations and safety within constrained rights-of-way. The concept was formally introduced by Chlewicki in 2003 at the 2nd Urban Street Symposium, where it was proposed as an alternative to conventional interchange forms, such as the standard diamond and the single-point diamond interchange (SPDI) (Chlewicki 2003). The operation of the DDI was first implemented in the United States on June 21, 2009, when the Missouri Department of Transportation (MoDOT) opened the nation's inaugural DDI at the interchange of Kansas Expressway (MO-13) and I-44 in Springfield, Missouri (Chilukuri et al. 2011; MoDOT 2010). Since then, the DDI has gained widespread adoption, with over 200 DDIs constructed nationwide as of 2019. DDIs offer compelling performance in both urban and suburban contexts. Beyond benefiting traffic efficiency, DDIs are also found to offer enhanced safety, cost-effectiveness, and design flexibility, and most of the time by reusing existing structures that require minimal expansion (MoDOT 2010).

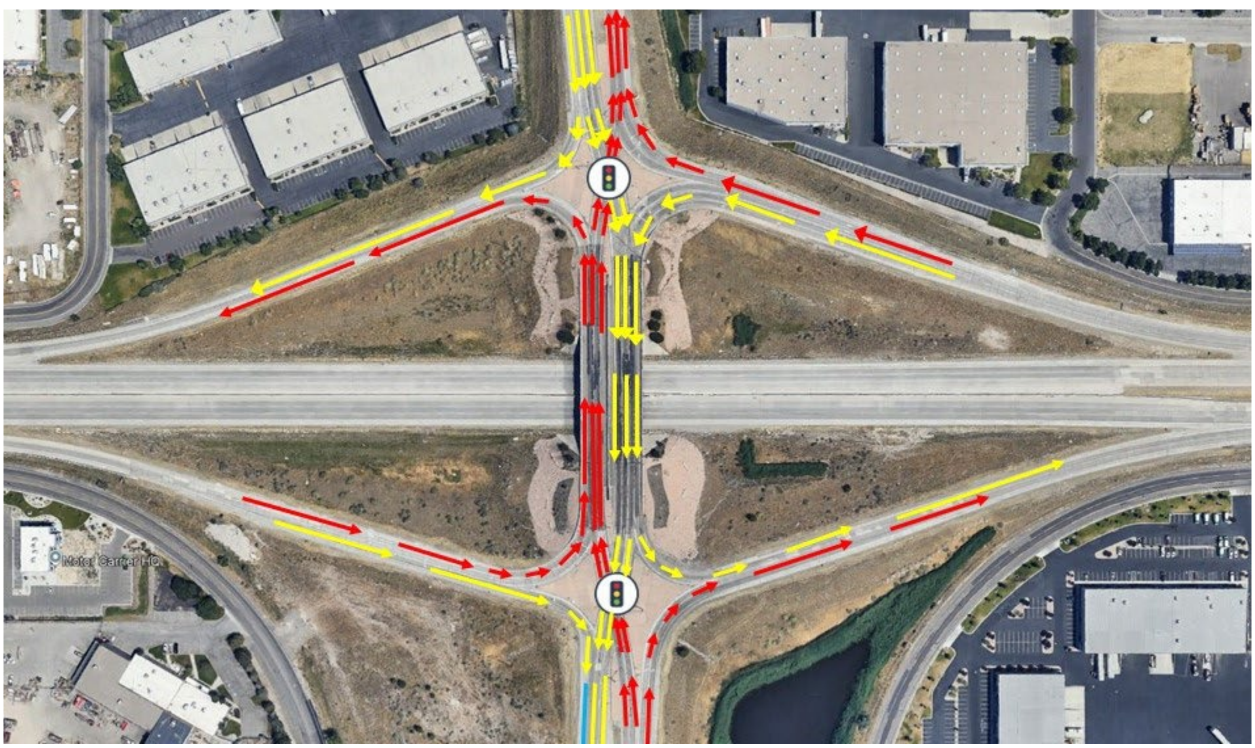

**Figure 1: Traffic movements at a typical DDI (SR-201 and Bangerter Highway, Utah)**

## Operational Characteristics and Safety Considerations

By design, DDIs can reduce vehicular conflict points from 30 (in standard diamond interchanges) to just 18, notably decreasing dangerous crossing conflicts from 10 to two (see Figure 2) (B. Claros et al. 2017a). The core functionality of a DDI lies in its unique crossover configuration, where vehicles shift to the left side of the roadway at ramp terminals and then cross back after traversing a bridge or underpass (Chilukuri et al. 2011; MoDOT 2010; Schroeder et al. 2014). The main intersections at DDIs operate with two-phase signals and left-turning drivers only pass through a single intersection, which typically reduces travel time and can lead to improved safety (Chilukuri et al. 2011). This maneuver eliminates conflicting left turns across opposing traffic, facilitating more efficient left-turn movements onto freeway ramps and thereby reducing signal phases and delays (Chilukuri et al. 2011; B. R. Claros et al. 2015; MoDOT 2010; Schroeder et al. 2014). This not only lowers the crash potential but also enables simplified signal phasing, which leads to reduced cycle lengths and intersection delays. The reduction in vehicle delay further improves fuel economy and lowers emissions, creating secondary environmental benefits (Almoshaogeh et al. 2020). The DDI offers significant improvements in traffic flow and safety compared with conventional diamond interchanges by reducing conflict points and simplifying signal operations; however, it has several limitations. It can be inefficient for high through-traffic volumes on the cross route, may confuse drivers due to its unfamiliar crossover pattern, and restricts straight-through off-ramp movements. Additionally, it can pose challenges for pedestrians due to nontraditional crossing patterns and may require more space and careful signal coordination when nearby intersections are close or heavily trafficked (Haq et al. 2022; MoDOT 2010).

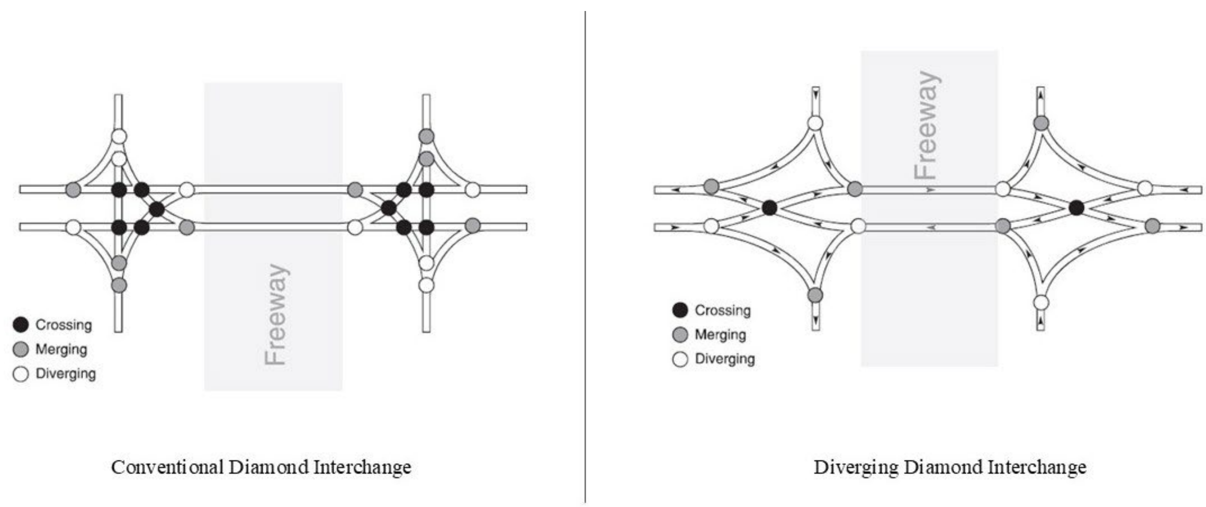


**Figure 2: Conflict points in conventional diamond interchange (left) vs. DDI (right) (Christopher Cunningham et al. 2021)**

## 1.3 Continuous Flow Intersection (CFI)

**Geometric Design**

Continuous flow intersections (CFIs), also known as displaced left-turn (DLT) intersections (Figure 3), are designed to increase vehicle mobility by relocating the left-turn lane (or lanes) to the far-left side of the road upstream of the main signalized intersection. The main idea is to eliminate conflicts between left-turning vehicles and opposing through traffic by relocating the left-turn movement several hundred feet upstream. Vehicles intending to turn left are redirected to cross opposing through lanes at a signalized crossover before the main intersection. After crossing, these vehicles travel within a separate lane positioned on the left side of opposing traffic. When they reach the main intersection, they complete their left-turn maneuver concurrently with opposing through movements (Wolfgram 2018; S. Park and Rakha 2010; Zlatkovic 2015; Qu et al. 2020; Zlatkovic 2019; Qi et al. 2018; Hughes et al. 2010; Chris Cunningham et al. 2022; Steyn et al. 2014; Mary Eileen Yahl 2013; Dhatrak et al. 2010; Esawey and Sayed 2007; Bared et al. 2005; Abdelrahman 2020).

A CFI intersection improves traffic operations by replacing the conventional four-phase signal cycle with a simplified two-phase structure that allows through-traffic and left-turning vehicles—shifted to upstream crossover points—to move at the same time. This arrangement increases the amount of usable green time, shortens overall cycle lengths, and supports smoother progression along major corridors. As a result, CFIs offer higher capacity, reduced delays during peak congestion, and better coordination between adjacent signals compared with conventional intersection designs (Hughes et al. 2010).

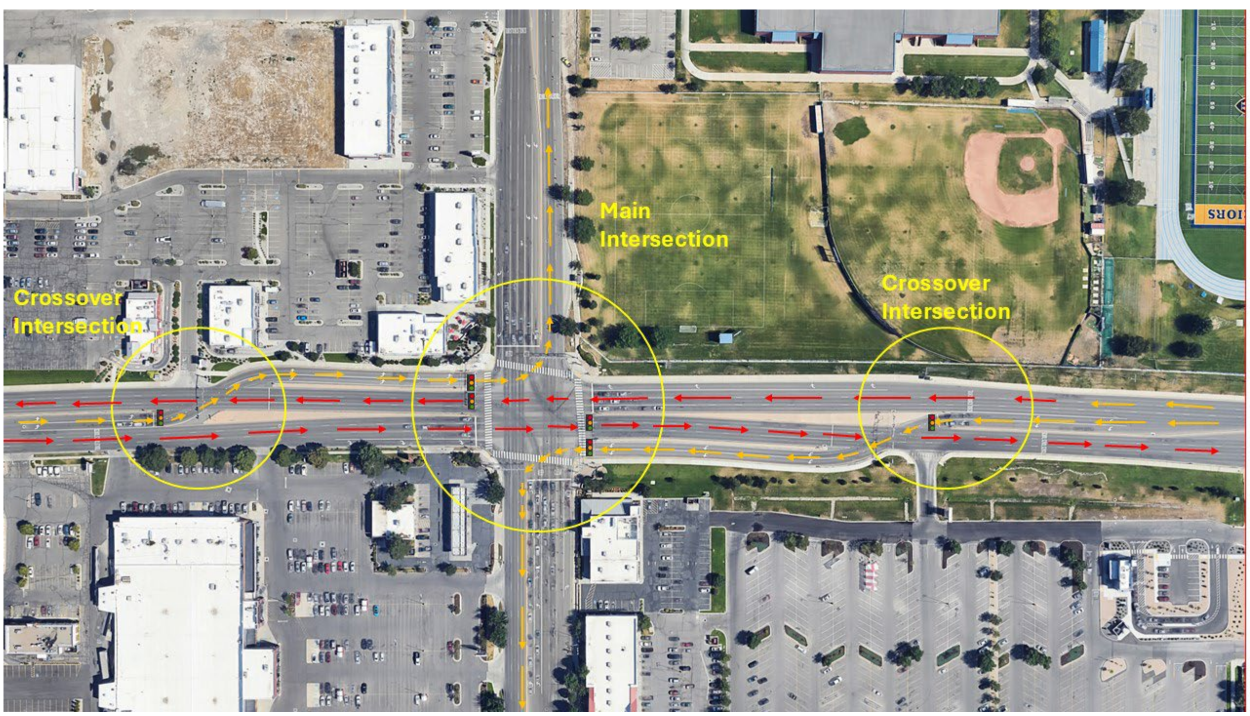


**Figure 3: Continuous flow intersection at Redwood @ 5400 S**

## Operational Characteristics and Safety Considerations

CFIs can be implemented in either partial or full configurations. A partial CFI displaces left-turn movements only on selected approaches—generally along the major roadway. A full CFI displaces left turns on all four approaches, typically requiring five signalized intersections: one at the primary intersection and four at the upstream crossovers. Achieving effective performance in a full configuration depends on precise coordination among all signalized locations to maintain smooth traffic flow (Steyn et al. 2014). Figure 3 illustrates the partial CFI located at Redwood Road and 5400 South. The intersection consists of two crossover intersections in addition to the main intersection. Traffic signals are installed at each crossover to manage vehicle movements as they cross the opposing through-lanes, with arrowheads in red and yellow indicating the direction of traffic flow.

CFIs have been shown to offer notable environmental advantages, including reductions in emissions, improvements in fuel economy, and decreases in overall traffic conflicts, with benefits maintained even under varying demand conditions (Wolfgram 2018; S. Park and Rakha 2010) and a smaller footprint than an interchange (Steyn et al. 2014). Nevertheless, CFIs pose several implementation challenges, such as potential driver confusion due to their unconventional layout (Abdelrahman et al. 2020; S. Park and Rakha 2010), increased right-of-way requirements compared with conventional intersections (LaDOTD 2007; Hughes et al. 2010; Steyn et al. 2014), more complex pedestrian and bicycle accommodations (Hughes et al. 2010; Steyn et al. 2014), and the need for closely coordinated signal operations to ensure optimal performance (Steyn et al. 2014).

The CFI layout (Figure 4) strengthens safety performance by reducing the number and severity of potential conflict points. Because left-turn movements are relocated before the main intersection, vehicles no longer cross opposing traffic in the central junction, removing several high-risk crossing conflicts. While three-leg intersections exhibit similar conflict counts across designs, four-leg CFIs show a meaningful reduction—from the typical 32 conflict points in a conventional layout to as few as 28 when all crossovers are implemented, as shown in Table 1. This decrease in vehicle-path interactions lowers exposure to severe right-angle crashes and contributes to the CFI's reputation for enhancing both operational efficiency and roadway safety. The Federal Highway Administration (FHWA) further analyzed CFIs on major roads and found a 6% to 12% reduction in total conflict points compared with conventional four-leg intersections (Steyn et al. 2014).

**Table 1: Conflict Points Comparison (Steyn et al. 2014)**

| Number of Intersection Legs | Number of Crossovers on CFI | Conflict Points (Conventional) | Conflict Points (CFI) |
|---|---|---|---|
| 3 | 1 | 9 | 9 |
| 4 | 2 | 32 | 30 |
| 4 | 4 | 32 | 28 |

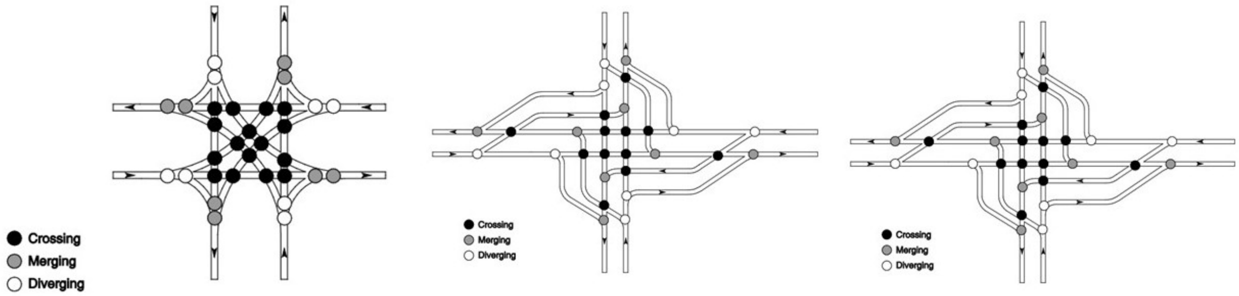


**Conflict point diagram for a conventional intersection.**

**Conflict point diagram for a DLT intersection with two displaced left turns**

**Conflict point diagram for a DLT intersection with four displaced left turns**

**Figure 4: Conflict point diagrams for a conventional intersection and CFIs with two and four displaced left turns (Hughes et al. 2010; Steyn et al. 2014)**

## 1.4 Project Motivation

Rapid growth in traffic demand in urban and suburban corridors has intensified the need for intersection and interchange designs that can simultaneously improve operational efficiency and roadway safety. Innovative designs such as DDIs and CFIs have emerged as promising alternatives to conventional configurations, offering increased capacity, reduced delay, and improved traffic progression. As these designs continue to be deployed across the United States, transportation agencies require robust and locally relevant evidence to support their planning, design, and operational decisions.

While DDIs and CFIs are widely recognized for their operational advantages, comprehensive evaluations that jointly consider operational performance and safety outcomes remain limited. Traditional safety assessment approaches often rely on historical crash data and post-implementation analyses, which, although valuable, do not fully support proactive safety evaluation during the planning and design stages. Conversely, microscopic traffic simulation is frequently used to assess operations but is rarely calibrated or validated with explicit consideration of safety performance. This disconnect can limit the ability of simulation tools to reliably inform safety-related decisions.

In Utah, the increasing number of implemented DDIs and CFIs provides a unique opportunity to address these gaps. The availability of multi-year crash, traffic, and geometric data enables both retrospective safety evaluations using statistically rigorous methods and prospective safety assessment through simulation-based analysis. There is a critical need to integrate these approaches to develop a unified, data-driven framework that supports both operational analysis and safety decision-making under local conditions.

This project is motivated by the goal of advancing the evaluation of innovative intersection and interchange designs by combining empirical crash-based safety analysis with safety-integrated microscopic simulation. By doing so, the research supports evidence-based transportation planning, improves confidence in alternative design implementation, and contributes transferable methodologies applicable at both regional and national levels.

## 1.5 Research, Objectives, and Tasks

The objective of this research is to comprehensively evaluate the operational and safety performance of DDIs and CFIs using complementary empirical and simulation-based approaches. The specific objectives are to:

1. Assess the operational performance of DDIs and CFIs using calibrated microscopic traffic simulation models.
2. Quantify the safety impacts of DDIs and CFIs through crash-based evaluations using statistically robust methodologies.
3. Develop locally calibrated safety performance measures and crash modification factors (CMFs) relevant to Utah conditions.
4. Integrate surrogate safety analysis into simulation model calibration to enable proactive safety assessment.
5. Establish a consistent, transferable framework that links operational efficiency and safety performance for innovative roadway designs.

## 1.6 Report Overview

This report is structured to provide a comprehensive evaluation of the operational and safety performance of innovative intersection designs, focusing on DDIs and CFIs. The report is organized into the following key chapters:

**Chapter 1: Introduction and Background**

This chapter sets the stage for the study by outlining the motivation for evaluating innovative intersection designs. It introduces the research objectives, presents the significance of the study, and provides a high-level overview of the report structure to guide the reader through the subsequent chapters.

**Chapter 2: Literature Review on Operational and Safety Performance**

A thorough review of existing literature is presented, covering previous studies on innovative intersection designs like DDIs and CFIs. This chapter discusses operational performance, safety evaluations, and methodologies used in earlier research. It also identifies gaps in the literature that this study aims to address.

**Chapter 3: Operational Performance Evaluation of DDI and CFI**

This chapter outlines the methodology used to assess the operational performance of DDIs and CFIs. It details the data collection process, the development and calibration of microscopic simulation models, and the evaluation of traffic performance measures such as traffic volume, speed, and delay.

**Chapter 4: Safety Evaluation Methodologies**

This section discusses the safety evaluation framework used in the study. It covers the crash data collection process, the development of safety performance functions (SPFs), and the application of the empirical Bayes (EB) before–after methodology for estimating CMFs. The chapter also highlights the integration of surrogate safety measures for proactive safety assessment.

**Chapter 5: Results and Discussion**

This chapter presents the results of both the operational and safety evaluations. It compares the performance of DDIs and CFIs, discusses key findings, and examines how the results align with or differ from previous studies. Implications for future intersection design and safety improvements are also explored.

**Chapter 6: Conclusion**

The conclusion summarizes the key findings of the study, including the significant operational and safety benefits of DDIs and CFIs. This chapter also outlines the limitations of the study and provides recommendations for future research and the continued application of these designs in high-traffic corridors.

# 2. LITERATURE REVIEW

## 2.1 Operational Evaluation of DDIs and CFIs

This chapter presents a comprehensive review of the literature related to innovative intersection designs, traffic simulation modeling, and advanced safety evaluation techniques. With increasing traffic demand and complexity in urban transportation systems, traditional intersection designs often face challenges in maintaining operational efficiency and safety. As a result, alternative intersection designs such as DDIs and CFIs have been developed to improve traffic performance under high-demand conditions.

In addition to geometric design improvements, advancements in traffic simulation and safety analysis methods have enabled more detailed evaluation of traffic systems. Microscopic traffic simulation models allow for the representation of individual vehicle behavior, while surrogate safety measures and statistical modeling approaches such as Extreme Value Theory (EVT) provide alternative methods for evaluating safety performance in the absence of reliable crash data.

This chapter reviews existing research on innovative intersection designs, simulation modeling techniques, calibration and validation practices, surrogate safety measures, and EVT-based crash estimation methods. The goal is to identify current research trends, highlight methodological approaches, and establish the foundation for the integrated framework developed in this study.

### 2.1.1 Innovative Intersection Design

The increasing demand for efficient and safe transportation systems has driven significant advancements in intersection design and traffic management strategies. Conventional signalized intersections, while widely used, often experience operational inefficiencies under high traffic volumes, including excessive delays, queue formation, and increased crash risk. These limitations have led researchers and transportation agencies to explore alternative intersection configurations that can better accommodate complex traffic movements and improve overall system performance (Hughes et al. 2010; Badgley et al. 2021).

Innovative intersection designs aim to address these challenges by modifying traditional traffic flow patterns and reducing the number and severity of conflict points. By redistributing traffic movements spatially and temporally, these designs seek to improve operational efficiency while enhancing safety. Research conducted by the FHWA has highlighted the potential benefits of such designs, including reductions in delay, improved throughput, and enhanced safety performance in comparison with conventional intersections (Badgley et al. 2021).

In addition to geometric design improvements, recent studies have emphasized the importance of integrating advanced analytical tools for evaluating traffic systems. The complexity of vehicle interactions at innovative intersections requires detailed modeling approaches that can capture dynamic traffic behavior. Consequently, simulation-based analysis and data-driven methodologies have become central to modern transportation research (Dowling et al. 2004).

Furthermore, the increasing availability of high-resolution traffic data has enabled more sophisticated analysis of traffic systems. This has led to the development of integrated evaluation frameworks that combine operational analysis with safety assessment, providing a more comprehensive understanding of traffic system performance (Ciuffo and Lima Azevedo 2014).

### 2.1.2 Traffic Flow Characteristics at Complex Intersections

Traffic flow behavior at complex intersections is influenced by multiple interacting factors, including traffic demand, signal timing, roadway geometry, and driver behavior. Unlike conventional intersections, innovative designs introduce non-standard vehicle trajectories and altered conflict patterns, which significantly impact traffic dynamics. Previous research has demonstrated that reducing conflict points and improving traffic stream coordination can significantly enhance traffic flow efficiency (Hunter et al. 2019; Hughes et al. 2010). The interaction between different traffic movements, particularly at merging, diverging, and crossing points, plays a crucial role in determining overall performance. Key operational indicators such as delay, travel time, queue length, and average speed are commonly used to evaluate traffic flow performance at intersections (Hunter et al. 2019). In addition, traffic flow characteristics are strongly influenced by vehicle composition and driver behavior. The presence of heavy vehicles, variations in acceleration and deceleration profiles, and differences in driver response can affect traffic performance, particularly under congested conditions. Studies have shown that driver behavior models, including gap acceptance and reaction time, are critical components in accurately representing traffic dynamics (Liu et al. 2025). Another important aspect of traffic flow at complex intersections is the impact of signal control strategies. Signal timing, phase sequencing, and coordination between adjacent intersections can significantly influence traffic performance. Efficient signal control is essential for minimizing delay and preventing queue spillback, especially in high-demand scenarios (Dowling et al. 2004).

### 2.1.3 Modeling Approaches for Traffic Performance Analysis

Traffic system analysis relies on a hierarchy of modeling approaches, including macroscopic, mesoscopic, and microscopic models. Each approach differs in terms of the level of detail and computational complexity. Macroscopic models describe traffic flow using aggregate variables such as density, flow, and speed, making them suitable for large-scale network analysis. Mesoscopic models provide a balance between detail and computational efficiency by combining elements of both aggregated and disaggregated approaches (B. [Brian] Park and Schneeberger 2003). However, for intersection-level analysis, particularly in the case of innovative intersection designs, microscopic simulation models are most used. These models simulate individual vehicle movements based on behavioral theories, including car-following and lane-changing models. By capturing the interactions between vehicles at a detailed level, microscopic models provide a more accurate representation of traffic dynamics (B. [Brian] Park and Schneeberger 2003; Dowling et al. 2004). Microscopic models are particularly valuable for analyzing complex traffic systems where interactions between vehicles are highly dynamic and non-linear. They allow researchers to evaluate the impact of geometric design, traffic control strategies, and driver behavior on overall system performance. In addition, these models support scenario-based analysis, enabling the evaluation of different traffic conditions and design alternatives. The selection of an appropriate modeling approach depends on the objectives of the study and the level of detail required. For studies focusing on operational performance and safety at complex intersections, microscopic simulation is generally preferred due to its flexibility and ability to represent detailed traffic behavior (B. [Brian] Park and Schneeberger 2003).

### 2.1.4 Simulation-Based Evaluation of Traffic Operations

Simulation-based approaches have become an essential tool in transportation engineering due to their ability to analyze complex systems under controlled conditions. Microscopic simulation tools, such as PTV VISSIM, enable detailed modeling of traffic networks, including vehicle interactions, signal control, and roadway geometry. Simulation models are widely used to evaluate key operational performance measures, including traffic volume, speed, delay, queue length, and travel time. These measures provide insights into how traffic systems respond to varying conditions, such as changes in demand, signal timing, and network configuration (Dowling et al. 2004). One of the primary advantages of simulation-based evaluation is the ability to test hypothetical scenarios without implementing physical changes in the real world. This allows researchers to assess the potential impact of different design alternatives and control strategies in a cost-effective manner. Additionally, simulation models can capture the dynamic nature of traffic systems, providing a more realistic representation of traffic behavior compared with analytical models (Astarita et al. 2012). However, the accuracy of simulation results depends on the quality of the model. Calibration and validation are critical steps in ensuring that simulation outputs accurately represent real-world conditions. Without proper calibration, simulation models may produce misleading results, which can negatively impact decision-making processes. Therefore, rigorous validation using observed data is essential for ensuring the reliability of simulation-based analysis (Astarita et al. 2012).

### 2.1.5 Safety Assessment Using Traffic Conflict Techniques

Safety evaluation is a fundamental aspect of traffic system analysis, particularly for assessing the effectiveness of innovative intersection designs. Traditional safety analysis methods rely on historical crash data; however, such data are often limited and may not adequately represent safety conditions, especially for newly implemented designs. To address these limitations, traffic conflict techniques have been developed as an alternative approach for safety assessment. Traffic conflicts are defined as interactions between vehicles that have the potential to result in a collision if no evasive action is taken. These interactions provide valuable insights into potential crash conditions and can be used to assess safety performance proactively (Gettman and Head 2003). Surrogate safety measures, such as time-to-collision (TTC), post-encroachment time (PET), and maximum deceleration (MaxD), are commonly used to quantify the severity of traffic conflicts. These measures are derived from vehicle trajectory data and provide a detailed representation of vehicle interactions (Gettman and Head 2003). The surrogate safety assessment model (SSAM) is widely used to analyze these measures and identify conflict events. SSAM enables the processing of large volumes of trajectory data and provides a systematic approach for evaluating safety performance. This method is particularly useful for analyzing innovative intersection designs, where traditional crash data may not be available (Gettman and Head 2003).

### 2.1.6 Statistical Approaches for Crash Estimation

Statistical modeling plays a critical role in translating traffic conflicts into meaningful safety indicators. Among various approaches, extreme value theory (EVT) has emerged as a powerful method for modeling rare and extreme events. The peaks over threshold (POT) approach is widely used in EVT-based traffic safety analysis. This method focuses on extreme observations that exceed a specified threshold and provides a probabilistic framework for estimating crash risk. EVT allows researchers to model the distribution of extreme events and estimate the likelihood of crash occurrence based on high-severity conflicts (Songchitruksa and Tarko 2006). Recent advancements have introduced bivariate EVT models, which consider multiple surrogate safety indicators simultaneously. By analyzing the joint behavior of variables such as TTC and MaxD, these models provide a more comprehensive representation of crash risk. Studies have shown that bivariate EVT models can improve the accuracy and reliability of crash estimation compared with traditional univariate approaches (Zheng et al. 2018). The integration of EVT with surrogate safety analysis represents a significant advancement in traffic safety research. These methods enable a more robust and data-driven approach to safety evaluation, particularly in simulation-based studies where direct crash data are not available.

### 2.1.7 Limitation of Existing Studies

Despite significant advancements in traffic modeling and safety analysis, several limitations remain in the existing literature. Many studies focus primarily on operational performance without adequately considering safety evaluation, resulting in incomplete assessment of intersection performance. Conversely, some studies emphasize safety analysis without incorporating operational efficiency, limiting the practical applicability of their findings. Another key limitation is the lack of integration between simulation-based analysis and advanced statistical methods. While simulation models are widely used for operational analysis, their integration with statistical approaches such as EVT remains limited. This gap restricts the development of comprehensive evaluation frameworks that can simultaneously assess both operational and safety performance. Furthermore, many studies rely on limited datasets and do not validate their models using independent data sources. This raises concerns about the generalizability and robustness of simulation results. Addressing these limitations is essential for improving the reliability of traffic system analysis and supporting more effective transportation planning and decision-making.

## 2.2 Safety Evaluation of DDIs and CFIs

### 2.2.1 Safety Literature on DDIs

Many prior studies have consistently demonstrated the safety advantages of DDIs through before–after evaluations, EB-based methods, and the development of CMFs. The first real-world implementation in Springfield, Missouri, provided early validation of the concept. A study reported a 46% reduction in total crashes, the complete elimination of left-turn crashes, and a 72% decrease in left-turn right-angle crashes following DDI conversion with one year of post-construction data (Chilukuri et al. 2011). Similarly, another analysis of crash data from seven early DDI sites across four states recommended CMFs of 0.67 for total crashes and 0.59 for injury crashes, citing consistent reductions in overall, angle, and turning crashes (Hummer et al. 2016). A broader national safety evaluation involving 26 DDI sites across 11 states reported CMFs of 0.633 for total crashes and 0.461 for fatal and injury crashes. The study observed significant reductions in angle crashes (CMF = 0.441) and rear-end crashes (CMF = 0.549), although a slight increase was noted in sideswipe crashes (CMF = 1.139) (Nye et al. 2019).

Building on these findings, an evaluation of 80 DDI sites across 24 states using comparison group analysis, EB, and cross-sectional modeling reported a 44% reduction in fatal and injury crashes, along with notable improvements in rear-end and angle/left-turn crash rates. The study also identified ramp terminal spacing and exit ramp speed as critical geometric factors influencing DDI safety performance (Abdelrahman et al. 2021). Together, these studies consistently indicate that DDIs outperform conventional diamond interchanges in reducing crashes, particularly those of higher severity. Furthermore, additional work contributed to the advancement of freeway interchange safety analysis by developing predictive methodologies that address limitations in the Highway Safety Manual (HSM), enabling the calibration of SPFs and CMFs across various crash severities and interchange configurations (Bonneson et al. 2021).

Several studies have also investigated crash trends along adjacent roadway segments and wrong-way entry points—not just at DDI ramp terminals—employing robust methodologies such as the EB approach and comparison group for development of CMFs to evaluate the effectiveness of DDIs in enhancing roadway safety. One study examined the effects of DDIs on adjacent intersections and speed-change lanes, finding no statistically significant safety impact in those areas, suggesting DDIs do not negatively influence surrounding roadway segments (B. Claros et al. 2017a). Another addressed concerns about wrong-way maneuvers by monitoring five DDI sites with video detection over six months; while wrong-way entries occurred more frequently at night and at entry points, no crashes were linked to them, indicating DDIs are generally safe when designed properly (Vaughan et al. 2015).

In addition to national and multi-state evaluations, several studies have focused specifically on state-level analyses to better understand localized DDI safety performance. An analysis of DDIs in Missouri using naïve Bayes, EB, and comparison group methods observed the largest safety improvements in fatal and injury crashes (59.3%–63.2%) and up to 47.9% reduction in total crashes, affirming DDI safety despite minor concerns such as wrong-way entries (B. R. Claros et al. 2015). Another study developed CMFs for DDI ramp terminals using data from 20 Missouri sites, showing significant crash reductions—up to 73.3% for FI crashes—through both comparison group and EB methods, offering a replicable approach for other interchange types (B. Claros et al. 2016). In a follow-up study, over 13,000 crash records from Missouri were analyzed, SPFs were developed using negative binomial (NB) regression, and the EB method was applied for evaluation. The study found that DDI ramp terminals experienced a 55% reduction in fatal and injury crashes, a 31.4% reduction in property damage only (PDO) crashes, and a 37.5% decrease in total crashes compared with conventional ramp terminal designs. The remaining crashes were predominantly minor rear-end collisions (B. Claros et al. 2017b). Another study evaluates the safety performance of two DDIs in Minnesota using before–after analyses. Applying naïve and empirical Bayes methods to crash and traffic volume data, the results show significant crash reductions, with CMFs of 0.48 and 0.42, confirming DDIs as an effective safety countermeasure (Qi et al. 2018). Previous research in Utah used the EB before–after method with SPFs from the HSM and FHWA's Interchange Safety Analysis Tool (ISAT) to analyze crash data from five DDI sites, revealing significant reductions in total, PDO, and FI crashes at most sites, though some showed minor or insignificant increases, emphasizing the need for further study with more data (Lloyd and Song 2017). Similarly, another study applied EB methods to a smaller sample of DDI sites in Utah and reported a 24.5% crash reduction (CMF = 0.755), but it noted that limited post-conversion data restricted the accuracy and generalizability of the findings (Zlatkovic 2015, 2019).

This study focuses on evaluating the safety performance of DDIs in Utah, with an emphasis on locally calibrated analyses to improve the accuracy of CMFs. By extending the EB approach, the study aims to assess the region-specific impacts of these innovative intersection designs, considering local geometric, traffic, and driver behavior factors. Using crash data from 2006 to 2021, this study provides a more comprehensive understanding of the safety outcomes associated with DDIs, particularly in the context of Utah's unique roadways and traffic conditions.

### 2.2.2 Safety Literature on CFIs

CFIs have gained increasing attention in recent years as transportation agencies seek innovative solutions to address growing traffic demands, improve safety, and enhance operational efficiency at congested intersections. A substantial body of research has examined the performance of CFIs and other displaced left-turn configurations from multiple perspectives—including safety, traffic operations, driver behavior, and environmental impacts. The following studies provide a comprehensive overview of the current state of knowledge, highlighting key findings that collectively inform the motivation and methodological direction of the present research.

A study investigated how CFIs impact safety and environmental performance compared with traditional signalized intersections. Using microsimulation models for CFIs in Missouri and Colorado, along with the SSAM, the study analyzed traffic conflict patterns and found that total conflicts decreased after implementing CFIs. Overall, the research provides strong evidence that CFIs enhance traffic safety and emissions performance, making them a promising alternative for both urban and rural intersections (Wolfgram 2018).

Another study evaluated CFIs through both field observations and simulation analyses to assess operational, safety, and environmental performance compared with conventional intersections. The methodology included before-and-after field studies to observe driver behavior and hazardous maneuvers, as well as microsimulation using VISSIM and INTEGRATION models to estimate operational efficiency, fuel consumption, and emissions. Findings showed that while drivers initially experienced confusion and unsafe maneuvers near the diverging areas, these issues declined by about 50% after one year as familiarity improved. Simulation results indicated that CFIs enhanced intersection performance, reducing delay, energy use (by 5%–11%), and emissions (HC, CO, NOx reduced by 1%–6%). Overall, CFIs proved more robust and efficient under varying traffic demands, offering significant operational and environmental benefits once drivers adapt to their layout (S. Park and Rakha 2010).

Several studies have investigated the safety performance of CFIs and related displaced left-turn treatments, providing an increasingly detailed understanding of how these innovative designs influence crash occurrence and severity. The following research efforts highlight key empirical findings from various states and methodological approaches, collectively forming the foundation for evaluating the safety effectiveness of CFIs. A study evaluated the safety effects of a DLT intersection installed at Airline Highway and Seigen Lane in Baton Rouge, Louisiana, by comparing four years of crash data before installation (2002–2005) with two years of data after installation (2006–2008). Using a simple before–after analysis, the study examined total crashes, fatal and injury crashes, and crash rates based on entering traffic volumes. The results showed notable safety improvements: total crashes decreased by about 24%, and fatal and injury crashes decreased by nearly 19%. Crash rates also declined by approximately 22%–24%. Although the analysis did not adjust for changes in traffic or other external factors, the findings suggest that the DLT intersection contributed to meaningful reductions in both the frequency and severity of crashes (LaDOTD 2007; Hughes et al. 2010).

One of the earliest studies focused on quantifying the safety effects of CFIs using the EB methodology to develop CMFs, applying six years of crash data from eight treatment sites and five control sites. The results showed that partial CFIs—those implementing displaced left turns on only two approaches—achieved approximately a 12% reduction in total crashes, corresponding to a CMF of 0.877. This study provided valuable early evidence supporting the safety effectiveness of the CFI design and offered a methodological foundation for subsequent large-scale evaluations (Zlatkovic and Kergaye 2018; Zlatkovic 2019).

Another study comprehensively evaluated the safety and operational performance of DLT intersections across Utah, Colorado, Louisiana, and Ohio using two approaches: a before-and-after analysis with comparison groups and a cross-sectional statistical model. Results showed that while DLTs improve traffic efficiency—reducing average delays by about 3.6 seconds per vehicle and accommodating higher traffic volumes—they also tend to increase crash frequencies. Specifically, total crashes rose by about 11%, fatal and injury crashes by 22%, property-damage-only (PDO) crashes by 7%, and single-vehicle crashes by 52%, although non-motorized crashes decreased by roughly 39%. Despite operational benefits, the safety disadvantages led to an unfavorable benefit–cost ratio. The authors recommend applying targeted safety measures, improving driver awareness, and conducting future studies with larger datasets to refine these findings (Abdelrahman 2020; Abdelrahman et al. 2020).

Another research study assessed the safety performance of two DLT intersections in San Marcos, Texas, using crash data from 2011 to 2018 obtained from TxDOT's CRIS database. Through statistical and collision-diagram-based analyses, they found that DLT implementation did not increase overall crash frequencies and significantly reduced left-turn- and right-turn-related crashes. However, new safety issues emerged concerning traffic signage, signal coordination, geometric design, and access management. The study emphasized that successful DLT implementation requires careful attention to these design and operational aspects, as well as driver understanding and acceptance, and provided recommendations to ensure safer future DLT applications (Qu et al. 2020).

Moreover, a study examining the adoption of CFIs found strong safety benefits, with an EB analysis of 16 sites revealing a 12.2% total crash reduction. The most influential factor was right-turn design: parallel right turns improved safety with a 29.6% crash reduction, while standard right turns increased crashes by 15.6%. Among sites using parallel right turns, both non-skewed and skewed intersections showed large safety gains (29.4% and 30.1% reductions, respectively), with non-skewed sites performing slightly better by severity and crash type. Although area type did not increase crashes overall, rural CFIs were significantly safer than urban/suburban ones (40.3% vs. 26.0% reduction). Additionally, 4-legged intersections provided the most consistent safety improvements, and 2-lane crossovers were the only crossover type with a significant crash reduction, achieving 34.9% (Chris Cunningham et al. 2022).

Additionally, the present study examines the operational and safety performance of CFIs and related displaced left-turn treatments. While CFIs have shown operational and environmental advantages, their safety performance varies based on site-specific conditions and driver adaptation. This research addresses these mixed findings by offering a data-driven, state-specific safety assessment, with the goal of generating reliable CMFs that can guide decision-making for future DDI and CFI implementations. The study provides valuable insights to inform transportation agencies and enhance safety planning for these innovative intersection treatments in Utah.

# 3. OPERATIONAL PERFORMANCE EVALUATION OF DDI AND CFI

This chapter presents a detailed description used to develop, calibrate, and validate microscopic traffic simulation models for innovative intersection designs. The study focuses on DDIs and CFIs, which involve complex traffic movements and required detailed modeling.

The simulation models were developed using PTV VISSIM and calibrated using three key performance measures: traffic volume, average speed, and crash frequency. While traffic volume and speed were used to ensure operational accuracy, safety performance was evaluated using surrogate safety measures derived from vehicle trajectory data.

Crash frequency was estimated by integrating the SSAM with a bivariate EVT approach, using TTC and MaxD as conflict indicators. This approach allows for more realistic real-world representation of crash risk in simulation models.

The overall methodology consists of four stages: pre-modeling, base model development, calibration, and validation. The methodological framework adopted in this study is illustrated in Figure 5, and the subsequent sections below describe each stage in detail.

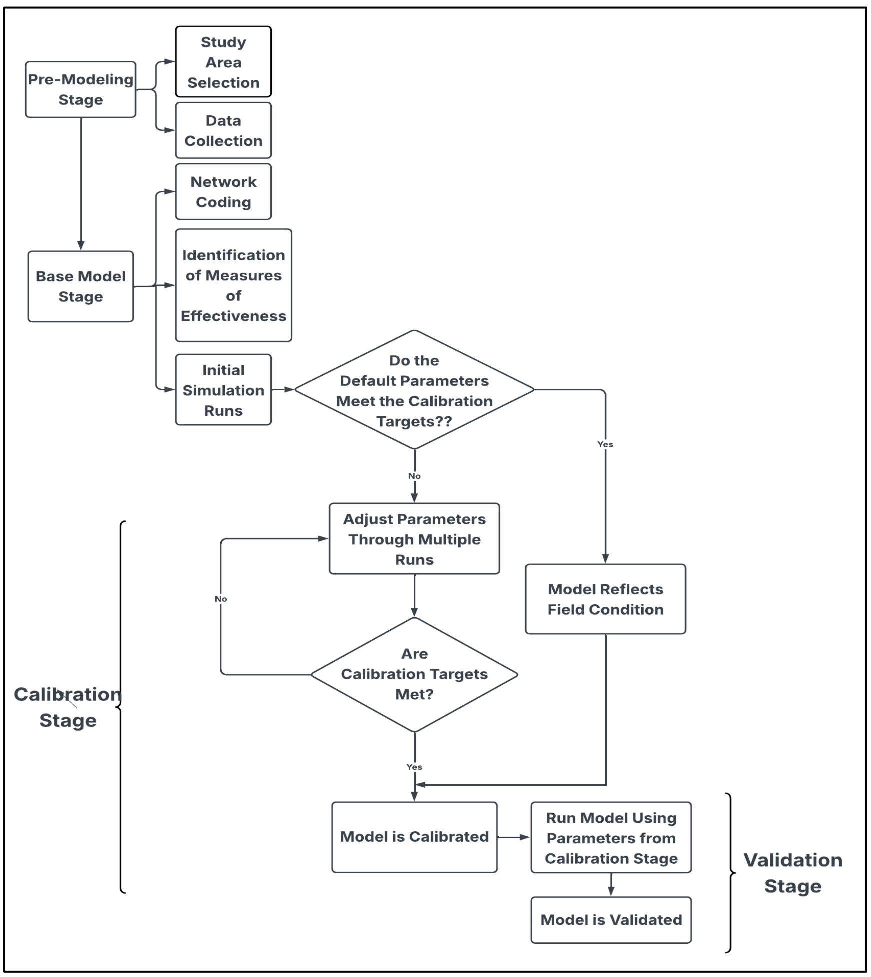


**Figure 5: Flowchart of methodological framework**

## 3.1 Pre-Modeling Stage

The pre-modeling stage involves the initial steps required for developing simulation models. This stage includes the selection of study sites and the collection of relevant field data to ensure that the models accurately represent real world traffic conditions. The selected study sites consist of a DDI and a CFI located in Utah. These sites were chosen due to their complex geometry and the availability of reliable traffic and crash data. Following site selection, key data such as traffic volumes, signal timing plans, vehicle speeds, and crash records were collected to support model development and calibration. These data serve as the foundation for accurately replicating both operational and safety conditions within the simulation environment. The study site and data collection are described in the following section.

### 3.1.1 Study Area Selection

This study focuses on two innovative intersection designs located in Salt Lake City, Utah: a DDI and a CFI. These sites were selected due to their unique geometric configurations and operational complexity, and the availability of reliable traffic, speed, and crash data required for both simulation and safety analysis. The first study site is a DDI located at the intersection of Bangerter Highway and State Route 201 (SR – 201). This design allows vehicles to temporarily cross to the opposite side of the roadway, enabling direct left-turn movement without conflicts with opposing traffic. As a result, the number of signal phases is reduced, improving traffic flow and operational efficiency. The second study site is a CFI located at the intersection of Bangerter Highway and 3100 South. In this design, left-turning vehicles are redirected to cross over opposing traffic upstream of the main intersection. This configuration allows left-turn and through movements to occur simultaneously at the primary intersection, reducing delay and enhancing overall intersection performance. Both intersections are situated along Bangerter Highway, a major arterial corridor with high traffic demand. Selecting these two sites allows for the evaluation of different innovative intersection designs under similar traffic conditions while capturing their distinct operational and safety characteristics. The layouts and configuration of the selected study sites are shown in Figure 6 and Figure 7.


**Figure 6: Aerial view of the diverging diamond interchange (DDI) at Bangerter Highway and SR-201**

**Figure 7: Aerial view of the continuous flow intersection (CFI) at Bangerter Highway and 3100 South**

### 3.1.2 Data Collection

Data collection was conducted to support the development, calibration, and validation of the simulation models. The required datasets include traffic volumes, signal timing plans, vehicle speeds, and crash records, which are essential for accurately representing both operational and safety conditions. These data were obtained from reliable sources, including transportation agency databases and field measurements, ensuring consistency and accuracy for simulation modeling. The collected data were further processed and organized for use in model development and performance evaluation. The details of each dataset are described in the following subsections.

### *Traffic Data*

Traffic data were collected to represent the volume and movement patterns at the selected study sites. Annual average daily traffic (AADT) data for 2016, 2019, and 2024 were obtained from the Utah Department of Transportation (UDOT) database. In addition, intersection approach volumes and turning movement counts for 2024 were used as the base reference for simulation modeling. To ensure consistency in simulation inputs, traffic data were extracted for the same calendar date, January 15, for both 2016 for calibration and 2019 for validation. The selected peak hour of analysis was from 4:15 PM to 5:15 PM, representing the period of highest traffic demand at both intersections. Since detailed turning movement data were not available for all years, the turning movements for 2016 and 2019 were estimated based on the proportional distribution of turning movements observed in 2024. This estimation was performed by scaling the 2024 turning movement volumes, using the corresponding AADT values for each target year, by using the following equation.

$$\text{Movement Volume}_{\text{target year}} = \text{Movement Volume}_{2024} * \frac{\text{AADT}_{\text{target year}}}{\text{AADT}_{2024}} \quad (1)$$

where Movement Volume represents the turning movement count, and AADT represents the annual average daily traffic for the corresponding year.

The AADT values used for scaling were 42,000 (2024) and 40,000 (2016) for the DDI, and 65,000 (2024) and 56,000 (2016) for the CFI. These values were used to compute the scaling factors applied to estimate turning movement volumes for the target years. A summary of the traffic volume conversion for selected movements is presented in Table 2, while the complete dataset is provided in Appendix A and B. The processed traffic data were used as input for defining traffic demand in the simulation models and served as a key component for traffic volume calibration.

**Table 2: Summary of Traffic Volume Conversion**

| Intersection | Movement | 2024 Volume Count | Estimated 2016 Volume | VISSIM Input |
|---|---|---|---|---|
| DDI (SB) | Left | 479 | 455 | 455 |
| CFI (EB) | Right | 89 | 76 | 76 |

### *Signal Timing Data*

Signal timing data were collected to accurately represent traffic control operations at the selected study sites. Signal timing plans, phasing sequences, and controller logic for both intersections were obtained from official UDOT documentation. The collected signal timing plans included detailed information on minimum green times, maximum green times, vehicle extension parameters, yellow change intervals, and red clearance intervals for each signal group. In addition, coordination parameters such as cycle length, phase splits, offsets, and coordination patterns were incorporated to reflect real-world signal operations along the corridor.

The phasing sequences and signal group configurations were carefully reviewed to ensure that the operational logic of each intersection was accurately represented. This included the correct implementation of protected and permitted movements, phase compatibility, and sequencing of signal groups based on field conditions. Detector settings and vehicle actuation parameters were also considered to replicate realistic traffic-responsive signal behavior.

All signal timing parameters were implemented in the VISSIM simulation environment using the ring-barrier controller framework. The cycle length, phase splits, and coordination settings were adjusted according to the field data to ensure consistency between simulated and observed conditions. The signal timing data were used as a critical input for model development and played an essential role in accurately reproducing intersection control operations during simulation. Detailed signal timing plans and controller settings are provided in Appendix C. A sample signal timing plan obtained from UDOT documentation is shown in Figure 8.

```
COORDINATOR PATTERN [   6]
USE SPLIT PATTERN.  6 SPLIT SUM ....111s
TS2 (PAT-OFF)..   1-3
CYCLE.........   100s STD (COS)......112
OFFSET VAL.....     0s
ACTUATED COORD...  NO TIMING PLAN....  1
ACT WALK REST....  NO SEQUENCE........ 1
PHASE RESRVCE....  NO ACTION PLAN....  6
SPLIT PREFERENCE PHASES
 PHASE[s]  1   2   3   4   5   6   7   8
SPT[  6]   7  41   7  45   7  52   7  34
PREF 1...  0   0   0   0   0   0   0   0
PREF 2...  0   0   0   0   0   0   0   0
SPLT EXT...0s. 0s  0s  0s
VEH PERM.  0s  0s  0s  DISP
RING DISP  -  12s  0s  0s (RING 2-4)
 PHASE[s]  9  10  11  12  13  14  15  16
SPT[  6]   0   0   0   0   0   0   0   0
PREF 1...  0   0   0   0   0   0   0   0
PREF 2...  0   0   0   0   0   0   0   0

SPLIT DEMAND PTRN.  0    0 XART PTRN.   0
PHASE..  1 2 3 4 5 6 7 8 9 0 1 2 3 4 5 6
COORD... . X . . . . . X . . . . . . . .
VE RCALL . . . . . . . . . . . . . . . .
PD RCALL . . . . . . . . . . . . . . . .
MX RCALL . . . . . . . . . . . . . . . .
OMIT.... . . . . . . . . X X X X X X X X
SF OUT.. . . . . . . . . (1-8)
```

**Figure 8: Sample signal timing plan for DDI, illustrating phase sequence and timing parameters**

### *Speed Data*

Vehicle speed data were collected to represent operating conditions at the selected study sites. Approach speeds were obtained from the UDOT Automated Traffic Signal Performance Measures (ATSPM) system, which provides high-resolution traffic data along with corresponding detector location information. The ATSPM data include vehicle speeds recorded at specific detection points along each approach, allowing for accurate representation of speed variations under real-world traffic conditions. The detector locations were carefully considered to ensure that the collected speeds reflect approach conditions prior to entering the intersection.

The speed data include average speed, 85th percentile speed, and 15th percentile speed, which were used to characterize the distribution of vehicle speeds for each approach. These measures provide a comprehensive understanding of traffic flow conditions and driver behavior. The collected speed data were used to define desired speed distributions in the VISSIM simulation models. These inputs play a critical role in capturing realistic vehicle behavior and were further used during the calibration process to match simulated speeds with observed field conditions. Sample approach speed profiles for the DDI and CFI obtained from ATSPM are shown in Figure 9 and Figure 10, respectively.

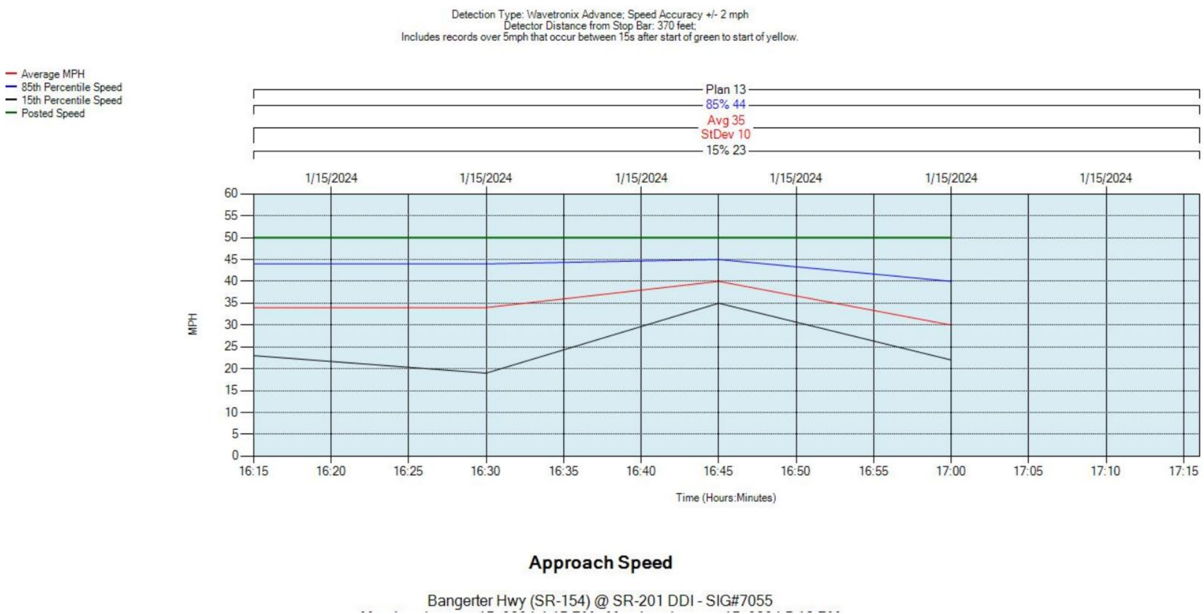


**Figure 9: Approach speed profile for DDI**

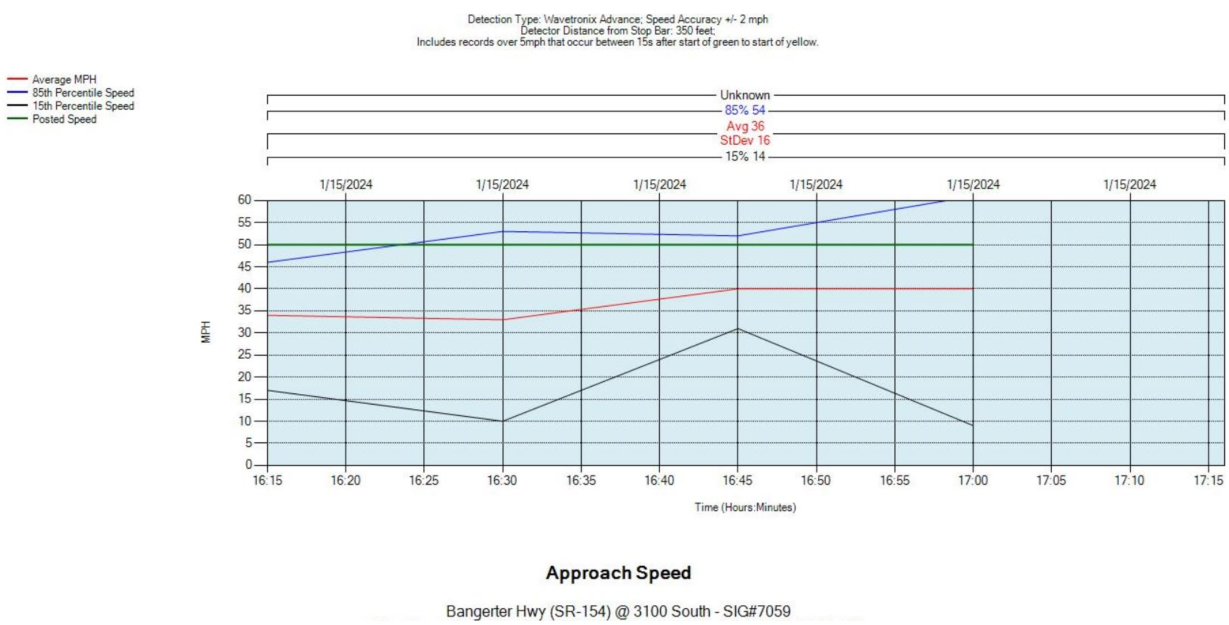


**Figure 10: Approach speed profile for CFI**

***Crash Data***

Crash data related to the study sites for 2016 and 2019 were obtained from the UDOT crash records database (Utah Department of Public Safety – Highway Safety Office 2026). The dataset included a comprehensive range of crash attributes, such as injury severity levels, manner of collision, roadway characteristics, environmental conditions, and contributing factors. The crash data for both years were compiled for the entire year to ensure sufficient sample size and statistical reliability for safety analysis.

In addition to the selected analysis years, a comprehensive crash dataset covering the period from 2010 to 2022 was obtained to support the identification of long-term safety trends and to enhance the robustness of the analysis. Due to the large size of the dataset, only a representative sample is presented in Appendix E, while the complete dataset is provided as a supplementary Excel file.

## 3.2 Base Model

In this section, the development of the base simulation models using PTV VISSIM is described in detail. The base models were created to replicate the geometric layout, traffic operations, and control strategies of the selected study intersections prior to calibration.

### 3.2.1 Base Model Development for DDI

The base simulation model for the DDI was developed using PTV VISSIM to accurately represent the geometric layout and traffic operations of the study site. The model development followed a systematic process, including network creation, speed assignment, traffic control implementation, and routing configuration, ensuring that the model closely reflects real-world conditions.

The modeling process began with the development of the roadway network using links and connectors, as shown in Figure 11. All approaches, ramps, and crossover sections were carefully created to match the actual geometry of the DDI. A standard 12-ft lane width was used in the model to represent typical roadway conditions. Attention was given to the crossover segments to ensure proper lane continuity and correct vehicle movement. The model included two main vehicle types, consisting of 90% passenger cars and 10% heavy goods vehicles (HGVs), to reflect the observed traffic composition.

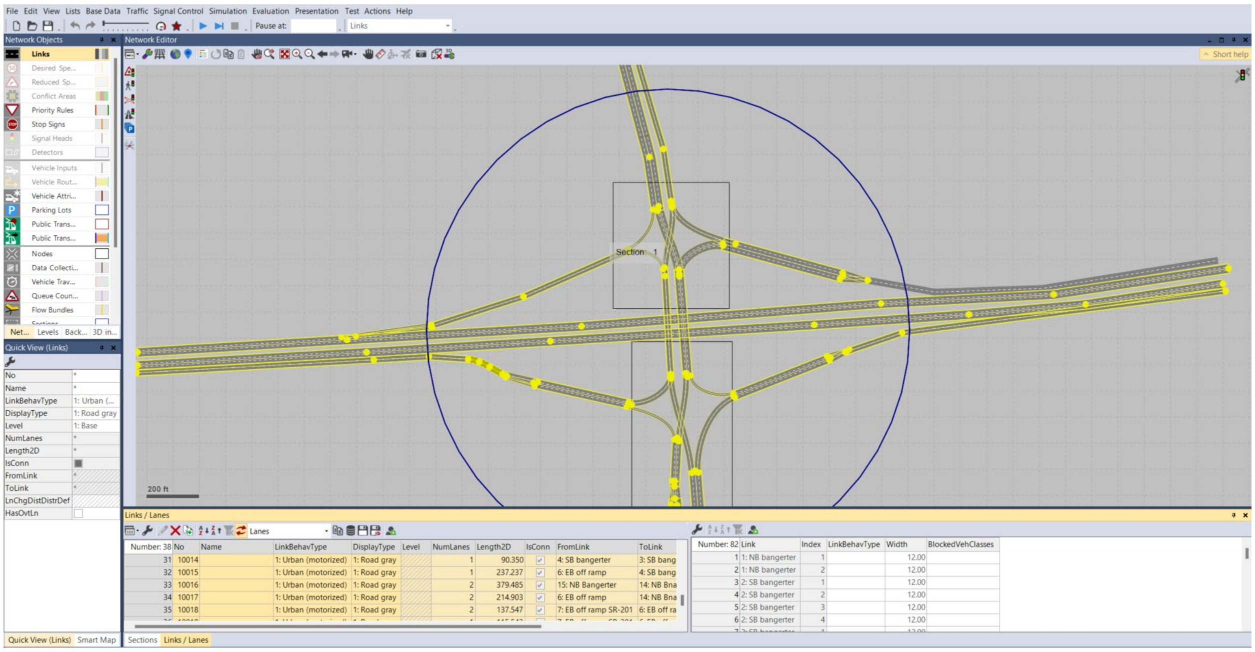


**Figure 11:Network geometry/links**

Following the network creation, desired speed decisions and distributions were defined based on the collected field speed data. These speed profiles were applied to different roadway segments to realistically represent driver behavior under varying traffic conditions. The desired speed along Bangerter Highway ranged from 15–55 mph, while SR-201 was modeled with desired speeds ranging from 35–65 mph, as illustrated in Figure 12 and Figure 13.

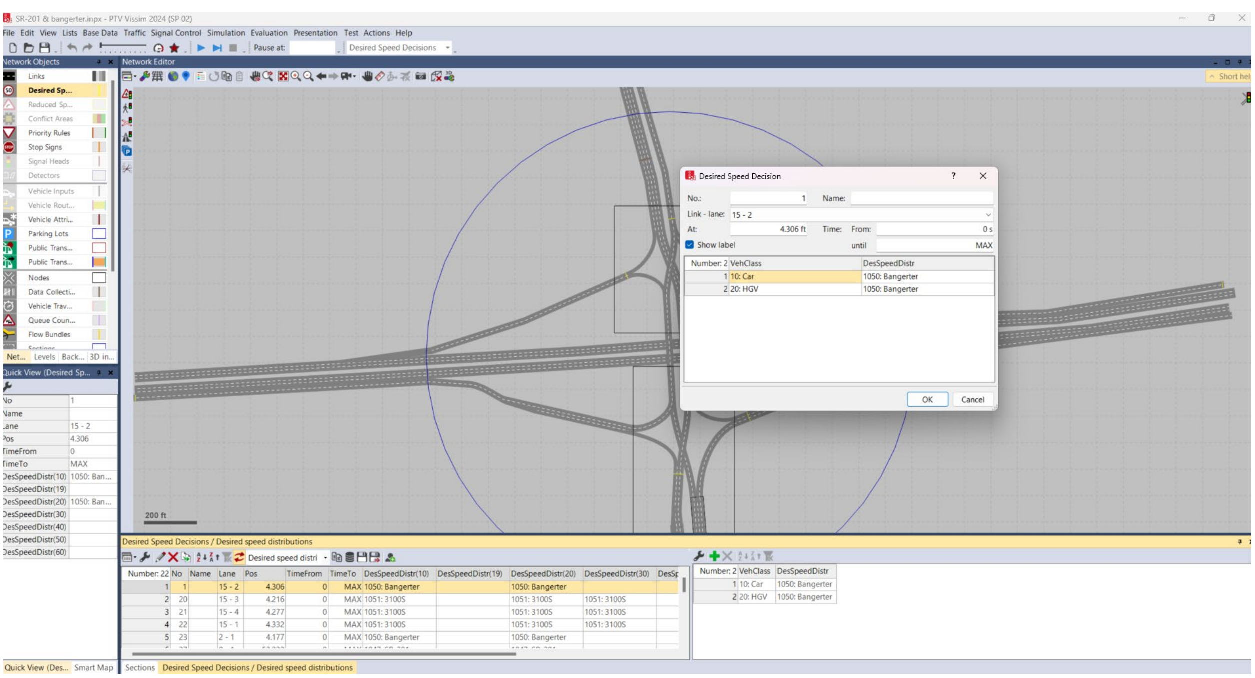


**Figure 12: Desired speed decision**

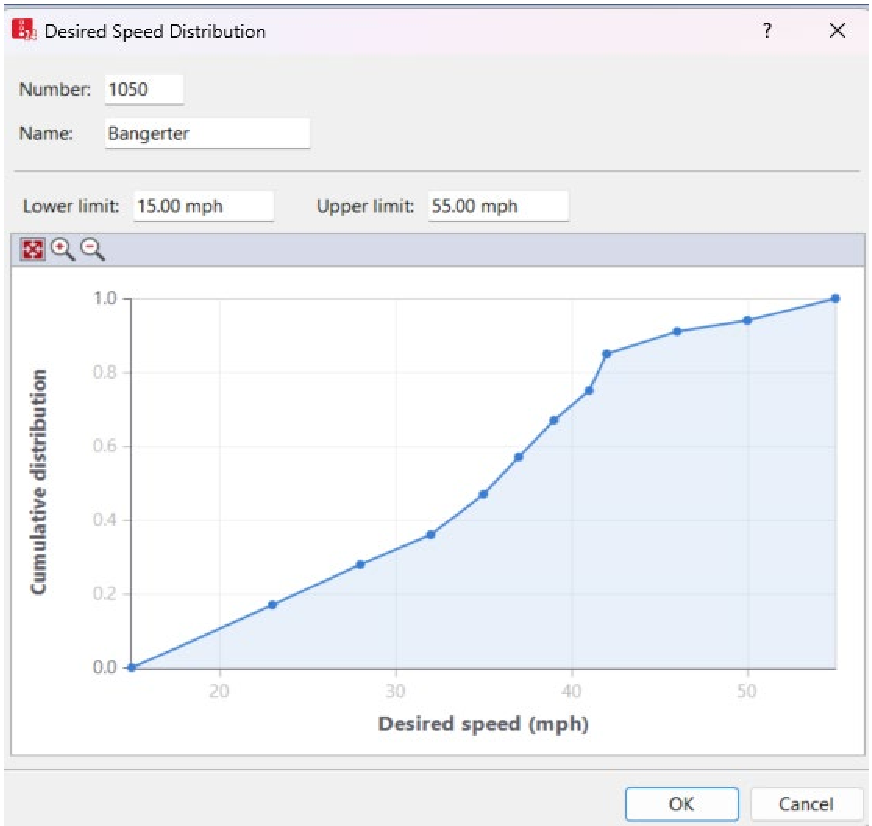


**Figure 13: Desired speed distribution**

To capture realistic vehicle deceleration behavior, reduced speed areas (Figure 14) were implemented at key locations such as turning movements and merging sections. Turning movements, including both left and right turns, were assigned reduced speed zones ranging from 15–25 mph to account for vehicle deceleration and maneuvering behavior. These areas allow vehicles to adjust their speeds appropriately when navigating complex intersection movements.

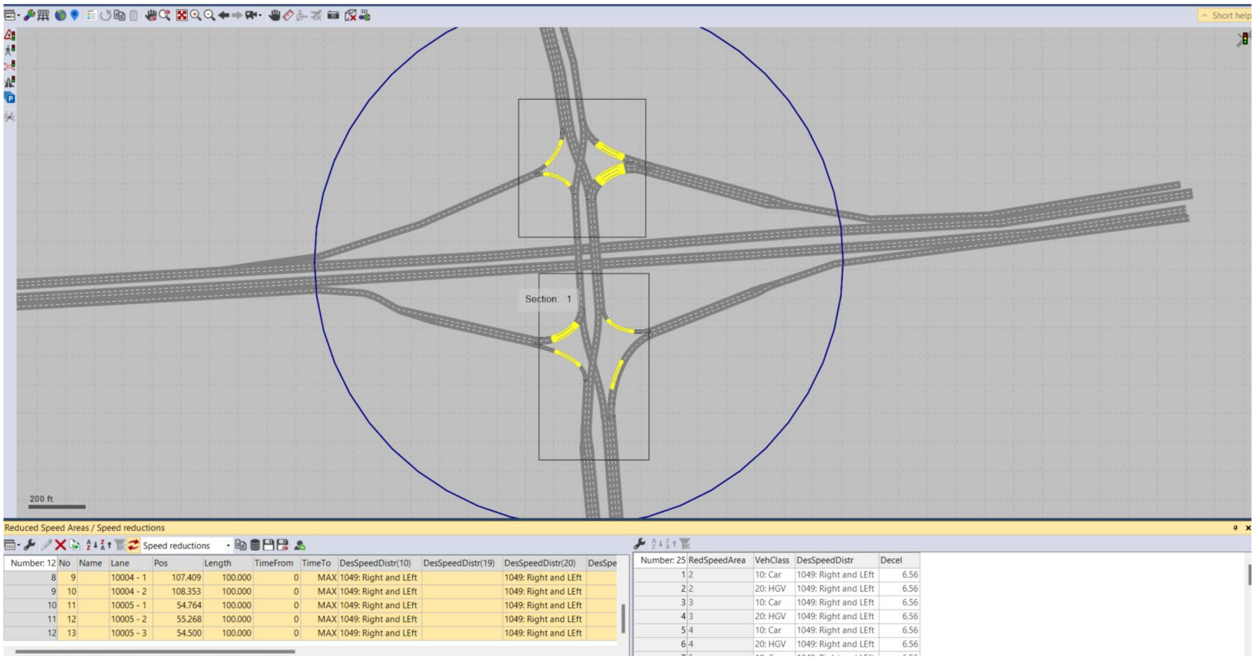

**Figure 14: Reduced speed areas**

Conflict areas were then defined at merging and crossing points within the intersection to model vehicle interactions. These areas (Figure 15) help simulate priority rules and gap acceptance behavior, which are critical for accurately representing traffic flow in unconventional intersection designs such as DDIs.

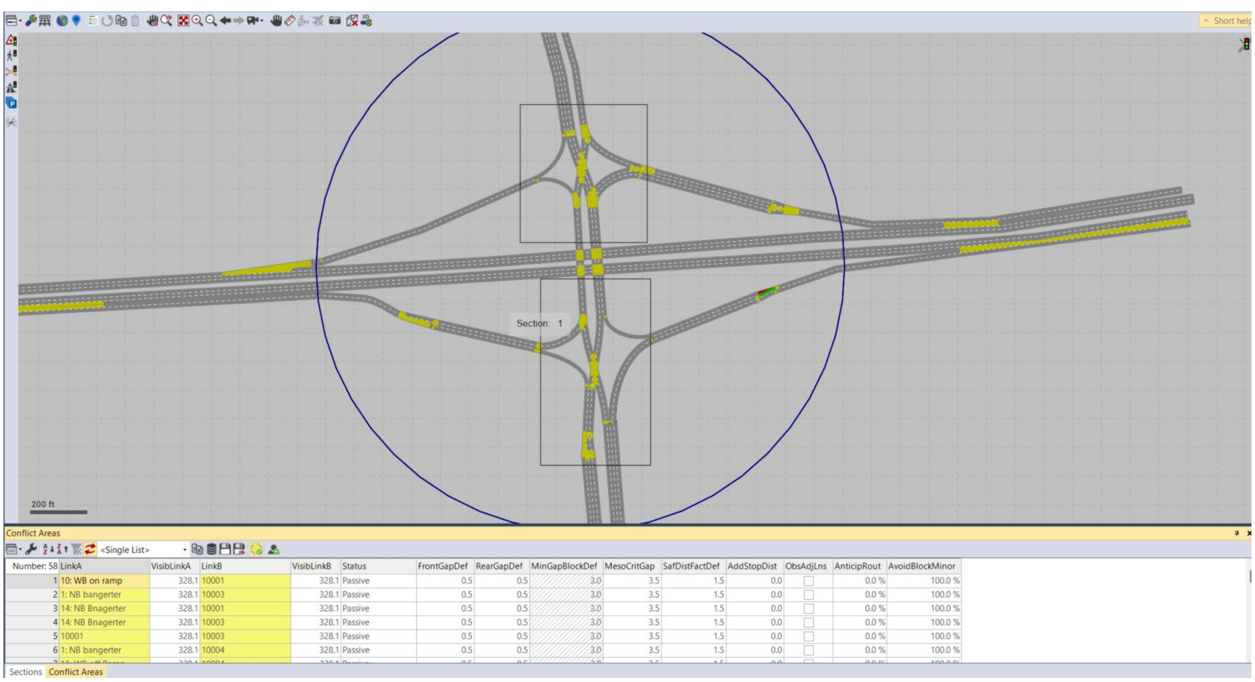

**Figure 15: Conflict areas**

Signal heads were placed at appropriate locations and assigned to corresponding signal groups to represent traffic signal control. The placement ensured that all movements were properly controlled according to the real-world signal configuration, as depicted in Figure 16.

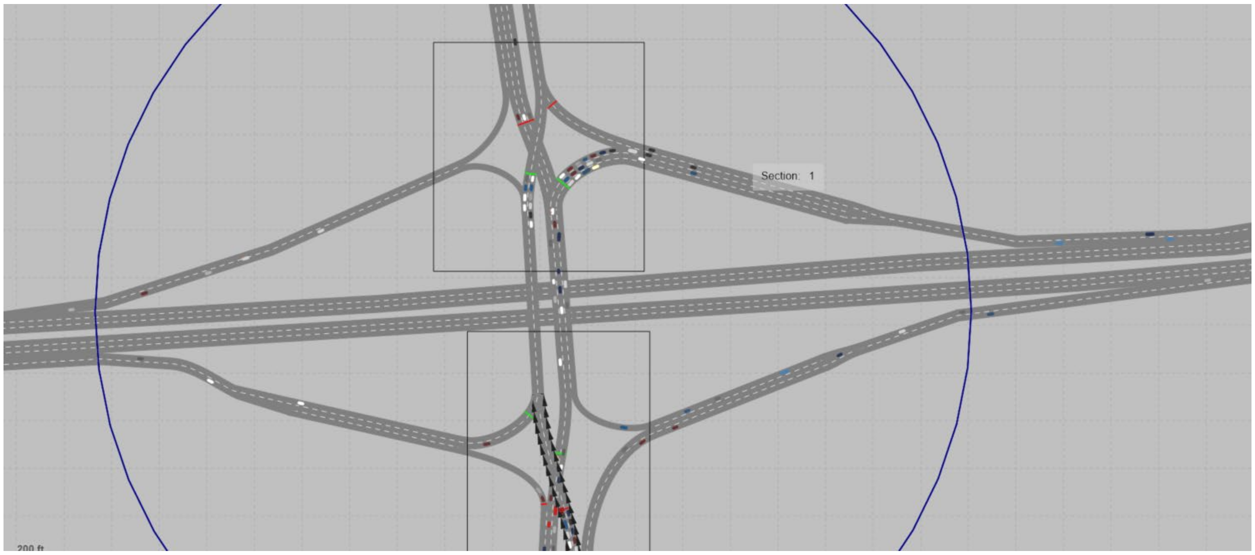


**Figure 16: Signal Head**

The placement ensured that all movements were properly controlled according to the real-world signal configuration. In addition, vehicle detectors (Figure 17) were placed at approximately 3 feet and 15 feet upstream of the signal heads to support signal control logic and accurately capture vehicle presence near the stop line.

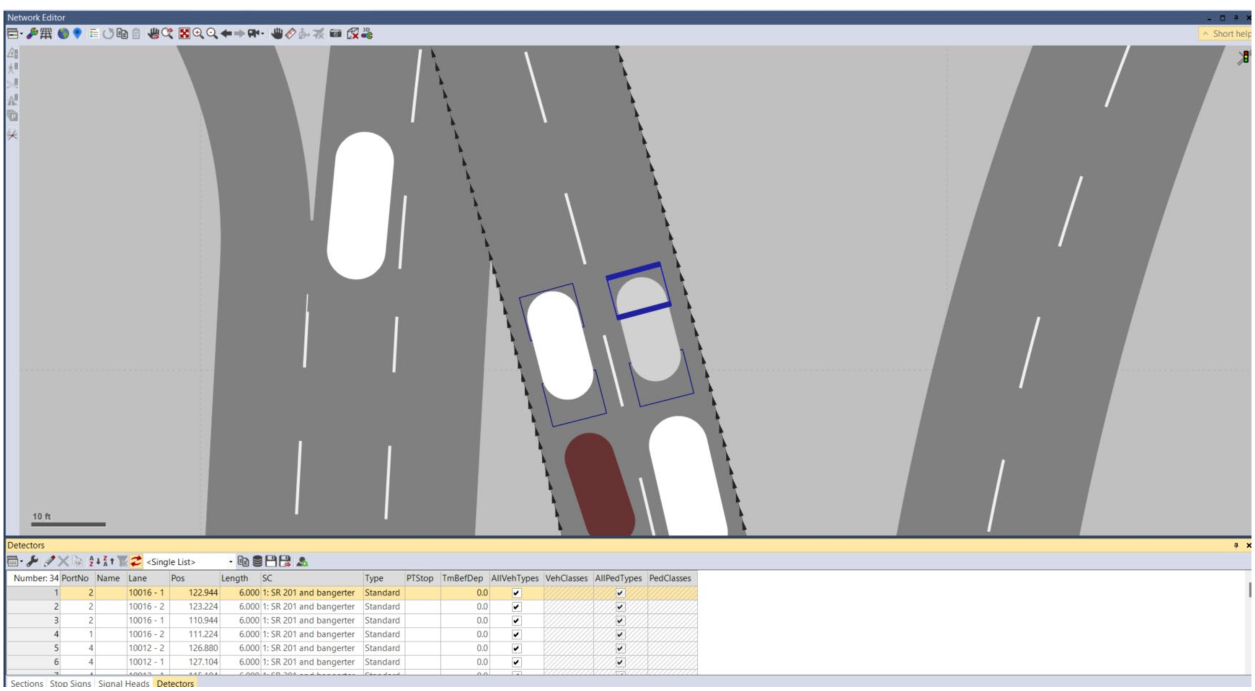


**Figure 17: Detectors**

Static vehicle routing decisions were defined to represent turning movements and route choices based on observed traffic patterns. This ensured that vehicles followed realistic paths through the intersection according to the traffic demand data, as shown in Figure 18.

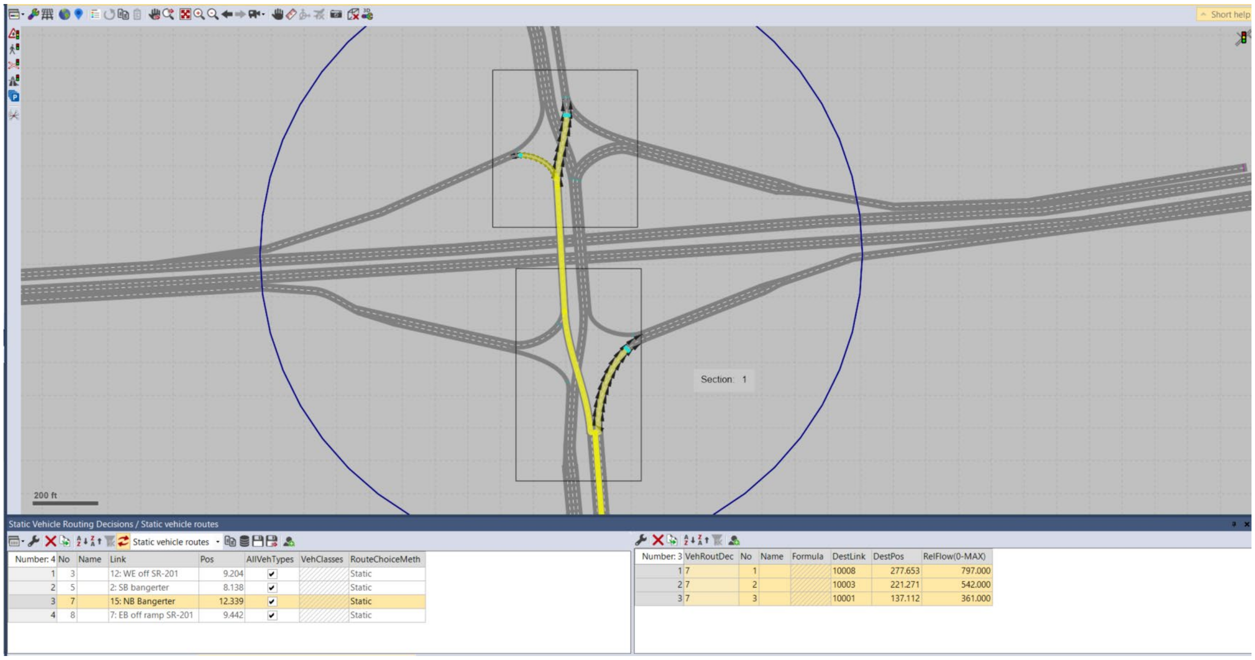


**Figure 18: Vehicle routing**

Nodes were defined to represent the intersection area for evaluation purposes. These nodes (Figure 19) were used to capture performance measures such as delay and travel time within the defined study area.

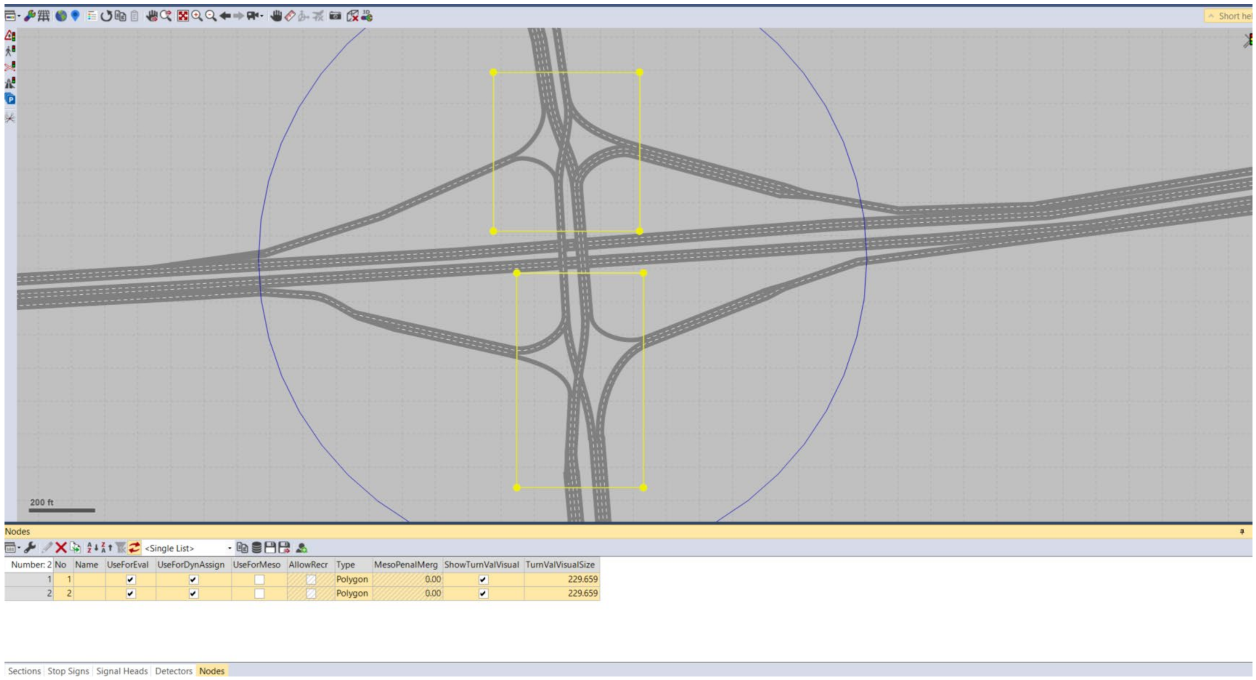


**Figure 19: Nodes**

In addition, data collection points were placed at selected locations along the network to extract traffic performance measures such as traffic volume and speed, as shown in Figure 20. These points were located approximately 380 feet upstream of the signal head on the southbound approach to capture representative approach conditions. The collected data were used later in the calibration and validation stages.

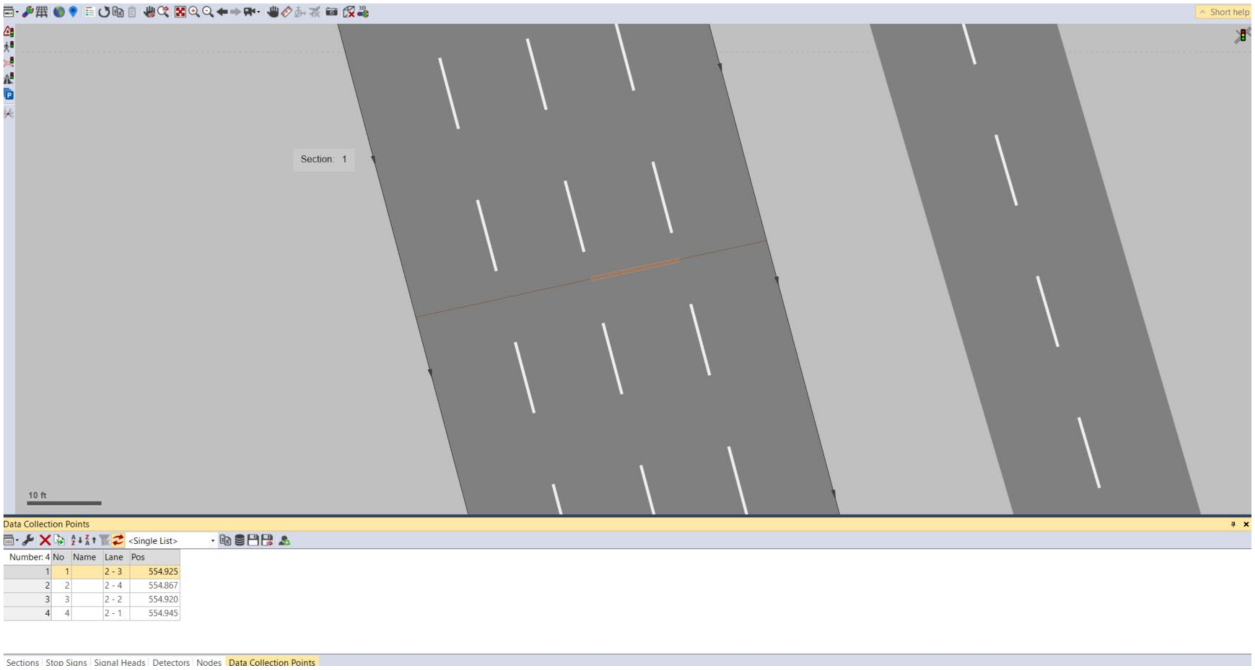


| Number: 4 | No | Name | Lane | Pos |
|---|---|---|---|---|
| 1 | 1 | | 2 - 3 | 554.925 |
| 2 | 2 | | 2 - 4 | 554.867 |
| 3 | 3 | | 2 - 2 | 554.920 |
| 4 | 4 | | 2 - 1 | 554.945 |

**Figure 20: Data collection points**

Signal control was implemented using the ring-barrier controller (Figure 21) framework in VISSIM. Signal controllers were defined and linked to signal groups, allowing for accurate representation of phase sequences and coordination strategies.

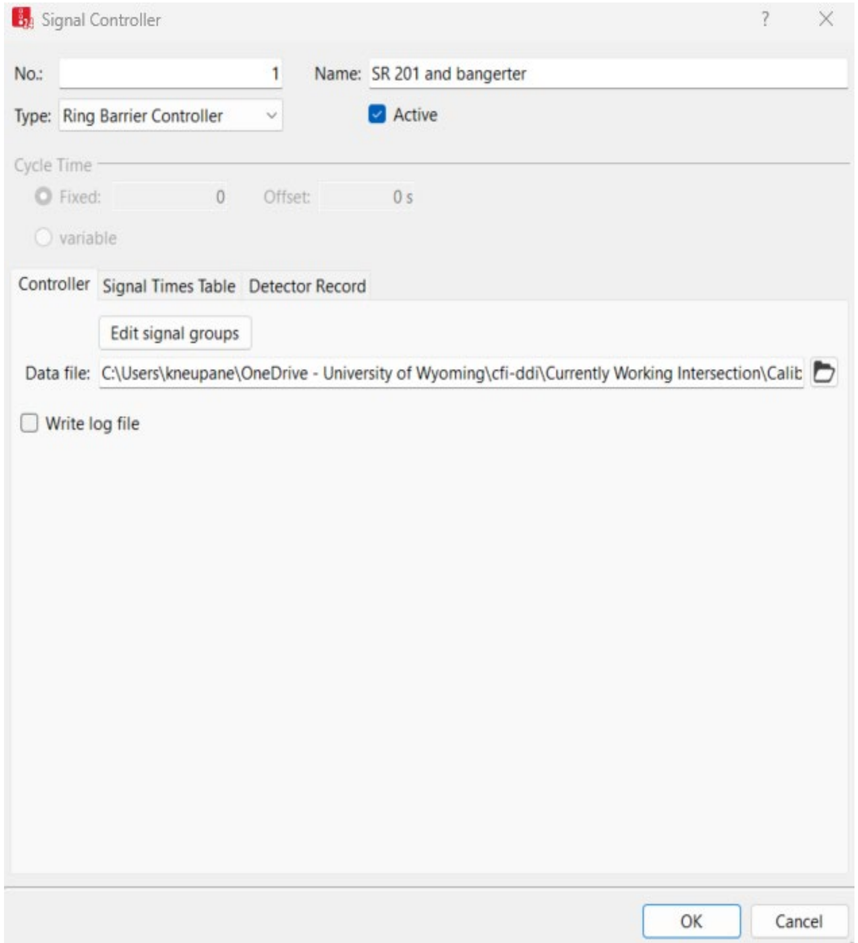


**Figure 21: Signal controller setup**

The signal timing plans, including cycle length, green splits, and phase sequences, were incorporated based on field data to ensure realistic traffic control operations, as shown in Figure 22.

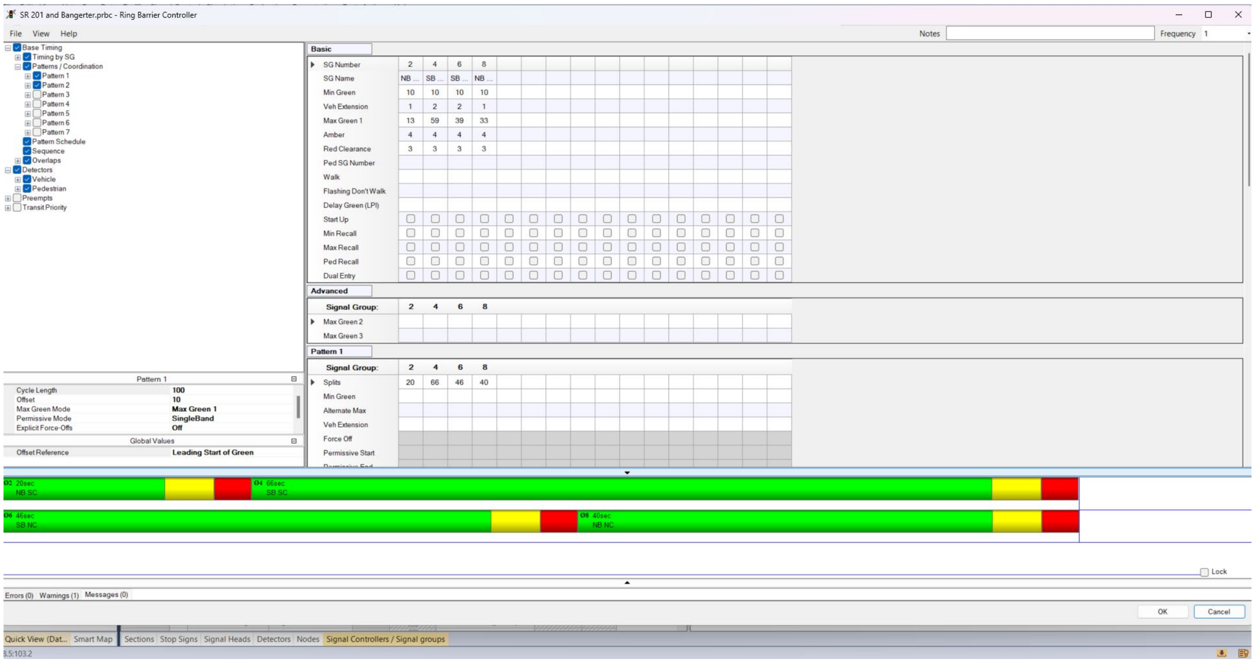

**Figure 22: Signal timing plan**

The base model (Figure 23) was developed using default driving behavior parameters without any calibration adjustments. This initial model provides a baseline representation of the intersection and serves as the foundation for subsequent calibration and validation stages.

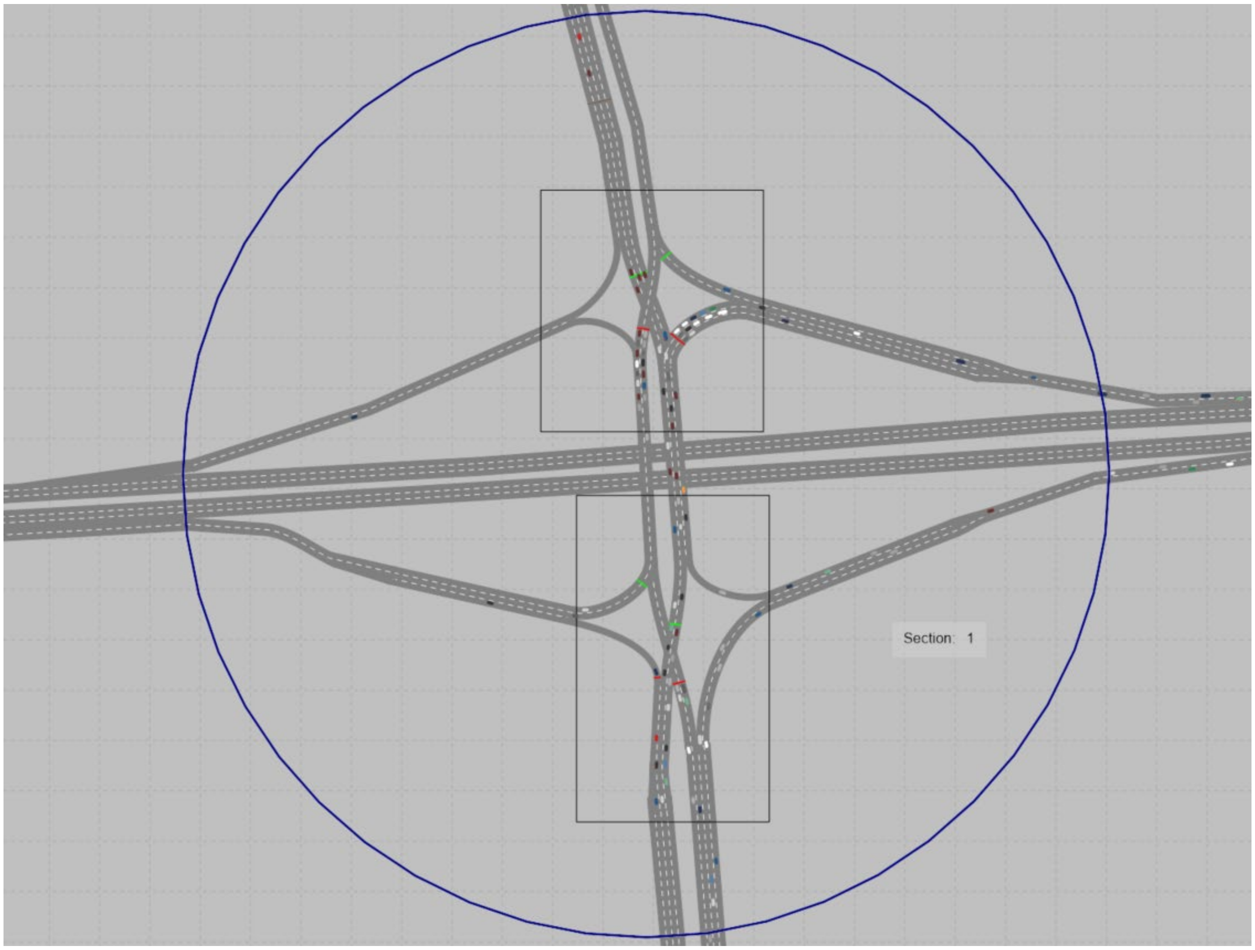


**Figure 23: Base model for DDI**

### 3.2.2 Base Model Development for CFI

The base simulation model for the CFI (Figure 24) was also developed in PTV VISSIM to represent the geometric configuration and traffic operations of the study site. The model was constructed in a structured manner, incorporating network geometry, traffic inputs, speed characteristics, and signal control elements to reflect real-world conditions.

The network was developed using links and connectors to replicate all approaches, turning movements, and upstream crossover sections characteristic of the CFI design. Attention was given to the displaced left-turn movements to ensure accurate representation of vehicle paths. A standard 12-ft lane width was applied, and the traffic composition consisted of 90% of passenger cars and 10% HGVs.

Desired speed decisions were assigned based on field data to capture realistic operating speeds across different roadway segments. The speed range along Bangerter Highway was set between 15–55 mph, while 3100 South was assigned a narrower range of 30–40 mph.

Reduced speed areas were incorporated at turning and merging locations to simulate deceleration behavior. Left and right turning movements were assigned reduced speed ranges of 15–25 mph to account for maneuvering conditions within the intersection. Conflict areas were introduced at key interaction points to model vehicle conflicts and priority behavior, ensuring realistic traffic flow representation.

Signal heads and corresponding signal groups were defined to replicate the field signal control system. Vehicle detectors were placed approximately 3 feet and 15 feet upstream of the signal heads to support signal operation and vehicle detection.

Vehicle route decisions were implemented to reflect observed patterns of turning and traffic demand. Nodes were defined within the intersection area to facilitate performance evaluation.

Data collection points were positioned to capture traffic performance measures such as speed and volume. For the CFI, these points were located approximately 350 feet upstream of the signal head on the northbound approach to represent approach conditions.

A circular buffer zone with a radius of 80 meters was defined around the intersection to capture safety-related interactions within the core area.

Signal control was implemented using the ring-barrier controller framework, with timing parameters such as cycle length and phase splits incorporated based on field data. The model was developed using default driving behavior parameters, providing a baseline for subsequent calibration and validation.

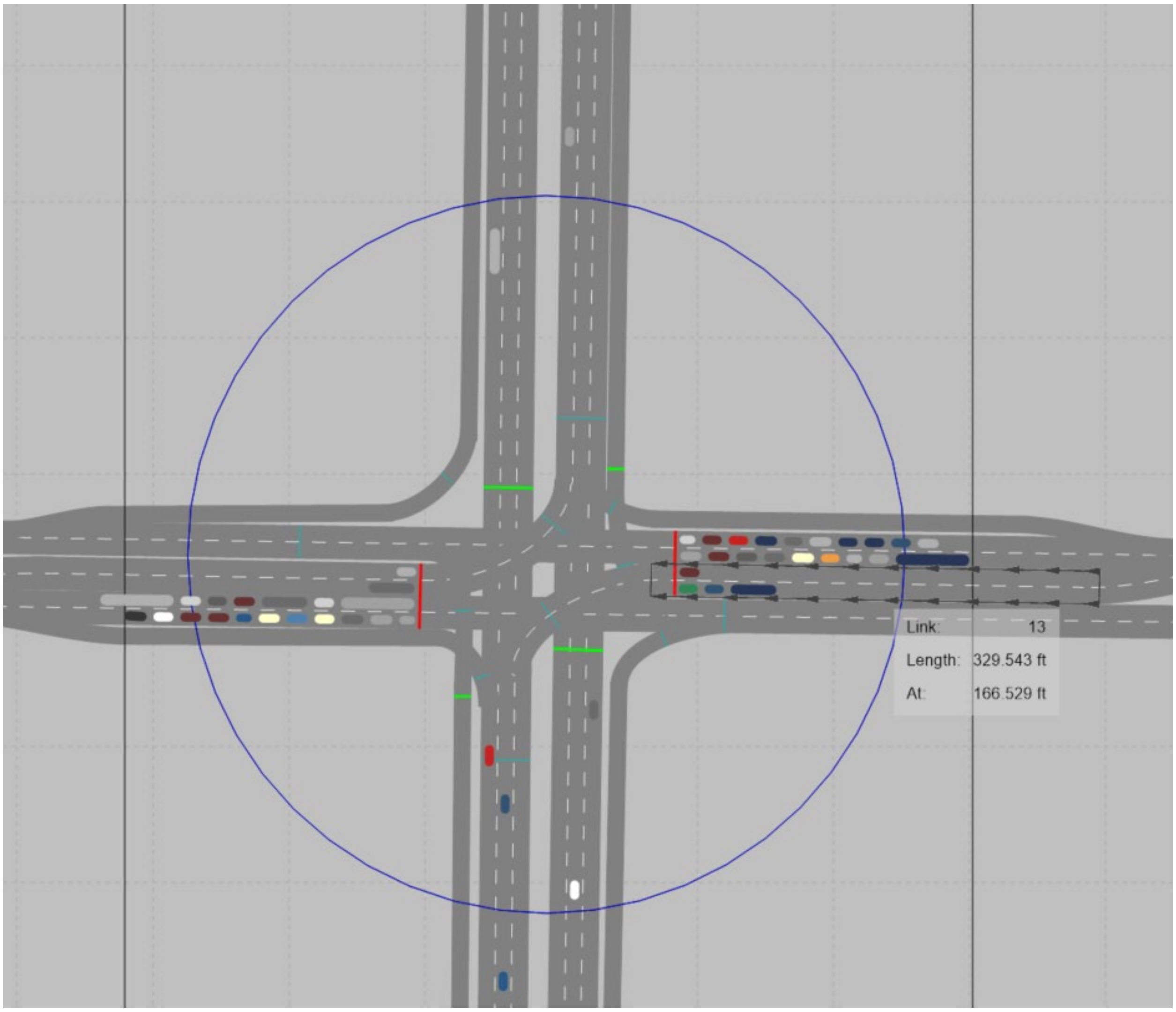


**Figure 24: Base model for CFI**

### 3.2.3 Identification of Measure of Effectiveness (MOEs)

Calibration and validation of microscopic traffic simulation models require the use of well-defined measures of effectiveness (MOEs) to ensure that the model accurately represents real-world traffic conditions. In this study, three key MOEs were selected: traffic volume, average approach speed, and crash frequency. These measures were chosen to provide a comprehensive evaluation of both operational performance and safety characteristics of the study intersections.

Traffic volume was used to assess the model's ability to replicate observed traffic demand and flow patterns across different movements and approaches. Accurate representation of traffic volume ensures that the model captures the correct distribution of vehicles within the network and reflects real-world traffic conditions.

Average approach speed was used as an indicator of prevailing traffic conditions and driver behavior. It provides insight into the level of congestion and operational efficiency of the intersection. Matching simulated speeds with observed field data is essential to ensure that the model realistically represents vehicle interactions and traffic flow dynamics.

Crash frequency was estimated using surrogate safety measures derived from vehicle trajectory data. Conflict data extracted from the SSAM were used to evaluate safety performance. This approach enables the estimation of crash risk based on vehicle interactions, providing a practical alternative to relying solely on observed crash data.

The selection of these three MOEs allows for a balanced assessment of both operational efficiency and safety performance within the simulation models. Furthermore, the same set of MOEs was consistently applied during both calibration and validation to ensure reliable model performance and predictive capability when tested against independent datasets.

### 3.2.4 Initial Simulation Runs

Initial simulation runs were conducted to verify that the developed network was functioning correctly and that the base model was properly configured prior to the calibration and validation process. During this stage, the model was executed using defined simulation parameters, including a total simulation period of 4,201 seconds, consisting of a 600-second warm-up period, a 3,600-second simulation run, and a 1-second wind-down period, as shown in Figure 25. A simulation resolution of 10 steps per second was used, and 10 simulation runs were performed with varying random seeds to ensure statistical reliability of the outputs. The simulation start time and conditions were set to represent typical traffic operations during the study period.

A detailed review of the model components was performed, including the geometric layout, signal timing implementation, vehicle routing, and overall traffic flow behavior under normal operating conditions. Attention was given to verifying lane connectivity, proper assignment of turning movements, detector placement, and the accuracy of signal control logic to ensure consistency with field conditions.

During the initial runs, several operational issues were identified and addressed. Speed profiles were examined to evaluate consistency in vehicle behavior and to detect any unrealistic variations or outliers. Instances of localized congestion were observed at certain approaches, which led to adjustments in traffic input distributions and minor refinements in signal coordination settings. Additionally, signal timing implementation was carefully reviewed to identify and correct any phase inconsistencies, overlaps, or mismatches with the actual signal plans.

All driver behavior parameters, including car-following and lane-changing models, were maintained at their default VISSIM settings during this stage. This approach ensured that the base model provided an unbiased representation of traffic behavior before any calibration adjustments were introduced. Overall, this step established a stable and reliable foundation for subsequent calibration and validation of the simulation model.

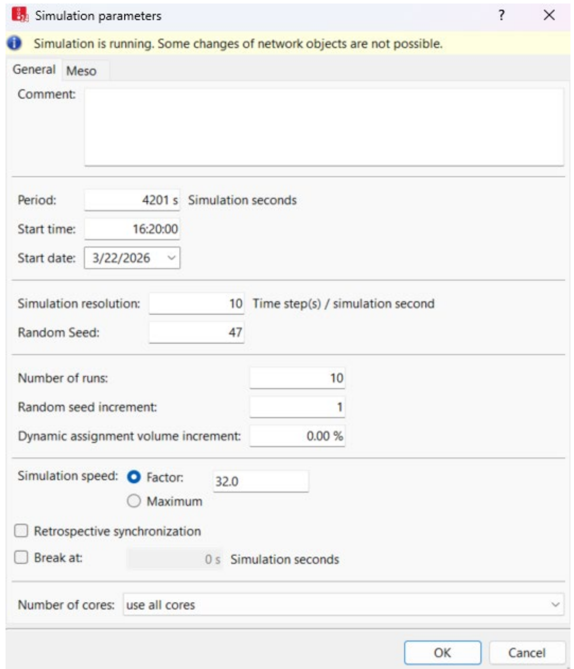


**Figure 25: Parameters**

## 3.3 Model Calibration

Calibration is a critical step in microsimulation modeling to ensure that simulated outputs closely match observed real-world conditions. In this study, calibration was performed using three MOEs: traffic volume, average approach speed, and crash frequency.

To account for the stochastic nature of the simulation, each scenario was run 10 times using different random seed values, and the average results were used for evaluation. The calibration was conducted sequentially, starting with traffic volume, followed by speed, and finally safety measures, to achieve reliable model performance.

### 3.3.1 Traffic Volume Calibration

To evaluate the accuracy of simulated traffic volumes, the following statistical metrics were used:

*Geoffrey E. Havers (GEH) Statistic:*

In microscopic traffic simulation, the GEH statistic is commonly used to assess how well simulated and observed traffic volumes match. The GEH equation is given by:

$$\mathrm{GEH} = \sqrt{\frac{2(\mathrm{S_i}-\mathrm{O_i})^2}{\mathrm{S_i}+\mathrm{O_i}}} \qquad (2)$$

where, $S_i$= simulated traffic volume (vph) obtained from VISSIM for turning movement i.

$O_i$= observed traffic volume (vph) for movement i.

GEH = Geoffrey E. Havers statistic for traffic volume validation.

The criteria for interpreting GEH values are summarized in Table 3.

**Table 3: GEH Performance Evaluation Criteria**

| GEH Value Range | Interpretation |
|---|---|
| GEH < 5 | Good match |
| 5 ≤ GEH ≤ 10 | Acceptable match |
| GEH > 10 | Poor match |

*Mean Absolute Percentage Error (MAPE):*

MAPE expresses the average magnitude of the error between observed and simulated traffic volumes. It provides a normalized measure of prediction accuracy that is easy to interpret. A value below 10% is considered excellent for traffic simulation studies.

$$MAPE = \frac{1}{n}\sum_{i=1}^{n}\left|\frac{O_i - S_i}{O_i}\right| \times 100 \qquad (3)$$

Where, $n =$ Total number of observations used in calculation

The interpretation of MAPE values is summarized in Table 4.

**Table 4: MAPE Performance Evaluation Criteria**

| MAPE (%) Range | Interpretation |
|---|---|
| MAPE < 10% | Very good match |
| 10% ≤ MAPE ≤ 20% | Acceptable match |
| 20% < MAPE ≤ 30% | Needs calibration tuning |
| MAPE > 30% | Model accuracy needs improvement |

*Root Mean Square Error (RMSE):*

RMSE is used to quantify the difference between observed and simulated traffic volumes by measuring the square root of the average squared deviations. It gives more weight to large errors, making it sensitive to outliers.

$$\mathrm{RMSE} = \sqrt{\frac{1}{n}\sum_{i=1}^{n}(O_i - S_i)^2} \qquad (4)$$

### 3.3.2 Traffic Speed Calibration

Speed accuracy was evaluated using average speeds collected from field detectors and the corresponding simulated values obtained from VISSIM data collection points. The comparison between observed and simulated speeds was performed using absolute error and percent error, defined as:

$$\text{Absolute Error} = |S_i - O_i| \quad (5)$$

$$\text{Percent Error} = \left|\frac{S_i - O_i}{O_i}\right| * 100 \quad (6)$$

An error value below 10% was considered acceptable for model calibration. Absolute and percent error metrics were selected due to their simplicity and ease of interpretation, providing direct comparison between observed and simulated values. These measures are also consistent with the approach used in traffic volume calibration.

### 3.3.3 Crash Frequency Calibration

A key component of the calibration process is ensuring that the simulated crash frequency is consistent with observed field crash data. This was achieved through a structured surrogate safety analysis approach.

*Surrogate Safety Measures:*

Surrogate safety measures are indirect indicators used to evaluate traffic safety based on vehicle interactions rather than observed crash data. These measures quantify the severity of potential conflicts and provide a proactive approach to safety assessment in microsimulation environments (Gettman and Head 2003).

Time-to-collision (TTC) is defined as the time remaining before two vehicles would collide if they continued at their current speeds and trajectories (Hayward 1972). Lower TTC values indicate higher collision risk and more severe traffic conflicts.

Maximum deceleration (MaxD) represents the highest rate of deceleration applied by a vehicle to avoid a potential collision (Archer 2005). Higher MaxD values indicate more abrupt braking and reflect more critical conflict situations.

Post-encroachment time (PET) is the time difference between when one vehicle leaves a conflict point and another vehicle arrives at the same point (Allen et al. 1978). Smaller PET values indicate a higher likelihood of conflict and reduced safety margins.

In this study, TTC and MaxD were selected as the primary surrogate safety measures for evaluating conflict severity.

*Conflict Detection Using SSAM:*

The SSAM, developed by the FHWA, was used in this study to conduct surrogate safety analysis based on vehicle trajectory data generated from microsimulation modeling in PTV VISSIM. This approach supports the assessment of safety conditions by identifying and analyzing vehicle interactions that represent potential collision risks, even in the absence of observed crashes.

Vehicle trajectory data generated from VISSIM, including time, position, speed, and acceleration for each vehicle, were exported after the simulation run and processed in SSAM using a *.trf* file as the input. The methodology used for SSAM analysis was based on the approach presented in the study by Ahmed (Ahmed et al. 2025). The SSAM analysis steps are shown in Figure 26.

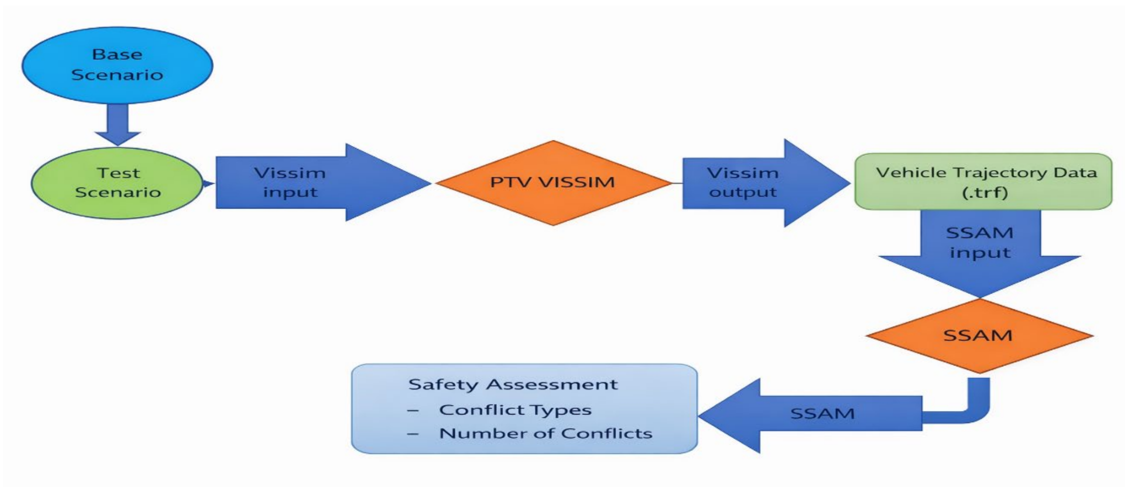


**Figure 26: Flow chart of SSAM analysis steps**

SSAM detects all potential traffic conflicts and provides detailed information on surrogate safety measures such as TTC, MaxD, and PET. To focus on critical interactions relevant for crash estimation, the detected conflicts were filtered using TTC and MaxD thresholds to identify severe conflicts.

The hourly number of severe conflicts generated from the simulation was converted into an annual estimate using a conversion equation. The peak hour percentages used in this calculation were derived from observed traffic data, and the detailed computations are provided in Appendix F. The conversion equation is expressed as follows:

$$\text{Conflicts}_{\text{year}} = \left(\frac{C_{\text{hour}}}{P_{\text{wd}}}\right) * D_{\text{wd}} + \left(\frac{C_{\text{hour}}}{P_{\text{nw}}}\right) * D_{\text{nw}} \qquad (7)$$

where,

$C_{\text{hour}}$= total number of conflicts per peak hour
$P_{\text{wd}}$= percentage of daily traffic occurring during the peak hour on workdays
$P_{\text{nw}}$= percentage of daily traffic occurring during the peak hour on non-workdays
$D_{\text{wd}}$= number of workdays in a year
$D_{\text{nw}}$= number of non-workdays in a year

In this study, a typical year was assumed to consist of 250 workdays and 115 non-workdays.

*Crash Estimation using EVT:*

Crash estimation in this study was performed using EVT, a statistical approach that focuses on modeling the behavior of the extreme tail of a distribution (Ali et al. 2023a). One commonly used method within EVT is the peaks over threshold (POT) approach. This method models only those values that exceed a predefined threshold, thereby capturing extreme events (Zheng et al. 2014).

The selection of TTC and MaxD thresholds used in the bivariate EVT model was guided by prior studies and empirical findings from surrogate safety literature (Gettman and Head 2003; Archer 2005; Hayward 1972). Previous research has commonly adopted threshold values of TTC ≤ 1.2–1.5 seconds and MaxD ≥ 6–8 m/s² to identify critical vehicle interactions with a higher likelihood of crash occurrence, particularly in signalized intersections and complex traffic environments (Archer 2005; Minderhoud and Bovy 2001; Tarko 2018).

To determine appropriate thresholds for this study, a sensitivity analysis was conducted to evaluate the influence of different TTC and MaxD combinations on conflict filtering and subsequent crash estimation. Based on this analysis, threshold values of TTC ≤ 1.2 s and MaxD ≥ 8 m/s² were selected for the DDI, and TTC ≤ 1.4 s and MaxD ≥ 7 m/s² for the CFI.

Let $Z$ represent a variable such as inverse TTC and let $u$ denote the selected threshold. The exceedances above this threshold are assumed to follow a generalized Pareto distribution (GPD) (Zheng et al. 2014), which is defined as:

$$P(Z > z \mid Z > u) = 1 - \left(1 + \frac{\xi(z-u)}{\sigma}\right)^{\left\{-\frac{1}{\xi}\right\}} \tag{8}$$

where
$\xi$=shape parameter
$\sigma$= scale parameter
$u$= threshold value
$z$= exceedance above the threshold

In the bivariate case, two conflict severity measures are modeled simultaneously, such as TTC and relative speed, or TTC and MaxD. This joint modeling approach captures the combined probability of both variables reaching extreme levels, which provides a more realistic representation of crash risk compared with univariate analysis (Ali et al. 2023b).

The joint behavior of threshold exceedances is represented using either a copula function or a joint GPD. For exceedances defined as $X > u_1$ and $Y > u_2$, the joint survival function is expressed as:

$$P\,(X > x,\ Y > y \mid X > u_1,\ Y > u_2) = G\,(x, y) \tag{9}$$

This function is typically estimated using parametric or semi-parametric methods, enabling the calculation of the annual probability of crashes based on the joint severity of traffic conflicts.

Finally, the estimated annual number of crashes is obtained using the following relationship:

$$Crashes_{\{year\}} = Conflicts_{\{year\}} \times P_{\{crash|conflict\}} \qquad (10)$$

Where,
$P_{\{crash|conflict\}}$ represents the probability that a traffic conflict results in a crash, as estimated from the bivariate EVT model.

*Thresholds:*

The calibration of the simulation model was guided by established performance measures and threshold targets recommended in the FHWA *Traffic Analysis Toolbox Volume III* (Dowling et al. 2004). These criteria were used to ensure that the simulated traffic conditions closely matched observed field conditions in terms of traffic volume, speed, operational behavior, and safety performance. The calibration targets adopted in this study are summarized in Table 5.

**Table 5: Calibration Parameters and Goals**

| Calibration Parameters | Calibration Target/Goal |
|---|---|
| Traffic Volume | Simulated and measured link volume for more than 85% of the links to be:<br>Within 100 vph for volumes less than 700 vph<br>Within 15% for volumes between 700 and 2,700 vph<br>Within 400 vph for volumes greater than 2,700 vph<br>Simulated and measured link volumes for more than 85% of links to have GEH ≤ 5 |
| Speed | Modeled average links speed to be within ± 10 mph of field speed on at least 85% of links. |
| Visualization Check | Check field consistency: queuing, weaving, signal patterns, lane usage, bottleneck, etc. |
| Crashes/Safety | Simulated conflicts converted to crash frequencies should be within ±25% of observed field crash frequency. |

*Calibration Framework and Parameter Tuning:*

The calibration process in this study followed a sequential approach rather than a multi-objective optimization framework. Specifically, the model was first calibrated for traffic volumes using the GEH statistic, RMSE, and MAPE to ensure alignment with observed turning movement counts.

Once acceptable volume targets were achieved, the average approach speeds were calibrated by adjusting the desired speed distribution curves in VISSIM. These adjustments involved modifying the mean and standard deviation of the assumed Gaussian distribution for desired speeds across different roadway segments. No other driver behavior parameters (e.g., car-following or lane-changing aggressiveness) were modified. This approach was intentionally adopted to avoid overfitting and to ensure model generalizability, particularly given the limited availability of detailed field data for these parameters.

After calibrating traffic operations, the model was further refined to match surrogate safety performance. Conflict data obtained from SSAM were processed and converted into annual crash estimates using a bivariate POT EVT approach. The bivariate EVT model jointly analyzed TTC and MaxD to estimate the likelihood of high-severity crashes.

Each calibration step was performed iteratively, using average outputs from multiple simulation runs, until the model achieved close agreement with field observations across all performance metrics. All calibration performance measures were computed based on aggregated values over the entire 3,600-second simulation period rather than at individual time steps. This approach ensured consistency in model calibration and supported the use of field-representative summary statistics.

## 3.4 Model Validation

The validation process evaluated the predictive capability and generalizability of the calibrated DDI and CFI microsimulation models. Independent traffic data from 2019 were used to assess whether the models, calibrated using 2016 data, could accurately reproduce real-world traffic conditions and safety outcomes without additional model adjustments.

For validation, only the input approach volumes were updated to reflect the observed 2019 conditions, specifically for the peak hour period from 4:30 PM to 5:30 PM on January 15, 2019. All other model parameters, including driver behavior characteristics, traffic composition, and speed distributions, were kept unchanged from the calibration phase to ensure an unbiased evaluation of model performance.

The validation results were assessed by comparing simulated and observed turning movement volumes, approach speeds, and estimated crash frequencies. The same performance metrics used during calibration were applied to maintain consistency in evaluation. Additionally, the conflict-to-crash conversion relationships developed during calibration were used without modification.

This approach ensured that the validation rigorously tested the model's ability to generalize to new traffic conditions based solely on changes in traffic demand without further calibration or tuning.

### 3.4.1 Calibration Results

***Traffic Volume***

The calibration of traffic volumes was evaluated by comparing simulated and observed turning movements at the study intersections for both the DDI and the CFI. Multiple statistical performance measures, including the coefficient of determination ($R^2$), GEH statistic, root mean square error (RMSE), and MAPE, were used to assess the accuracy of the simulation model.

For the DDI model, a strong linear relationship was observed between simulated and field-measured traffic volumes, as shown in Figure 27. The regression analysis yielded an $R^2$ value of 0.9926, indicating an excellent level of agreement. Similarly, the CFI model demonstrated a high degree of correlation with an $R^2$ value of 0.9967, as illustrated in Figure 28. These results confirm that the simulation models accurately replicate observed traffic demand patterns across all turning movements.

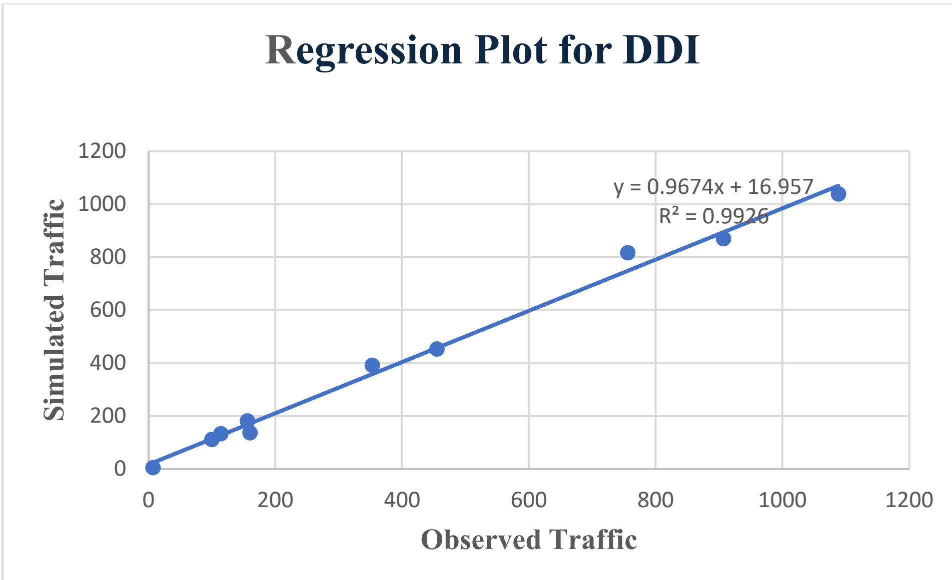


**Figure 27: Regression plot for DDI**

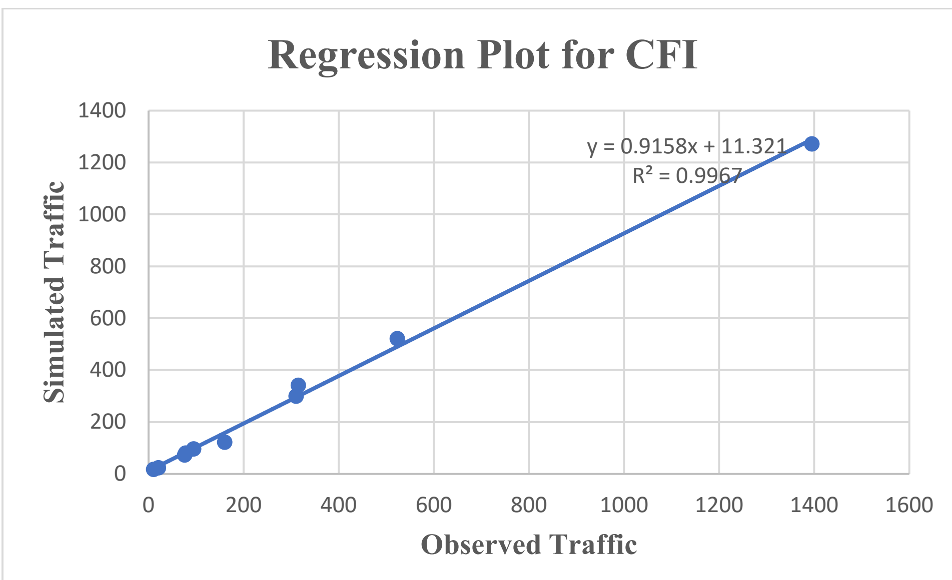


**Figure 28: Regression plot for CFI**

The GEH statistics were used as the primary calibration criterion to evaluate the consistency between simulated and observed volumes. As presented in Table 6 for the DDI and Table 7 for the CFI, all movements exhibited GEH values less than 5, satisfying the recommended calibration threshold. For the DDI, GEH values ranged approximately between 0.09 and 2.14, while for the CFI, values ranged between 0.08 and 3.36, indicating a strong match across all approaches and movements.

**Table 6: Traffic Volume Calibration Result for DDI**

| Movement | Simulated Volume (Veh/h) | Observed Volume (veh/h) | GEH |
|---|---|---|---|
| EB Left | 111 | 100 | 1.11 |
| EB Right | 132 | 114 | 1.62 |
| WB Left | 869 | 907 | 1.27 |
| WB Right | 181 | 156 | 1.92 |
| NB Left | 136 | 160 | 1.97 |
| NB Right | 816 | 756 | 2.14 |
| NB Through | 391 | 353 | 1.97 |
| SB Left | 453 | 455 | 0.09 |
| SB Right | 5 | 7 | 0.81 |
| SB Through | 1,038 | 1,088 | 1.53 |

**Table 7: Traffic Volume Calibration Result for CFI**

| Movement | Simulated Volume (Veh/h) | Observed Volume (veh/h) | GEH |
|---|---|---|---|
| EB Left | 96 | 95 | 0.10 |
| EB Right | 73 | 76 | 0.34 |
| EB Through | 341 | 315 | 1.43 |
| WB Left | 122 | 160 | 3.2 |
| WB Right | 18 | 11 | 1.83 |
| WB Through | 300 | 310 | 0.57 |
| NB Left | 80 | 78 | 0.22 |
| NB Through | 521 | 523 | 0.08 |
| SB Left | 23 | 21 | 0.42 |
| SB Through | 1,272 | 1,395 | 3.36 |

In addition to GEH, error-based performance metrics were computed to further quantify model accuracy. The DDI model produced an RMSE of 32.62 and a MAPE of 11.43%, reflecting a reasonable level of deviation given the variability in field traffic conditions. The CFI model exhibited improved performance, with an RMSE of 41.73 and a MAPE of 12.51%, indicating a closer fit between simulated and observed values.

Overall, both models successfully met the calibration criteria, with more than 85% of movements falling within acceptable error thresholds. The strong agreement observed across regression analysis, GEH statistics, and error metrics demonstrate that the calibrated models reliably reproduce real-world traffic volumes. These results provide a solid foundation for subsequent analyses, including speed calibration and safety evaluation using surrogate measures.

### *Average Speed*

Average speeds from the simulation were compared with field observations for selected approaches at both intersections. For the DDI, the simulated speed (28.29 mph) closely matched the observed speed (28.00 mph), with a percentage error of 1.04%. Similarly, for the CFI, the simulated speed (32.60 mph) showed strong agreement with the observed speed (32.31 mph), with a percentage error of 0.90%.

As summarized in Table 8, the percentage errors for both cases are well within the acceptable ±10% calibration threshold, indicating a good match between simulated and observed speeds.

**Table 8: Speed Calibration Results for DDI and CFI**

| Intersection | Approach | Observed Speed (mph) | Simulated Speed (mph) | Absolute Error (mph) | Percent Error (%) |
|---|---|---|---|---|---|
| DDI | NB | 28.00 | 28.29 | 0.29 | 1.04 |
| CFI | SB | 32.31 | 32.60 | 0.29 | 0.90 |

### *Crash Frequency*

Crash frequency calibration was evaluated using conflict data processed through the bivariate POT-EVT approach. The relationship between TTC and MaxD and the applied thresholds are illustrated in Figure 29 (DDI) and Figure 30 (CFI).

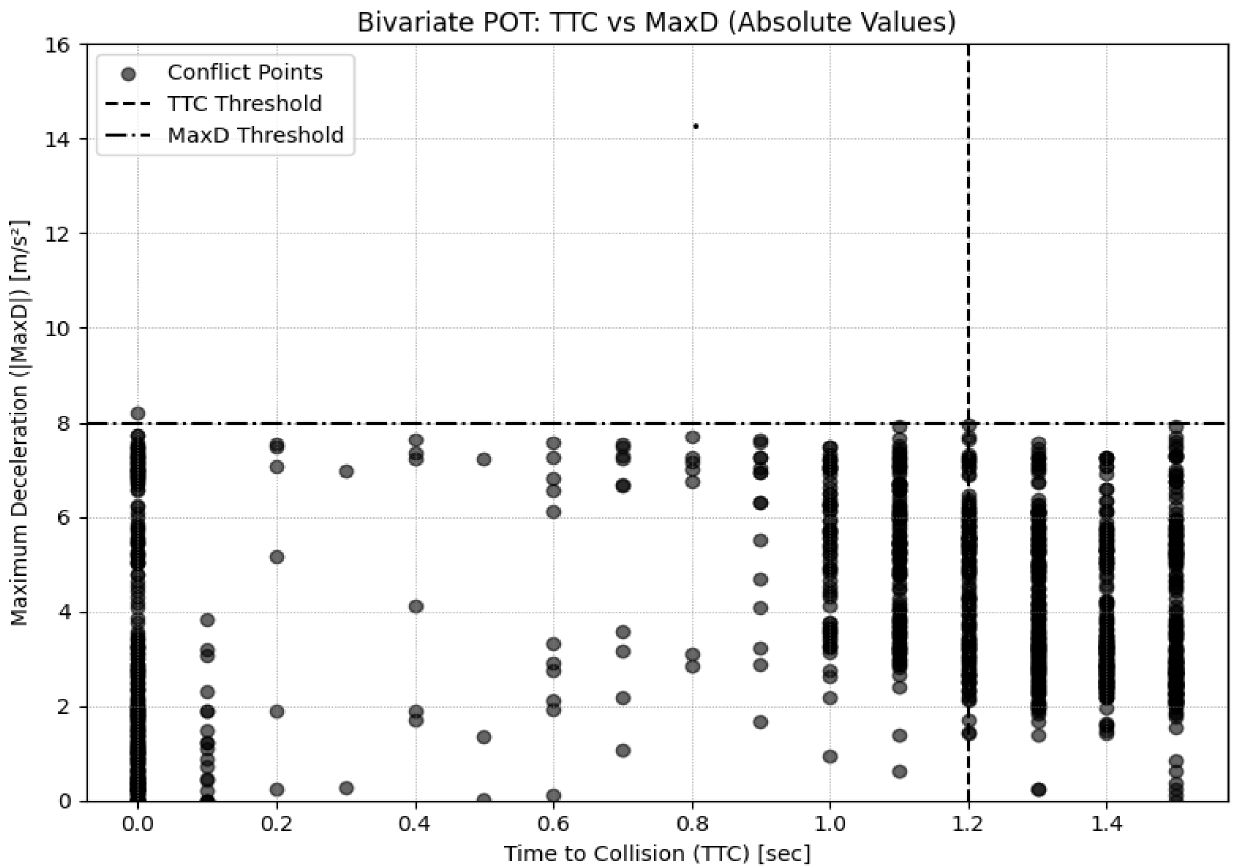


**Figure 29: Bivariate POT analysis of DDI conflicts (TTC ≤ 1.2 s, MaxD ≥ 8 m/s²)**

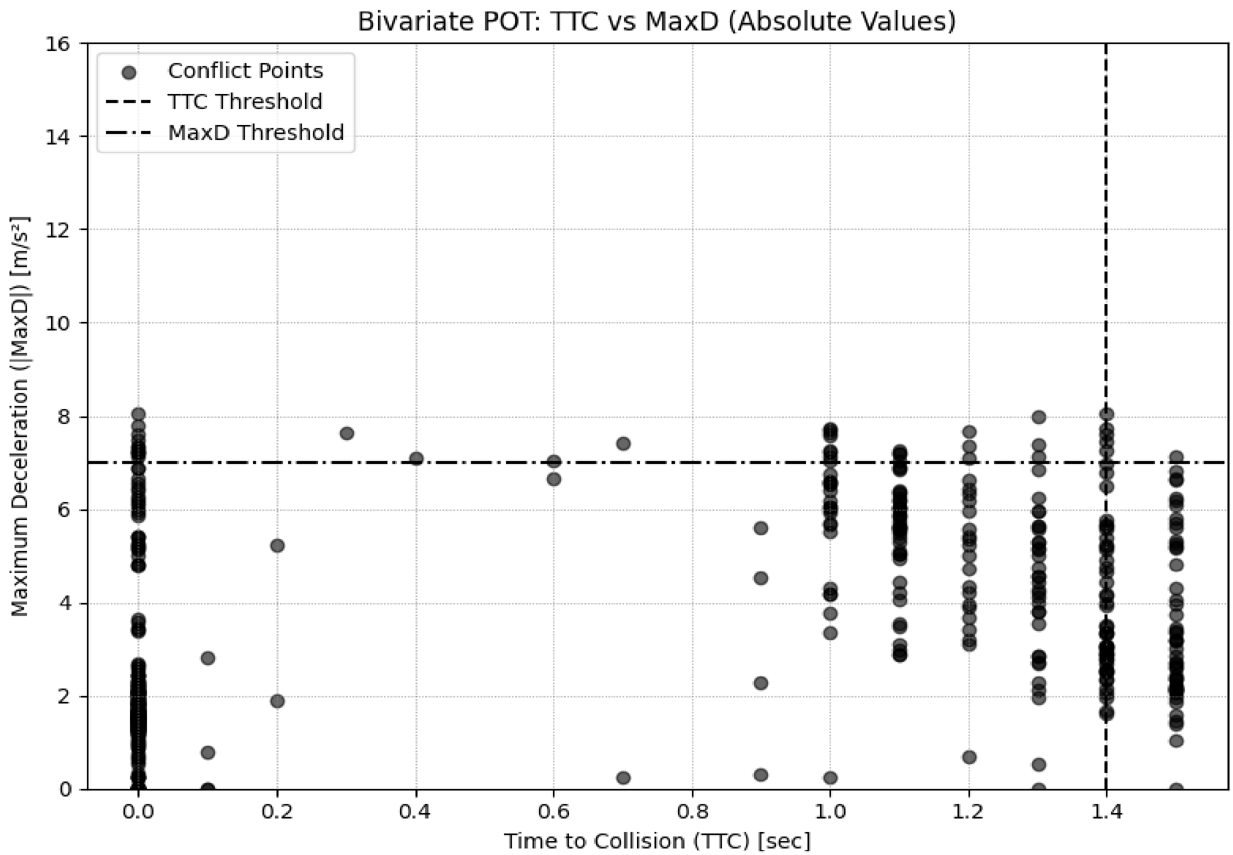


**Figure 30: Bivariate POT analysis of CFI conflicts (TTC≤1.4 s, MaxD≥7 m/s²)**

For the DDI, using thresholds of TTC ≤ 1.2 s and MaxD ≥ 8 m/s², the model estimated 22.31 crashes/year, compared with the observed 25 crashes/year. For the CFI, with thresholds of TTC ≤ 1.4 s and MaxD ≥ 7 m/s², the estimated crash frequency was 17.93 crashes/year, closely matching the observed value of 18 crashes/year.

As summarized in Table 9 and Table 10, the differences between simulated and observed crash frequencies are small for both intersections, indicating good agreement. The results confirm that the calibrated models are capable of capturing high-risk traffic interactions and producing realistic crash estimates.

**Table 9: Crash Frequency Calibration for DDI**

| Conflict Type | Conflicts per Hour | Conflicts per Year | Crashes per Year (Simulated) | Crashes per Year (Observed) |
|---|---|---|---|---|
| Crossing | 110 | 604,348.4 | 2.13 | 5 |
| Rear-End | 1,052 | 5,014,117 | 17.65 | 19 |
| Lane Change | 131 | 719,724 | 2.53 | 1 |
| Total | | | 22.31 | 25 |

Table 10: Crash Frequency Calibration for CFI

| Conflict Type | Conflicts per Hour | Conflicts per Year | Crashes per Year (Simulated) | Crashes per Year (Observed) |
|---|---|---|---|---|
| Crossing | 9 | 48,904.6 | 0.31 | 3 |
| Rear-End | 450 | 2,445,229.6 | 15.68 | 14 |
| Lane Change | 56 | 304,295.2 | 1.94 | 1 |
| Total | | | 17.93 | 18 |

### 3.4.2 Validation Results

***Traffic Volume***

The validation of traffic volumes was carried out by comparing simulated turning movement counts with observed field data for the 2019 dataset at both the DDI and the CFI. The same statistical measures used during calibration, including the coefficient of determination ($R^2$) and GEH statistics, were applied to evaluate model performance under independent traffic conditions.

For the DDI model, a strong linear relationship was observed between simulated and observed traffic volumes, as shown in Figure 31. The regression analysis produced an $R^2$ value of 0.9854, indicating that the model maintained a high level of accuracy under validation conditions. Similarly, the CFI model demonstrated excellent agreement, with an $R^2$ value of 0.992, as illustrated in Figure 32. These results indicate that the calibrated models are capable of generalizing well to new traffic datasets without further parameter adjustment.

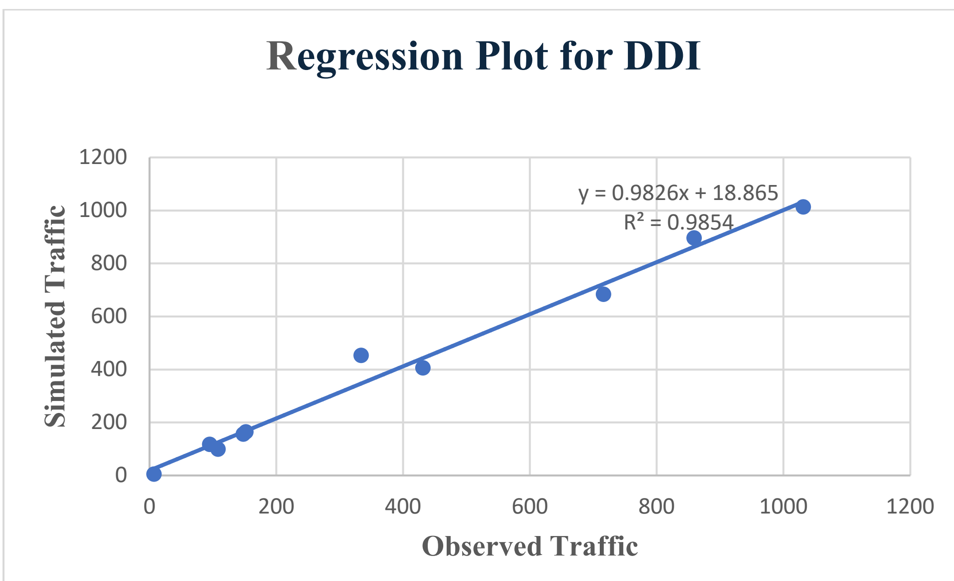


Figure 31: Regression plot for DDI

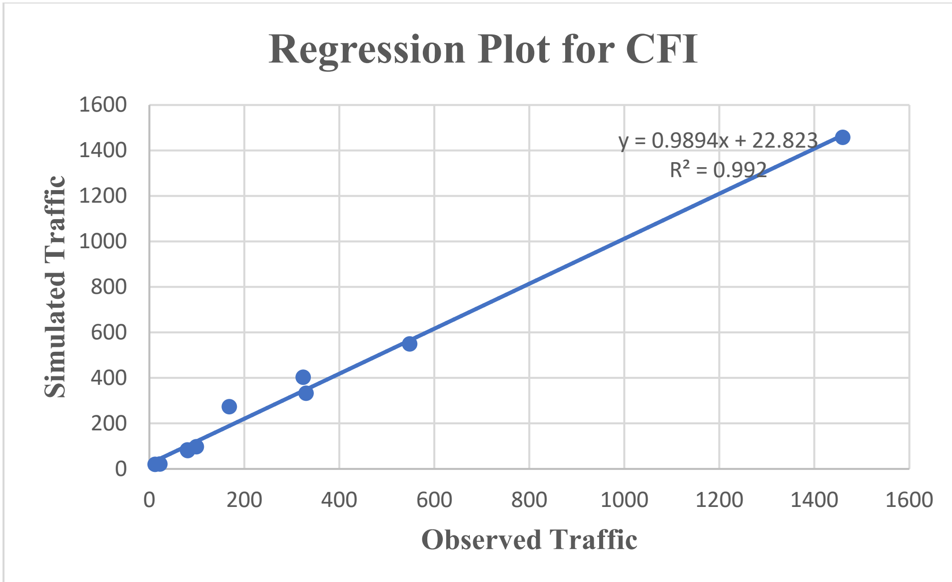


**Figure 32: Regression plot for CFI**

The GEH statistics were used to evaluate the agreement between simulated and observed traffic volumes during validation. As shown in Table 11 for the DDI and Table 12 for the CFI, 9 out of 10 movements satisfied the GEH < 5 criterion for both intersections, indicating satisfactory model performance. For the DDI, GEH values ranged from 0.39 to 6.04, while for the CFI, values ranged from 0.11 to 7.13, demonstrating consistent agreement across all approaches.

**Table 11: Traffic Volume Validation Result for DDI**

| Movement | Simulated Volume (Veh/h) | Observed Volume (veh/h) | GEH |
|---|---|---|---|
| EB Left | 118 | 95 | 2.22 |
| EB Right | 100 | 108 | 0.78 |
| WB Left | 897 | 859 | 1.28 |
| WB Right | 157 | 148 | 0.72 |
| NB Left | 165 | 152 | 1.03 |
| NB Right | 684 | 716 | 1.20 |
| NB Through | 454 | 334 | 6.04 |
| SB Left | 407 | 431 | 1.17 |
| SB Right | 6 | 7 | 0.39 |
| SB Through | 1,014 | 1,031 | 0.53 |

**Table 12: Traffic Volume Validation Result for CFI**

| Movement | Simulated Volume (Veh/h) | Observed Volume (veh/h) | GEH |
|---|---|---|---|
| EB Left | 97 | 99 | 0.20 |
| EB Right | 83 | 80 | 0.33 |
| EB Through | 333 | 330 | 0.16 |
| WB Left | 274 | 168 | 7.13 |
| WB Right | 20 | 12 | 2 |
| WB Through | 403 | 324 | 4.14 |
| NB Left | 80 | 81 | 0.11 |
| NB Through | 550 | 548 | 0.08 |
| SB Left | 21 | 22 | 0.21 |
| SB Through | 1,458 | 1,460 | 0.05 |

In addition to the GEH statistics, error-based performance measures were used to further assess model accuracy during validation. For the DDI model, an RMSE of 43.10 and a MAPE of 11.25% were obtained, indicating a reasonable level of agreement with observed traffic volumes. For the CFI model, the RMSE was 41.92 and the MAPE was 16.71%, reflecting a satisfactory correspondence between simulated and field data.

Overall, the validation results indicate that both models maintained acceptable performance when applied to independent traffic data, with most movements meeting the established evaluation criteria. Despite minor deviations observed in a limited number of movements, the consistency in regression results, GEH statistics, and error-based measures demonstrate that the calibrated models are capable of reliably reproducing traffic volumes under different conditions. These findings confirm the robustness and transferability of the models, supporting their use for further analysis, including speed validation and safety evaluation based on surrogate measures.

***Average Speed***

Average speeds from the simulation were compared with field observations for selected approaches at both intersections under validation conditions. For the DDI, the simulated speed of 28.55 mph showed close agreement with the observed speed of 28.00 mph, resulting in a percentage error of 1.96%. Similarly, for the CFI, the simulated speed of 32.44 mph closely matched the observed speed of 32.31 mph, with a percentage error of 0.40%.

As summarized in Table 13, the percentage errors for both intersections remain well within the acceptable ±10% threshold, confirming that the model maintains good accuracy when applied to independent validation data.

**Table 13: Speed Validation Results for DDI and CFI**

| Intersection | Approach | Observed Speed (mph) | Simulated Speed (mph) | Absolute Error (mph) | Percent Error (%) |
|---|---|---|---|---|---|
| DDI | NB | 28.00 | 28.55 | 0.55 | 1.96 |
| CFI | SB | 32.31 | 32.44 | 0.13 | 0.40 |

### *Crash Frequency*

Crash frequency validation was conducted using conflict data obtained from SSAM and analyzed through the bivariate POT-EVT framework. The distribution of conflicts with respect to TTC and MaxD, along with the applied thresholds, are presented in Figure 33 (DDI) and Figure 34 (CFI).

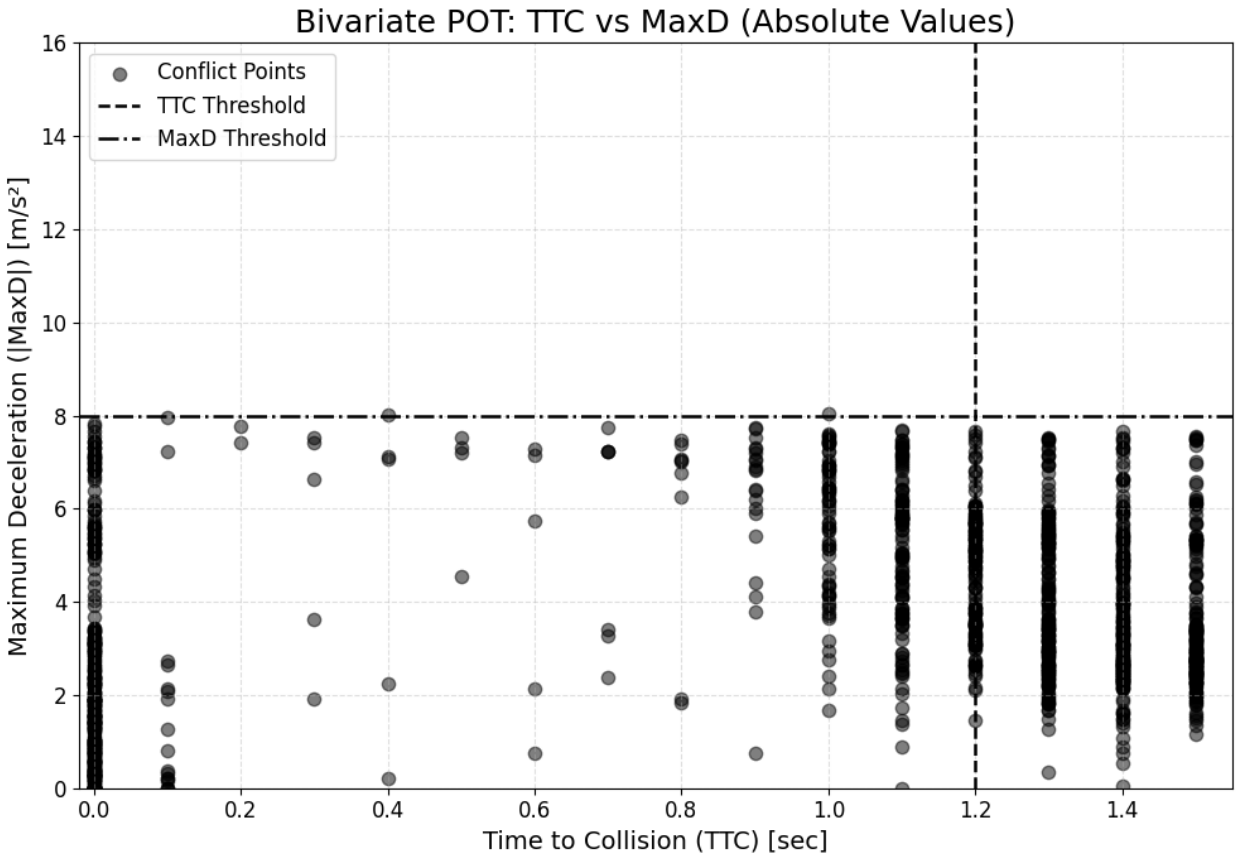


**Figure 33:Bivariate POT analysis of DDI conflicts (TTC ≤ 1.2 s, MaxD ≥ 8 m/s²)**

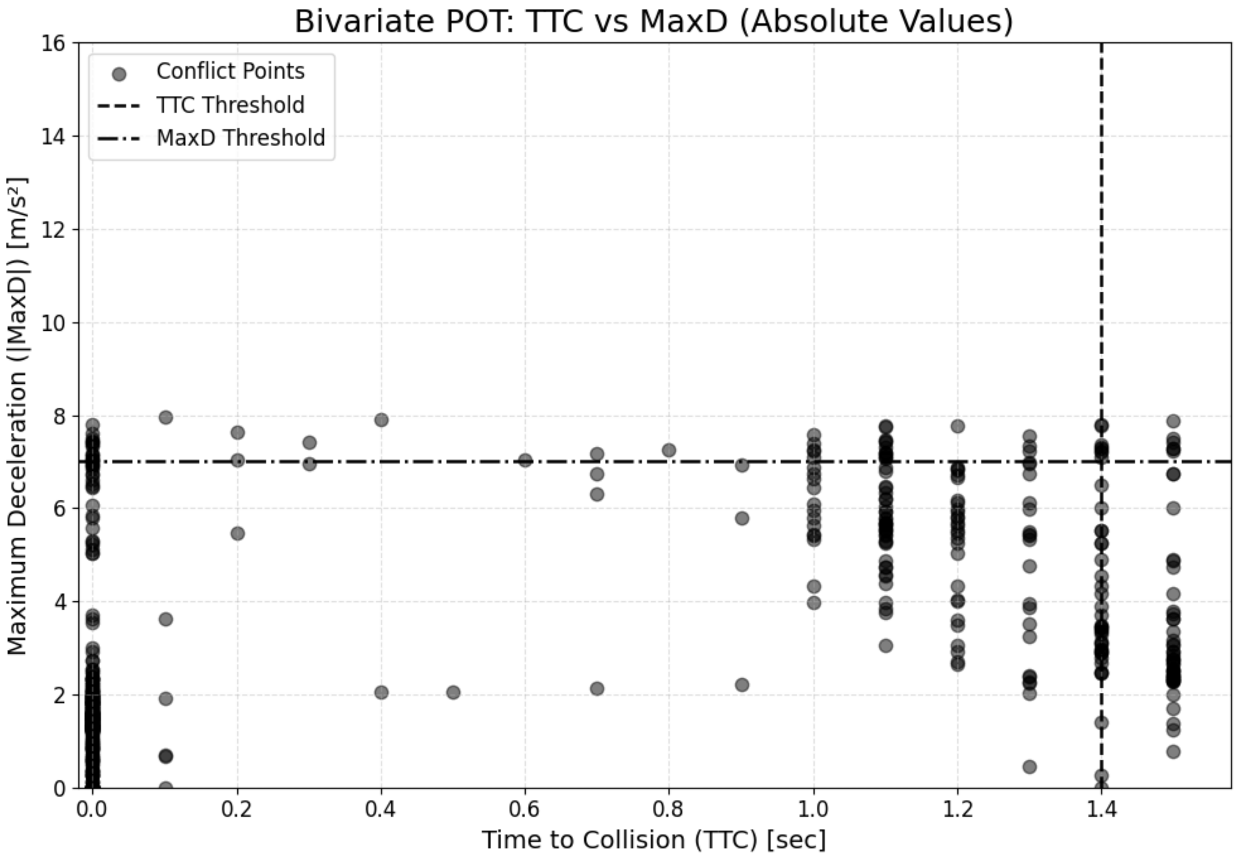


**Figure 34: Bivariate POT analysis of CFI conflicts (TTC≤1.4 s, MaxD≥7 m/s²)**

For the DDI, using thresholds of TTC ≤ 1.2 s and MaxD ≥ 8 m/s², the model estimated an annual crash frequency of 21.90 crashes/year, compared to the observed 8 crashes/year. For the CFI, with thresholds of TTC ≤ 1.4 s and MaxD ≥ 7 m/s², the estimated crash frequency was 19.64 crashes/year, compared with the observed 20 crashes/year.

As summarized in Table 14 and Table 15, the CFI model shows very close agreement between simulated and observed crash frequencies, while the DDI model exhibits a higher deviation, particularly in rear-end conflicts. Despite this difference, the overall trend of conflict-based crash estimation remains consistent, indicating that the models are capable of capturing the relative severity and distribution of traffic conflicts under validation conditions.

**Table 14: Crash Frequency Validation for DDI**

| Conflict Type | Conflicts per Hour | Conflicts per Year | Crashes per Year (Simulated) | Crashes per Year (Observed) |
|---|---|---|---|---|
| Crossing | 116 | 637,312.8 | 2.24 | 2 |
| Rear-End | 1,034 | 492,834 | 17.34 | 5 |
| Lane Change | 120 | 659,289.1 | 2.32 | 1 |
| Total | | | 21.9 | 8 |

**Table 15: Crash Frequency Validation for CFI**

| Conflict Type | Conflicts per Hour | Conflicts per Year | Crashes per Year (Simulated) | Crashes per Year (Observed) |
|---|---|---|---|---|
| Crossing | 26 | 141,279.93 | 0.91 | 7 |
| Rear-End | 483 | 2,624,546.40 | 16.82 | 9 |
| Lane Change | 55 | 298,861.39 | 1.92 | 4 |
| Total | | | 19.64 | 20 |

## 3.5 Conclusion and Discussion

This study developed and evaluated microscopic simulation models to assess the operational and safety performance of two innovative intersection designs: the DDI and the CFI. The models were built using VISSIM and evaluated using traffic volume, speed, and safety-related measures. The study introduced a combined framework integrating surrogate safety analysis with EVT to estimate crash frequency from simulated traffic conflicts. The models were calibrated and validated using real-world data to ensure their reliability and applicability. Overall, the study demonstrates that simulation-based approaches, when integrated with advanced safety analysis techniques, can effectively evaluate both operational and safety performance of complex intersection designs.

### 3.5.1 Key Findings

The study demonstrates that the developed simulation models are capable of reliably representing traffic operations under both calibration and validation conditions. The consistency observed across different datasets indicates that the models are not only well-fitted but also generalizable to varying traffic scenarios. In terms of safety assessment, the integration of surrogate safety measures with the EVT framework proved effective in capturing crash-related risk from simulated traffic interactions. The approach provides a practical alternative for safety evaluation, particularly in situations where sufficient crash data may not be available. A key observation from the study is the difference in predictive performance between the two intersection types. The CFI model exhibited more stable and consistent crash estimation under validation conditions, while the DDI model showed higher sensitivity to changes in traffic conditions and conflict characteristics. Overall, the findings suggest that the proposed modeling framework is suitable for evaluating both operational and safety performance of complex intersection designs, while also highlighting the importance of considering intersection-specific characteristics in safety analyses.

### 3.5.2 Discussion of Results

The results of this study provide important insights into the performance of simulation-based safety evaluation for complex intersection designs. While the models demonstrated strong agreement with field data during calibration, the validation results highlight differences in how each intersection type responds to changing traffic conditions.

One key observation is the variation in crash prediction accuracy between the DDI and CFI models. The CFI maintained consistent performance during validation, suggesting that its traffic flow patterns and conflict characteristics are more stable and predictable. In contrast, the DDI exhibited greater deviation in estimated crash frequency. This can be attributed to the more complex vehicle interactions within the DDI, including weaving maneuvers and unconventional movement paths, which introduce higher variability in conflict generation and severity.

Another important factor influencing the results is the sensitivity of the EVT-based approach to threshold selection and conflict characteristics. Small changes in TTC and MaxD distributions can significantly affect the number of severe conflicts identified, particularly in intersections where traffic interactions are more dynamic. This explains why the DDI model, which involves more complex conflict patterns, showed higher variability in crash estimation under validation conditions.

Additionally, differences between simulated and real-world driving behavior may contribute to the observed deviations. Although the simulation models were calibrated to match field conditions, driver behavior in real traffic can vary due to factors such as reaction time, aggressiveness, and compliance with traffic control, which are difficult to fully capture in simulation environments.

Despite these differences, the overall framework demonstrated strong capability in identifying relative safety performance and capturing high-risk interactions. The integration of microsimulation, surrogate safety analysis, and EVT provides a robust approach for evaluating safety in complex intersections, particularly in scenarios where historical crash data are limited or unreliable.

### 3.5.3 Implications

The findings of this study have important implications for both traffic engineering practice and safety analysis of complex intersection designs. The results demonstrate that microsimulation models, when properly calibrated and validated, can serve as reliable tools for evaluating traffic operations and safety performance under varying conditions. The integration of surrogate safety measures with EVT provides a practical approach for estimating crash risks without relying solely on historical crash data. This is particularly valuable for newly implemented or proposed intersection designs, where sufficient crash records may not yet be available.

From a design and planning perspective, the results highlight that different intersection types may exhibit varying levels of predictability in safety performance. The more consistent results observed for the CFI suggest that certain innovative designs may offer more stable traffic behavior, while the higher variability observed in the DDI indicates the need for careful evaluation of complex traffic interactions during design and analysis. Overall, this study supports the use of simulation-based safety assessment as a decision-making tool for engineers and planners, enabling more informed evaluation of alternative intersection designs and their potential safety impacts.

### 3.5.4 Limitations, Recommendations, and Future Work

While the study provides valuable insights into the operational and safety performance of innovative intersection designs, several limitations should be acknowledged. These limitations are primarily related to data availability, modeling assumptions, and the inherent constraints of simulation-based analysis.

1. The analysis is based on a limited number of study sites, which may restrict the generalizability of the findings to other intersection configurations or traffic conditions.
2. The accuracy of the simulation results depends on the quality and completeness of the input data, including traffic volumes, signal timing, and field speed measurements.
3. The surrogate safety measures (TTC and MaxD) and selected threshold values may influence the identification of severe conflicts, introducing sensitivity in crash estimation results.
4. The EVT-based crash estimation approach assumes that extreme conflict events follow a specific statistical distribution, which may not fully represent all real-world traffic conditions.
5. Driver behavior in the simulation environment is modeled using predefined parameters, which may not capture the full variability of real-world driving behavior.
6. The SSAM tool relies on trajectory data from simulation, and any inaccuracies in vehicle interactions within the simulation model can affect conflict detection and classification.
7. The validation results showed variability in crash prediction for certain intersection types (e.g., DDI), indicating potential limitations in modeling complex traffic interactions.

Based on the findings and limitations of this study, several areas for future research are recommended to further enhance the reliability and applicability of simulation-based safety analysis.

1. Future studies can include a larger number of intersections with varying geometric designs and traffic conditions to improve the generalizability of the results.
2. Additional surrogate safety measures, such as PET or deceleration rate to avoid collision (DRAC), can be incorporated to provide a more comprehensive safety assessment.
3. Advanced calibration techniques, including automated or optimization-based methods, can be explored to improve the accuracy of simulation models.
4. Further research can investigate the sensitivity of EVT-based crash estimation to different threshold values and modeling assumptions.
5. Real-world trajectory data or connected vehicle data can be integrated to improve the representation of driver behavior and conflict dynamics.
6. The proposed framework can be extended to evaluate emerging transportation technologies, such as connected and autonomous vehicles, and their impact on intersection safety.

# 4. SAFETY EVALUATION OF DIVERGING DIAMOND INTERCHANGE (DDIS)

## 4.1 Data Collection

Crash data were obtained from the UDOT Traffic and Safety Division, while AADT data were sourced from UDOT's Open Data Portal (UDOT 2025). Crash and AADT data were collected for 2006 through 2021. The study includes six DDIs as treatment sites, and the years of implementation of each DDI are provided in parentheses, as shown in Table 16. The "before" period spans from 2006 to the year prior to DDI implementation, while the "after" period extends from one year after implementation through the end of the analysis in 2021. For comparison, six ramp terminal sites across Utah were selected: three conventional diamond interchanges (I-80 at 700 East, I-80 at State Street, and SR-201 at 5600 West) and three SPDIs (I-15 at 4500 South, I-15 at 3300 South, and I-15 at 600 North). Table 16 provides key geometric and configuration details of all sites, including ramp terminal spacing, interchange configuration type, and the number of lanes. These attributes support the analysis of DDI safety performance using historical crash and traffic volume data.

**Table 16:** Geometric and Configuration Details of DDI Treatment and Comparison Sites

| Group | Site Location | Ramp Terminal Spacing (ft) | Configuration Type | Lanes |
|---|---|---|---|---|
| DDI Treatment | SR-201 @ Bangerter (2011) | 830 | Overpass | 5 |
| | I-15 @ Pioneer X (2010) | 960 | Overpass | 8 |
| | I-15 @ 500 E AF (2011) | 910 | Overpass | 4 |
| | I-15 @ UT-130 (2014) | 502 | Underpass | 4 |
| | I-15 @ 1100 S (2014) | 757 | Overpass | 4 |
| | I-215 @ Redwood Rd (2019) | 976 | Overpass | 6 |
| Comparison Group | I-80 @ 700 E | 450 | Underpass | 10 |
| | I-80 @ State | 215 | Underpass | 8 |
| | SR-201 @ 5600 W | 805 | Overpass | 5 |
| | I-15 @ 4500 S | 540 | Underpass | 8 |
| | I-15 @ 3300 S | 512 | Underpass | 8 |
| | I-15 @ 600 N | 770 | Overpass | 6 |

Because separate AADT values for entrance and exit ramps were not available, it was assumed that ramp traffic volumes were approximately 15% of the crossroad AADT values. (Zlatkovic 2015) Additionally, to assess the sensitivity of the calculated CMF value, 10% and 20% of the main crossroad AADT were also considered as the ramp traffic volume. Table 17 and Table 18 presents the AADT for each ramp terminal direction at the selected treatment (DDI) and comparison (diamond or SPDI) sites from 2006 to 2021. For each site, AADT of ramp terminals crossover are provided.

**Table 17: Annual Average Daily Traffic at Ramp Terminals (Crossovers) of Treatment Site, 2006–2021**

| Year | Treatment Sites: Cross Roads (AADT, veh/day) | | | | | | |
|---|---|---|---|---|---|---|---|
| | Crossover Roads | SR-201 Bangerter | I-15 Pioneer X | I-15 500 E AF | I-15 @ UT-130 | I-15 @ 1100 S | I-215 @ Redwood Rd |
| 2006 | Crossover 1 | 37,375 | 15,790 | 19,785 | - | 18,520 | 10,745 |
| | Crossover 2 | 37,375 | 15,790 | 19,785 | - | 18,520 | 8,990 |
| 2007 | Crossover 1 | 39,320 | 24,680 | 20,060 | 4,000 | 17,570 | 13,845 |
| | Crossover 2 | 39,320 | 24,680 | 20,060 | 4,000 | 17,570 | 9,565 |
| 2008 | Crossover 1 | 39,240 | 23,740 | 19,080 | 3,805 | 18,905 | 13,170 |
| | Crossover 2 | 39,240 | 23,740 | 19,080 | 3,805 | 18,905 | 9,095 |
| 2009 | Crossover 1 | 39,200 | 23,910 | 18,965 | 3,780 | 19,720 | 13,090 |
| | Crossover 2 | 39,200 | 23,910 | 18,965 | 3,780 | 19,720 | 8,990 |
| 2010 | Crossover 1 | 36,730 | 25,715 | 18,890 | 3,765 | 20,210 | 13,035 |
| | Crossover 2 | 36,730 | 23,810 | 18,890 | 3,765 | 20,210 | 8,230 |
| 2011 | Crossover 1 | 41,610 | 23,740 | 18,830 | 13,000 | 17,495 | 13,000 |
| | Crossover 2 | 33,830 | 25,640 | 18,830 | 13,000 | 17,495 | 8,205 |
| 2012 | Crossover 1 | 41,780 | 23,265 | 18,455 | 12,740 | 17,720 | 12,740 |
| | Crossover 2 | 33,965 | 25,125 | 18,455 | 12,740 | 17,720 | 8,040 |
| 2013 | Crossover 1 | 44,035 | 24,500 | 17,995 | 12,420 | 17,685 | 12,420 |
| | Crossover 2 | 35,800 | 32,020 | 17,995 | 12,420 | 17,685 | 11,635 |
| 2014 | Crossover 1 | 37,335 | 25,575 | 18,190 | 12,560 | 18,355 | 12,560 |
| | Crossover 2 | 45,925 | 33,430 | 18,190 | 12,560 | 18,355 | 11,760 |
| 2015 | Crossover 1 | 38,270 | 26,830 | 18,975 | 13,200 | 19,770 | 13,100 |
| | Crossover 2 | 47,075 | 35,070 | 18,975 | 13,200 | 19,770 | 12,265 |
| 2016 | Crossover 1 | 39,916 | 28,011 | 19,980 | 14,348 | 20,679 | 13,793 |
| | Crossover 2 | 49,099 | 36,612 | 19,980 | 14,348 | 20,679 | 12,917 |
| 2017 | Crossover 1 | 40,235 | 28,767 | 20,519 | 14,190 | 21,093 | 14,165 |
| | Crossover 2 | 49,492 | 37,601 | 20,519 | 14,190 | 21,093 | 13,266 |
| 2018 | Crossover 1 | 40,034 | 29,141 | 20,724 | 14,147 | 21,325 | 14,307 |
| | Crossover 2 | 49,245 | 38,090 | 20,724 | 14,147 | 21,325 | 13,399 |
| 2019 | Crossover 1 | 38,192 | 29,432 | 21,097 | 14,303 | 21,282 | 14,565 |
| | Crossover 2 | 46,980 | 38,471 | 21,097 | 14,303 | 21,282 | 13,640 |
| 2020 | Crossover 1 | 33,227 | 25,606 | 18,840 | 12,873 | 19,963 | 13,007 |
| | Crossover 2 | 40,872 | 33,470 | 18,840 | 12,873 | 19,963 | 12,181 |
| 2021 | Crossover 1 | 39,640 | 28,371 | 20,423 | 14,688 | 22,458 | 14,100 |
| | Crossover 2 | 48,760 | 37,085 | 20,423 | 14,688 | 22,458 | 13,204 |

**Table 18: Annual Average Daily Traffic at Ramp Terminals (Crossovers) of Comparison Group, 2006–2021**

| Year | Comparison Group: Crossroads (AADT, veh/day) | | | | | | |
|---|---|---|---|---|---|---|---|
| | Crossover Roads | I-80 700 E | I-80 State | SR-201 5600 W | I-15 4500 S | I-15 3300 S | I-15 600 N |
| 2006 | Crossover 1 | 41,260 | 33,420 | 20,070 | 40,380 | 45,485 | 12,855 |
| | Crossover 2 | 34,650 | 35,795 | 31,080 | 29,395 | 30,470 | 12,855 |
| 2007 | Crossover 1 | 41,920 | 33,890 | 20,350 | 40,945 | 46,120 | 13,730 |
| | Crossover 2 | 35,205 | 36,295 | 31,515 | 29,805 | 29,130 | 13,730 |
| 2008 | Crossover 1 | 40,535 | 33,040 | 19,580 | 28,675 | 23,360 | 13,055 |
| | Crossover 2 | 34,040 | 34,520 | 38,060 | 39,390 | 44,370 | 13,055 |
| 2009 | Crossover 1 | 39,645 | 32,845 | 19,715 | 28,875 | 23,125 | 12,980 |
| | Crossover 2 | 33,295 | 34,310 | 38,235 | 39,665 | 44,680 | 12,980 |
| 2010 | Crossover 1 | 38,295 | 32,710 | 19,735 | 28,905 | 24,585 | 12,925 |
| | Crossover 2 | 32,160 | 34,175 | 38,365 | 39,705 | 44,725 | 12,925 |
| 2011 | Crossover 1 | 47,270 | 32,615 | 19,165 | 28,065 | 24,805 | 12,885 |
| | Crossover 2 | 32,710 | 34,070 | 40,400 | 38,555 | 43,430 | 12,885 |
| 2012 | Crossover 1 | 45,235 | 31,960 | 17,960 | 35,150 | 24,580 | 12,630 |
| | Crossover 2 | 31,300 | 33,390 | 40,280 | 38,440 | 43,300 | 12,630 |
| 2013 | Crossover 1 | 45,100 | 33,665 | 18,425 | 36,065 | 30,280 | 12,315 |
| | Crossover 2 | 31,250 | 32,555 | 41,325 | 39,435 | 44,425 | 12,315 |
| 2014 | Crossover 1 | 47,130 | 34,035 | 19,235 | 41,170 | 46,380 | 12,450 |
| | Crossover 2 | 32,610 | 32,555 | 41,325 | 36,065 | 30,280 | 19,865 |
| 2015 | Crossover 1 | 47,835 | 35,500 | 16,095 | 43,190 | 48,650 | 12,985 |
| | Crossover 2 | 33,100 | 34,330 | 45,255 | 39,495 | 32,970 | 20,945 |
| 2016 | Crossover 1 | 50,227 | 37,380 | 16,803 | 45,089 | 50,793 | 13,671 |
| | Crossover 2 | 34,756 | 36,147 | 47,248 | 41,235 | 34,685 | 22,054 |
| 2017 | Crossover 1 | 51,382 | 32,510 | 17,257 | 46,306 | 52,164 | 14,040 |
| | Crossover 2 | 35,555 | 37,123 | 48,524 | 42,348 | 35,621 | 22,649 |
| 2018 | Crossover 1 | 50,252 | 32,835 | 17,226 | 46,908 | 52,842 | 14,180 |
| | Crossover 2 | 34,773 | 37,494 | 49,155 | 42,899 | 34,552 | 22,875 |
| 2019 | Crossover 1 | 49,900 | 33,426 | 17,398 | 47,377 | 53,370 | 14,435 |
| | Crossover 2 | 34,530 | 38,169 | 49,647 | 43,328 | 34,172 | 23,287 |
| 2020 | Crossover 1 | 41,217 | 29,849 | 15,136 | 41,218 | 46,432 | 12,890 |
| | Crossover 2 | 28,522 | 34,085 | 43,193 | 37,695 | 30,037 | 20,795 |
| 2021 | Crossover 1 | 47,606 | 32,356 | 16,771 | 45,670 | 51,447 | 13,973 |
| | Crossover 2 | 32,943 | 36,948 | 47,858 | 41,766 | 32,560 | 22,542 |

To collect crash data for interchanges, an R script was developed to automate the extraction process by using the exact geographic coordinates of ramp terminal center points, the crash year, and the defined buffer size to accurately identify all relevant crashes within those areas. To isolate interchange-related crashes, those occurring on the mainline freeway, expressway, or interstate segments located above or below the interchange ramps were excluded, and a specific ramp influence area was defined. This influence area was defined as either 250 feet (typically the distance from a ramp or intersection to the beginning of turn lanes) or half the distance between adjacent ramps or intersections in a diamond interchange, whichever was shorter. This approach minimized the likelihood of double-counting crashes that occurred between adjacent ramps (Zlatkovic 2015; Abdelrahman 2020; Abdelrahman et al. 2021; Bonneson et al. 2021). Also, for crash data from DDI sites before construction, the ramp terminal locations that existed prior to the DDI were used to define the influence area.

In Figure 35, Figure 36, and Figure 37, representative examples of each interchange type are shown: DDI, conventional diamond interchange, and SPDI. Each image displays the buffer circle with its center point, the year of crash data collection, buffer size and its coverage, and crash point markers, which are color-coded for each severity type for visual clarity. Crash severity classifications included all crashes categorized as fatal (K), suspected serious injury (A), suspected minor injury (B), possible injury (C), and PDO (O) that occurred within the defined buffer zones surrounding each ramp terminal. Table 19 and Table 20 provide FI (severity levels K, A, B, and C) and PDO (severity level O) crash frequency from year 2006–2021for treatment and comparison group sites.


**Figure 35: Influence area at diverging diamond interchange ramp terminals (SR-201 Bangerter)**


**Figure 36: Influence area at diamond interchange ramp terminals (I-80 700 E)**


**Figure 37: Influence area at SPUI ramp terminals (I-15 4500 S)**

**Table 19: Crash Severity (crashes/year) for DDI Treatment Sites (2006–2021)**

| Year | Treatment Site: FI and PDO Crashes, Crash/Year | | | | | | | | | | | |
|---|---|---|---|---|---|---|---|---|---|---|---|---|
| | SR-201 Bangerter | | I-15 Pioneer X | | I-15 500 E AF | | I-15 @ UT-130 | | I-15 @ 1100 S | | I-215 @ Redwood Rd | |
| | FI | PDO | FI | PDO | FI | PDO | FI | PDO | FI | PDO | FI | PDO |
| 2006 | 5 | 15 | 3 | 12 | 8 | 4 | - | - | 3 | 0 | 0 | 2 |
| 2007 | 9 | 15 | 5 | 6 | 7 | 6 | 0 | 0 | 4 | 0 | 3 | 6 |
| 2008 | 8 | 10 | 1 | 2 | 7 | 8 | 0 | 0 | 1 | 5 | 6 | 0 |
| 2009 | 14 | 15 | 1 | 0 | 2 | 7 | 0 | 0 | 1 | 4 | 0 | 2 |
| 2010 | 7 | 17 | 2 | 0 | 1 | 4 | 0 | 0 | 0 | 1 | 0 | 2 |
| 2011 | 2 | 16 | 0 | 2 | 2 | 2 | 0 | 0 | 0 | 4 | 0 | 1 |
| 2012 | 5 | 14 | 2 | 0 | 0 | 0 | 0 | 2 | 0 | 6 | 0 | 0 |
| 2013 | 2 | 25 | 1 | 3 | 0 | 1 | 0 | 0 | 0 | 10 | 0 | 2 |
| 2014 | 1 | 13 | 2 | 2 | 0 | 0 | 0 | 3 | 0 | 5 | 0 | 9 |
| 2015 | 10 | 22 | 1 | 4 | 1 | 2 | 0 | 10 | 0 | 4 | 0 | 7 |
| 2016 | 11 | 23 | 1 | 0 | 0 | 0 | 0 | 9 | 0 | 2 | 0 | 5 |
| 2017 | 2 | 20 | 3 | 0 | 1 | 2 | 0 | 6 | 0 | 4 | 0 | 8 |
| 2018 | 8 | 21 | 4 | 5 | 3 | 5 | 0 | 7 | 0 | 2 | 0 | 10 |
| 2019 | 4 | 3 | 5 | 5 | 2 | 3 | 0 | 6 | 1 | 2 | 0 | 10 |
| 2020 | 3 | 5 | 4 | 2 | 1 | 3 | 0 | 0 | 0 | 1 | 0 | 6 |
| 2021 | 6 | 9 | 4 | 6 | 1 | 3 | 0 | 4 | 0 | 2 | 0 | 3 |

**Table 20: Crash Severity (crashes/year) for Comparison Group (2006–2021)**

| Year | Comparison Group: FI and PDO Crashes, Crash/Year | | | | | | | | | | | |
|---|---|---|---|---|---|---|---|---|---|---|---|---|
| | I-80 700 E | | I-80 State | | SR-201 5600 W | | I-15 4500 S | | I-15 3300 S | | I-15 600 N | |
| | FI | PDO | FI | PDO | FI | PDO | FI | PDO | FI | PDO | FI | PDO |
| 2006 | 10 | 10 | 15 | 14 | 10 | 7 | 8 | 22 | 9 | 15 | 1 | 1 |
| 2007 | 9 | 8 | 14 | 29 | 8 | 10 | 7 | 20 | 8 | 14 | 1 | 5 |
| 2008 | 12 | 10 | 12 | 19 | 9 | 5 | 6 | 15 | 4 | 7 | 2 | 2 |
| 2009 | 4 | 6 | 11 | 11 | 1 | 2 | 2 | 12 | 6 | 10 | 5 | 7 |
| 2010 | 2 | 12 | 11 | 17 | 2 | 8 | 4 | 9 | 2 | 6 | 0 | 1 |
| 2011 | 7 | 3 | 19 | 17 | 2 | 10 | 5 | 12 | 8 | 10 | 0 | 3 |
| 2012 | 5 | 11 | 12 | 17 | 6 | 9 | 0 | 13 | 4 | 16 | 2 | 4 |
| 2013 | 3 | 15 | 18 | 26 | 8 | 18 | 14 | 40 | 0 | 13 | 1 | 2 |
| 2014 | 11 | 8 | 6 | 16 | 7 | 20 | 6 | 31 | 4 | 15 | 0 | 3 |
| 2015 | 5 | 17 | 18 | 24 | 6 | 11 | 14 | 28 | 5 | 15 | 1 | 5 |
| 2016 | 12 | 14 | 11 | 12 | 3 | 19 | 8 | 28 | 7 | 23 | 1 | 0 |
| 2017 | 7 | 20 | 13 | 21 | 9 | 15 | 10 | 37 | 8 | 24 | 1 | 5 |
| 2018 | 4 | 9 | 2 | 16 | 7 | 18 | 14 | 32 | 11 | 15 | 2 | 4 |
| 2019 | 1 | 5 | 6 | 14 | 6 | 5 | 4 | 19 | 4 | 7 | 3 | 0 |
| 2020 | 1 | 3 | 3 | 11 | 2 | 3 | 2 | 10 | 4 | 11 | 1 | 2 |
| 2021 | 4 | 2 | 2 | 18 | 8 | 14 | 6 | 13 | 5 | 11 | 1 | 3 |

## 4.2 Safety Performance Functions (SPF)

SPFs, typically modeled using negative binomial distribution, predict crash frequencies based on traffic volumes and roadway geometric and operational characteristics. While the HSM outlines SPFs for several facility types, it does not include models for interchanges and freeways. To address this, Bonneson et al. (2021) developed SPFs for freeway segments, ramp segments, and ramp terminal intersections (Bonneson et al. 2021). Given the operational similarity of DDI ramp terminals, especially their signalized connections to crossroads, the D4 SPF is deemed suitable for estimating crash frequencies at DDI locations (Zlatkovic 2019). This model serves as the predictive basis for the EB analysis conducted in this study, with CMFs applied to account for different geometric changes beyond the standard four-leg signalized (4SG) diamond interchange.

**D4 Configuration:** The D4 configuration refers to a standard 4SG diamond or SPDI ramp terminal. It typically includes two ramps (one entrance and one exit) connecting to a crossroad at a signalized intersection. This configuration is commonly used to model crash frequencies at ramp terminals, as it represents a prevalent interchange layout in freeway systems.

The general SPF for a D4 interchange configuration is expressed as follows (Bonneson et al. 2021):

$$N_{spf} = e^{b_{0,D4}+b_{xrd,D4}\,ln\left(\frac{AADT_{xrd}}{1000}\right)+b_{rmp,D4}\,ln\left(\frac{AADT_{ex}}{1000}+\frac{AADT_{en}}{1000}\right)} \quad (11)$$

Where:

$N_{SPF}$: Predicted number of crashes (crashes/year) for a D4 interchange configuration under base conditions; applied to each ramp separately when applicable

$AADT_{xrd}$: AADT of the crossroad (vehicles/day)

$AADT_{ex}$: AADT of the exit ramp (vehicles/day)

$AADT_{en}$: AADT of the entering ramp (vehicles/day)

$b_{0,D4}$, $b_{xrd,D4}$, $b_{rmp,D4}$: Calibrated coefficients for the D4 ramp terminal configuration, representing the intercept, crossroad AADT, and ramp AADT, respectively

Table 21 presents the calibrated coefficients and statistical parameters for the D4 configuration SPF, with separate values reported for FI crashes and PDO crashes (Bonneson et al. 2021).

**Table 21: SPF Coefficients and Dispersion Parameters for D4 Configuration (Bonneson et al. 2021)**

| Crash Type | $b_{0,D4}$ | $b_{xrd,D4}$ | $b_{rmp,D4}$ | Inverse Dispersion (K), mi⁻¹ | Overdispersion (k = 1/K) |
|---|---|---|---|---|---|
| FI | -3.044 | 1.255 | 0.114 | 11.5 | 0.087 |
| PDO | -3.058 | 0.879 | 0.545 | 7.21 | 0.139 |

In negative binomial SPFs, the overdispersion parameter (k) captures the extra variability in crash counts that exceeds what a Poisson model can explain, allowing NB regression to better estimate crash frequencies by adjusting the variance. The k parameter is essential in EB estimation, where modeling the uncertainty in crash predictions requires accounting for this inherent variability across similar sites. The k parameter is estimated during SPF development and is shown in Table 21 for the D4 interchange configuration SPFs.

### *Predicted Crash Frequency for Local Conditions*

The predicted average crash frequency under local (Utah) conditions is calculated as:

$$N_{rt,D4} = C_{UT} * CMF_{comb} * N_{spf,D4} \qquad (12)$$

Where:

$N_{rt,D4}$: Predicted average crash frequency for the D4 configuration under local conditions (crashes/year)

$C_{UT}$: Calibration factor for Utah-specific crash conditions

$CMF_{comb}$: Combined crash modification factor, which accounts for geometric features such as channelized turns, location, access points, and segment length

$N_{SPF,D4}$: Predicted crash frequency from the base SPF model (Equation 11)

The local calibration factor ($C_{UT}$) was used to tailor SPF predictions to Utah-specific roadways and traffic conditions, and was computed based on the ratio of observed to predicted crash totals over the study period (2006–2021):

$$C_{UT} = \frac{\sum_{2008}^{2021} N_{observed}}{\sum_{2008}^{2021} N_{rt,D4}} \qquad (13)$$

In addition to the local calibration factor, CMFs were applied to account for geometric design features, specifically protected left-turn phasing on crossroads and right-turn channelization at exit ramps. These CMFs were combined into a single adjustment factor ($CMF_{comb}$) to refine the base crash predictions generated by the SPFs. Table 22 presents both the individual and combined CMFs for signalized ramp terminals, categorized by crash severity type (FI and PDO). The table also includes the proportion of AADT affected by each treatment, enabling the development of more accurate, context-sensitive crash frequency estimates for the Utah setting.

**Table 22: CMFs for Treatments at Signalized Ramp Terminals (Bonneson et al. 2021)**

| Crash Type | Junction | Leg | Prop. AADT | Channelization Type | CMF | $CMF_{comb}$ |
|---|---|---|---|---|---|---|
| FI | Ramp terminal | Exit ramp | 0.12 | 2 legs (Right-turn channelization) | 1.45 | 0.87 |
| | | Crossroad | 0.78 | 1 leg (Protected left turn) | 0.6 | |
| PDO | Ramp terminal | Exit ramp | 0.12 | 2 legs (Right-turn channelization) | 1.91 | 1.38 |
| | | Crossroad | 0.78 | 1 leg (Protected left turn) | 0.72 | |

The calibration factor for local conditions ($C_{UT}$) was determined to be 0.699 for FI crashes and 1.099 for PDO crashes. These calibration factors account for Utah-specific roadway, environmental, and traffic characteristics, ensuring that the CMFs derived are both accurate and regionally relevant. This local calibration strengthens the applicability of the results for regional safety planning and decision-making. The results as shown in Table 23 and Table 24 are the predicted number of FI and PDO crashes under Utah conditions calculated using Equation 12 for the comparison group.

**Table 23: Predicted Number of FI Crashes for the Comparison Group**

| Comparison Site | FI Predicted Number of Crashes (crash/yr) | | | | | |
|---|---|---|---|---|---|---|
| | I-80 700 E | I-80 State | SR-201 5600 W | I-15 4500 S | I-15 3300 S | I-15 600 N |
| 2006 | 7.36 | 6.47 | 4.33 | 6.58 | 7.42 | 1.67 |
| 2007 | 7.52 | 6.60 | 4.41 | 6.71 | 7.35 | 1.82 |
| 2008 | 7.18 | 6.26 | 5.17 | 6.36 | 6.43 | 1.70 |
| 2009 | 6.96 | 6.21 | 5.20 | 6.42 | 6.45 | 1.69 |
| 2010 | 6.64 | 6.17 | 5.22 | 6.43 | 6.62 | 1.68 |
| 2011 | 7.95 | 6.15 | 5.44 | 6.18 | 6.46 | 1.67 |
| 2012 | 7.49 | 5.98 | 5.30 | 7.04 | 6.42 | 1.63 |
| 2013 | 7.46 | 6.09 | 5.49 | 7.29 | 7.25 | 1.57 |
| 2014 | 7.92 | 6.14 | 5.57 | 7.53 | 7.52 | 2.31 |
| 2015 | 8.08 | 6.55 | 5.80 | 8.26 | 8.18 | 2.47 |
| 2016 | 8.64 | 7.03 | 6.16 | 8.76 | 8.71 | 2.65 |
| 2017 | 8.91 | 6.53 | 6.39 | 9.08 | 9.04 | 2.75 |
| 2018 | 8.65 | 6.62 | 6.47 | 9.25 | 9.00 | 2.79 |
| 2019 | 8.56 | 6.78 | 6.56 | 9.37 | 9.03 | 2.86 |
| 2020 | 6.59 | 4.13 | 3.87 | 5.56 | 5.39 | 1.68 |
| 2021 | 8.03 | 6.49 | 6.24 | 8.91 | 8.54 | 2.73 |

**Table 24: Predicted Number of PDO Crashes for Comparison Group**

| Comparison Site | PDO Predicted Number of Crashes (crash/yr) | | | | | |
|---|---|---|---|---|---|---|
| | I-80 700 E | I-80 State | SR-201 5600 W | I-15 4500 S | I-15 3300 S | I-15 600 N |
| 2006 | 13.15 | 11.51 | 17.58 | 11.72 | 13.29 | 2.81 |
| 2007 | 13.45 | 11.74 | 19.18 | 11.96 | 13.16 | 3.08 |
| 2008 | 12.82 | 11.12 | 9.14 | 11.32 | 11.48 | 2.87 |
| 2009 | 12.42 | 11.02 | 9.21 | 11.43 | 11.51 | 2.85 |
| 2010 | 11.82 | 10.96 | 9.25 | 11.45 | 11.82 | 2.83 |
| 2011 | 14.28 | 10.91 | 9.65 | 10.98 | 11.53 | 2.82 |
| 2012 | 13.41 | 10.60 | 9.40 | 12.56 | 11.45 | 2.74 |
| 2013 | 13.36 | 10.80 | 9.75 | 13.03 | 12.96 | 2.64 |
| 2014 | 14.21 | 10.89 | 20.49 | 13.46 | 13.48 | 3.95 |
| 2015 | 14.52 | 11.65 | 21.72 | 14.83 | 14.71 | 4.24 |
| 2016 | 15.56 | 12.54 | 24.21 | 15.76 | 15.70 | 4.56 |
| 2017 | 16.07 | 11.62 | 24.52 | 16.37 | 16.31 | 4.74 |
| 2018 | 15.57 | 11.78 | 25.82 | 16.68 | 16.25 | 4.80 |
| 2019 | 15.42 | 12.09 | 27.08 | 16.92 | 16.31 | 4.93 |
| 2020 | 11.74 | 14.48 | 30.29 | 19.31 | 18.70 | 6.10 |
| 2021 | 14.42 | 11.54 | 25.70 | 16.05 | 15.39 | 4.70 |

### *Predicted Crashes for Treatment Sites (Before and After)*

To account for time-specific crash rates (e.g., annual variation), the crash prediction model is modified as follows. From comparison sites, the yearly modification factor ($a_y$) is calculated as:

$$a_y = \frac{\sum_{Year} N_{Observed}}{\sum_{Year} N_{rt,D4}} \tag{14}$$

The yearly modification factor ($a_y$) is defined as the ratio of observed to predicted crashes for a given year, aggregated across all sites. It captures year-to-year variations in crash frequency that may result from changes in external factors such as traffic volumes, enforcement levels, or weather conditions. By quantifying these fluctuations, $a_y$ serves as a temporal adjustment factor that refines the predicted crash estimates for treatment sites, ensuring they align more closely with observed trends over time. This enhances the accuracy of the safety effectiveness evaluation.

Table 25 shows the yearly modification factors ($a_y$) for FI and PDO crashes at comparison sites, used to adjust predicted crashes at DDI sites by accounting for external yearly trends. The values fluctuate over time, with higher ratios in early years and lower values from 2019 to 2021, indicating an overall decline in crash rates at comparison sites. This adjustment improves the accuracy of DDI safety evaluations.

**Table 25: Yearly Modification Factor $a_y$ for FI and PDO Crashes**

| Year | $a_y$ for FI | $a_y$ for PDO |
|---|---|---|
| 2006 | 1.567 | 0.985 |
| 2007 | 1.366 | 1.185 |
| 2008 | 1.359 | 0.987 |
| 2009 | 0.88 | 0.821 |
| 2010 | 0.641 | 0.912 |
| 2011 | 1.211 | 0.914 |
| 2012 | 0.857 | 1.164 |
| 2013 | 1.252 | 1.823 |
| 2014 | 0.919 | 1.216 |
| 2015 | 1.245 | 1.225 |
| 2016 | 1.001 | 1.087 |
| 2017 | 1.124 | 1.361 |
| 2018 | 0.935 | 1.034 |
| 2019 | 0.556 | 0.539 |
| 2020 | 0.477 | 0.397 |
| 2021 | 0.635 | 0.695 |

Using this yearly modification factor $a_y$, the predicted number of crashes for treatment sites is computed as:

$$N_{rt,D4} = a_y \cdot C_{UT} \cdot CMF_{comb} \cdot N_{SPF,\ D4} \qquad (15)$$

The results as shown in Table 26 and Table 27 are the predicted number of FI and PDO crashes under Utah conditions calculated using Equation 15 for the treatment group.

**Table 26: Predicted Number of FI Crashes for Treatment Sites**

| Treatment Sites | FI Predicted Number of Crashes (crash/yr) | | | | | |
|---|---|---|---|---|---|---|
| | SR-201 Bangerter | I-15 Pioneer X | I-15 500 E AF | I-15 @ UT-130 | I-15 @ 1100 S | I-215 @ Redwood Rd |
| 2006 | 11.26 | 3.46 | 4.72 | - | 4.31 | 1.82 |
| 2007 | 10.53 | 5.56 | 4.19 | 0.46 | 3.49 | 2.02 |
| 2008 | 10.44 | 5.25 | 3.89 | 0.43 | 3.84 | 1.88 |
| 2009 | 6.75 | 3.43 | 2.50 | 0.27 | 2.64 | 1.20 |
| 2010 | 4.50 | 2.62 | 1.81 | 0.20 | 1.99 | 0.83 |
| 2011 | 8.84 | 4.94 | 3.41 | 2.05 | 3.08 | 1.57 |
| 2012 | 6.29 | 3.40 | 2.34 | 1.41 | 2.22 | 1.08 |
| 2013 | 9.87 | 6.16 | 3.31 | 1.99 | 3.23 | 1.91 |
| 2014 | 7.68 | 4.80 | 2.47 | 1.48 | 2.50 | 1.42 |
| 2015 | 10.76 | 6.95 | 3.54 | 2.15 | 3.74 | 2.04 |
| 2016 | 9.16 | 5.92 | 3.05 | 1.94 | 3.20 | 1.76 |
| 2017 | 10.40 | 6.90 | 3.56 | 2.15 | 3.69 | 2.05 |
| 2018 | 8.59 | 5.84 | 3.00 | 1.78 | 3.12 | 1.73 |
| 2019 | 4.79 | 3.52 | 1.83 | 1.07 | 1.85 | 1.05 |
| 2020 | 3.40 | 2.50 | 1.34 | 0.80 | 1.45 | 0.77 |
| 2021 | 5.76 | 3.82 | 2.00 | 1.27 | 2.27 | 1.15 |

**Table 27: Predicted Number of PDO Crashes for Treatment Sites**

| Treatment Sites | PDO Predicted Number of Crashes (crash/yr) | | | | | |
|---|---|---|---|---|---|---|
| | SR-201 Bangerter | I-15 Pioneer X | I-15 500 E AF | I-15 @ UT-130 | I-15 @ 1100 S | I-215 @ Redwood Rd |
| 2006 | 12.64 | 3.71 | 5.11 | - | 4.65 | 1.90 |
| 2007 | 16.35 | 8.42 | 6.27 | 0.63 | 5.19 | 2.94 |
| 2008 | 11.87 | 6.76 | 4.71 | 0.49 | 4.80 | 2.28 |
| 2009 | 9.87 | 5.65 | 3.90 | 0.40 | 4.24 | 1.88 |
| 2010 | 10.34 | 6.47 | 4.31 | 0.45 | 4.88 | 1.98 |
| 2011 | 10.61 | 6.47 | 4.31 | 2.61 | 3.98 | 1.98 |
| 2012 | 13.55 | 8.10 | 5.39 | 3.23 | 5.16 | 2.45 |
| 2013 | 22.23 | 14.52 | 8.26 | 4.87 | 8.06 | 4.66 |
| 2014 | 18.25 | 11.20 | 5.60 | 3.30 | 5.67 | 3.15 |
| 2015 | 19.04 | 12.08 | 5.99 | 3.57 | 6.35 | 3.37 |
| 2016 | 17.94 | 11.40 | 5.72 | 3.57 | 6.00 | 3.22 |
| 2017 | 22.73 | 14.83 | 7.44 | 4.40 | 7.74 | 4.19 |
| 2018 | 17.15 | 11.47 | 5.73 | 3.33 | 5.97 | 3.23 |
| 2019 | 8.36 | 6.07 | 3.07 | 1.76 | 3.10 | 1.73 |
| 2020 | 5.05 | 3.67 | 1.92 | 1.12 | 2.09 | 1.08 |
| 2021 | 11.36 | 7.42 | 3.77 | 2.36 | 4.32 | 2.13 |

## 4.3 Empirical Bayes Before- After Analysis

This study applies a robust data-driven methodology to assess the safety effectiveness of DDIs in Utah, using the EB before–after evaluation approach. The EB method is a well-established statistical technique in roadway safety research that addresses key biases such as regression-to-the-mean and site selection effects. By combining observed crash data with expected crash frequencies derived from SPFs, the method offers a more accurate estimate of the treatment's safety impact. The following steps are needed to conduct an EB before-after evaluation:

***Predicted Crashes in After Period (Had Treatment Not Been Applied)***

Let $\hat{\pi}_j$ represent the predicted number of crashes in the after period for site $j$, had the treatment not been applied. Then:

$$\hat{\pi}_j = C_j . M_j \qquad (16)$$

Where:

$$C_j = \frac{\sum(predicted\ crashes\ in\ after\ period\ for\ site\ j)}{\sum(predicted\ crashes\ in\ before\ for\ site\ j)} = \frac{\sum N_{rt,D4}(treatment\ sites,\ \ after\ period)}{\sum N_{rt,D4}(treatment\ sites,\ \ before\ period)}$$

$M_j = w . P_j + (1 - w) . K_j$

$K_j$: total observed crashes in the before period for site $j$

$P_j$: total predicted crashes in the before period for site $j$

$w = \frac{1}{1+ k*P_j}$ : Weight-based on the overdispersion parameter $k$

The total predicted crash across all sites is:

$$\hat{\pi}_j = \sum_j \hat{\pi}_j \quad (17)$$

***Variance of Predicted Crashes***

Variance of predicted crashes is calculated as:

$$VAR\{\hat{\pi}\} = \sum_j VAR\{\hat{\pi}_j\} \quad (18)$$

Where:

$VAR\{\hat{\pi}_j\} = C_j^2 * VAR\{M_j\}$

$VAR\{M_j\} = M_j * (1 - w)$

***Observed Crashes in After Period***

The observed crashes in after period is estimated as:

$$\hat{\lambda} = \sum_j \hat{\lambda}_j \quad (19)$$

with variance:

$$VAR\{\hat{\lambda}\} = \sum_j VAR\{\hat{\lambda}_j\} \quad (20)$$

Where:

- $\hat{\lambda}_j = \sum observed\ crashes\ in\ after\ period\ for\ site\ j$
- $VAR\{\hat{\lambda}_j\} = \hat{\lambda}_j$

***Estimate of CMF for Treatment***

The estimated CMF for the treatment is denoted as $\hat{\theta}$ and calculated as:

$$\hat{\theta} = \frac{\hat{\lambda}}{\hat{\pi}\,(1+ {VAR\{\hat{\pi}\}}/{\hat{\pi}^2})} \quad (21)$$

with variance:

$$VAR\{\hat{\theta}\} = \hat{\theta}^2 * \frac{{1}/{\hat{\lambda}} + {VAR\{\hat{\pi}\}}/{\hat{\pi}^2}}{\left(1+ {VAR\{\hat{\pi}\}}/{\hat{\pi}^2}\right)^2} \quad (22)$$

and standard deviation:

$$\sigma\{\hat{\theta}\} = \sqrt{VAR\{\hat{\theta}\}} \quad (23)$$

***Crash Reduction Estimate***

The reduction in crashes δ is estimated as:

$$\delta = \hat{\pi} - \hat{\lambda} \quad (24)$$

with variance:

$$\mathrm{VAR}\{\ \delta\ \} = \mathrm{VAR}\ \{\hat{\pi}\} + \mathrm{VAR}\ \{\hat{\lambda}\ \} \quad (25)$$

## 4.4 Crash Reductions and CMF Estimates

From Table 28, the EB analysis conducted in this study demonstrates that DDIs significantly reduce both FI and PDO crashes at freeway interchange ramp terminals in Utah at baseline assumption (i.e., ramp traffic volumes were approximately 15% of the main crossroad AADT). Based on our analysis, the predicted number of FI crashes ($\hat{\pi}$) was 169, while the observed number after DDI implementation ($\hat{\lambda}$) was 89, resulting in an estimated CMF of $\hat{\theta}$= 0.522. This corresponds to a 47.8% reduction in FI crashes, with a standard deviation of 0.071. Similarly, PDO crashes decreased from a predicted count of about 374 to 271 observed crashes, yielding a CMF of $\hat{\theta}$ = 0.719, which equates to a 28.07% reduction with a standard deviation of 0.071. These reductions are statistically significant and highlight the effectiveness of DDIs in improving safety outcomes, particularly in reducing both the frequency and severity of crashes.

**Table 28: Crash Prediction and Reduction Statistics at Different AADT Levels**

| **Parameter** | **15% of AADT (Baseline)** | | **10% of AADT** | | **20% of AADT** | |
|---|---|---|---|---|---|---|
| | **FI** | **PDO** | **FI** | **PDO** | **FI** | **PDO** |
| $\hat{\pi}$ (Predicted crashes) | 169 | 374 | 170 | 369 | 168 | 372 |
| VAR ($\hat{\pi}$) | 223 | 854 | 226 | 834 | 221 | 849 |
| $\hat{\lambda}$ (Observed crashes) | 89 | 271 | 89 | 271 | 89 | 271 |
| VAR ($\hat{\lambda}$) | 89 | 271 | 89 | 271 | 89 | 271 |
| $\hat{\theta}$ (Estimated CMF) | 0.522 | 0.719 | 0.518 | 0.731 | 0.524 | 0.723 |
| Crash Reduction | 47.8% ± 7.14% | 28.07% ± 7.07% | 48.17% ± 7.09% | 26.93% ± 7.20% | 47.55% ± 7.18% | 27.67% ± 7.12% |
| VAR ($\hat{\theta}$) | 0.005 | 0.005 | 0.005 | 0.005 | 0.005 | 0.005 |
| σ($\hat{\theta}$) | 0.071 | 0.071 | 0.071 | 0.072 | 0.072 | 0.071 |
| δ (Crash reduction count) | 80.171 | 103.449 | 81.378 | 97.622 | 79.377 | 101.379 |
| VAR(δ) | 311.928 | 1,125.39 | 314.844 | 1,104.88 | 310.022 | 1,119.694 |

Table 29 presents a sensitivity analysis of CMFs with respect to varying ramp traffic volume assumptions, expressed as a percentage of main crossroad AADT. As shown, the estimated CMFs for both FI crashes and PDO crashes exhibit minimal variation across the 10%, 15%, and 20% ramp traffic volume scenarios. The CMF values at 15% volume (0.522 for FI and 0.719 for PDO) serve as the baseline. Relative to this baseline, the FI CMF decreases slightly (–0.71%) at 10% and increases marginally (+0.47%) at 20%, while the PDO CMF increases by +1.58% at 10% and +0.55% at 20%. These small percentage changes indicate that the CMFs are relatively insensitive to moderate variations in ramp traffic volume, suggesting the model's robustness and stability under varying ramp traffic AADT assumptions.

**Table 29: Sensitivity of Estimated CMFs to Ramp Traffic Volume Assumptions**

| Ramp Traffic Volume (% of crossroad AADT) | FI Crashes | PDO Crashes | % Change from 15% (FI) | % Change from 15% (PDO) |
|---|---|---|---|---|
| 10% | 0.518 | 0.731 | -0.71% | 1.58% |
| 15% | 0.522 | 0.719 | - | - |
| 20% | 0.524 | 0.723 | 0.47% | 0.55% |

## 4.5 Comparison with Previous DDI Studies

As summarized in Table 30, CMFs reported in prior DDI studies for FI crashes range from 0.312 to 0.59, while CMFs for PDO crashes range from 0.626 to 0.92. Our study's findings, 0.522 for FI and 0.719 for PDO crashes, are consistent with this range. This reinforces the demonstrated safety benefits of DDIs, particularly in the Utah context. Notably, the CMFs from our study were derived using a longer post-conversion period (2006–2021), a large sample size, and a regionally calibrated EB approach, offering a more detailed and stable assessment of long-term DDI performance specific to Utah's traffic and roadway conditions.

**Table 30: Summary of CMFs for FI and PDO Crashes in DDI Studies (FHWA 2025)**

| Study | CMF (FI) | CMF (PDO) | State | Study Method (Data Range) |
|---|---|---|---|---|
| (Chilukuri et al. 2011) | – | 0.63 | MO | Simple before/after (2004–2010) |
| (Hummer et al. 2016) | 0.59 | – | KY, MO, NY, TN | Comparison group |
| (B. Claros et al. 2017a) | 0.45 | 0.686 | MO | Empirical Bayes or full Bayes |
| (Nye et al. 2019) | 0.461 | 0.695 | GA, ID, KS, KY, MN, MO, NY, NC, UT, VA, WY | Comparison group (2006–2017) |
| (Nye et al. 2019) | 0.312 | 0.626 | UT | Comparison group (2006–2016) |
| (Abdelrahman et al. 2021) | 0.558 | 0.92 | CO, FL, GA, ID, IN, IA, KS, KY, MI, MN, MO, NV, NM, NY, NC, OH, OR, PA, TN, TX, UT, VA, WI, WY | Empirical Bayes or full Bayes |
| Our Study (2025) | 0.522 | 0.719 | UT | Empirical Bayes or full Bayes (2006–2021) |

The slightly lower CMF for FI crashes compared with PDO crashes suggests that DDIs are especially effective at mitigating more severe crash types. This aligns with the intended safety benefits of DDI designs, which reduce vehicle conflict points, streamline turning movements, and simplify signal phasing—all of which are critical factors in preventing high-severity collisions.

Overall, the findings support the effectiveness of DDIs as a safety countermeasure, particularly in improving outcomes for all types of crashes. The study also contributes a regionally specific, data-driven reference point that can aid future DDI planning, evaluation, and implementation efforts within Utah and potentially in other jurisdictions with similar roadway environments.

## 4.6 Conclusion

This study set out to develop reliable, state-specific CMFs for DDIs through a safety evaluation using a robust EB before–after methodology. By analyzing a 16-year crash dataset (2006–2021) from multiple DDI sites across Utah, this study addressed key limitations in the existing literature, i.e., reliance on aggregated multi-state data. The methodology incorporated spatially consistent crash extraction, clearly defined influence areas, and localized calibration to ensure a context-sensitive analysis aligned with Utah's unique traffic and geometric conditions.

The results affirm the safety benefits of DDIs, particularly in reducing FI and PDO crashes. The estimated CMFs, 0.522 for FI and 0.719 for PDO, fall within the comparable range reported in previous studies, offering greater multiple years stability and regional specificity. The lower CMF for FI crashes indicates that DDIs are especially effective at mitigating severe crash outcomes. Statistical confidence in these estimates, as evidenced by their variance and standard errors, reinforces the reliability of the findings and supports their application in practical safety planning.

Overall, this research provides a replicable framework for evaluating DDI safety performance in other regions by combining multiple years of data with rigorous analytical methods. The Utah-based CMFs can directly inform state-level transportation planning, design standards, and investment decisions. More broadly, the study contributes to improved crash prediction and safer interchange design practices at both regional and national levels by supporting data-driven decision-making in the implementation of safety countermeasures.

While this study focuses on crash severity at DDIs, future research should explore CMFs for different manners of collision. The current comparison group combines conventional diamond interchanges and single-point diamond interchanges; separating these for comparison with treatment sites may yield more accurate CMF estimates. Additionally, geometric and contextual factors, such as crossover angle, ramp terminal configuration, proximity to adjacent intersections, and rural versus urban settings, may influence CMFs and warrant further investigation. Additionally, the availability of ramp terminal entry and exit AADT would give more accurate results.

# 5. SAFETY EVALUATION OF CONTINUOUS FLOW INTERSECTIONS (CFI)

## 5.1 Data Collection

Crash data were obtained from UDOT's Traffic and Safety Division, while annual average daily traffic (AADT) data were sourced from UDOT's Open Data Portal (UDOT 2025), along with signal phasing information collected from Google Earth and site visits. Crash and AADT data were collected for 2006 through 2021. The study included eight CFI sites as treatment locations and, for the comparison group, 4SG intersections across Utah. The "before" period spans from 2006 to the year prior to CFI implementation, while the "after" period extends from one year after implementation through the end of the analysis in 2021. Three CFI sites (Bangerter Highway at 5400 S, 6200 S, and 7000 S) were later converted to single point diamond interchange (SPDI) in 2017, 2019, and 2016, respectively. Therefore, the "after" period for these sites was considered only up to the year prior to their conversion to SPDI.

**Table 31: Annual Average Daily Traffic at Major and Minor Road of the Treatment Sites**

| Year | Treatment Sites: AADT (veh/day) | | | | | | | |
|---|---|---|---|---|---|---|---|---|
| | Bangerter @ 3100 S | | Bangerter @ 4100 S | | Bangerter @ 4700 S | | Bangerter @ 5400 S | |
| | Major | Minor | Major | Minor | Major | Minor | Major | Minor |
| 2006 | 50,405 | 18,825 | 52,555 | 32,030 | 57,320 | 35,450 | 51,145 | 36,380 |
| 2007 | 51,110 | 18,335 | 53,290 | 32,480 | 58,120 | 34,395 | 51,860 | 36,890 |
| 2008 | 49,170 | 17,440 | 51,265 | 30,885 | 55,915 | 33,085 | 49,890 | 35,080 |
| 2009 | 49,515 | 17,335 | 51,625 | 30,700 | 56,305 | 33,320 | 50,240 | 38,380 |
| 2010 | 49,565 | 17,265 | 51,675 | 30,580 | 56,360 | 31,840 | 50,290 | 38,225 |
| 2011 | 48,125 | 17,210 | 41,330 | 30,485 | 54,725 | 30,915 | 48,830 | 40,105 |
| 2012 | 47,980 | 16,870 | 41,205 | 29,875 | 54,560 | 30,825 | 48,685 | 39,300 |
| 2013 | 49,230 | 16,445 | 42,275 | 29,130 | 55,980 | 31,625 | 49,950 | 38,320 |
| 2014 | 51,395 | 16,625 | 44,135 | 29,450 | 58,445 | 33,015 | 52,150 | 38,740 |
| 2015 | 53,915 | 17,340 | 46,300 | 30,485 | 61,310 | 34,635 | 57,775 | 40,405 |
| 2016 | 56,286 | 18,261 | 48,336 | 32,102 | 64,006 | 36,157 | 60,315 | 42,546 |
| 2017 | 57,806 | 18,754 | 49,641 | 32,969 | 65,734 | 37,133 | 61,944 | 43,695 |
| 2018 | 58,557 | 18,942 | 50,286 | 33,299 | 66,589 | 37,616 | - | - |
| 2019 | 59,143 | 19,283 | 50,789 | 33,898 | 67,255 | 37,992 | - | - |
| 2020 | 51,454 | 17,220 | 44,186 | 30,271 | 58,512 | 33,053 | - | - |
| 2021 | 61,385 | 18,666 | 48,958 | 32,814 | 64,831 | 36,623 | - | - |
| Year | Bangerter @ 6200 S | | Bangerter @ 7000 S | | Redwood @ 5400 S | | Redwood @ 6200 S | |
| | Major | Minor | Major | Minor | Major | Minor | Major | Minor |
| 2006 | 62,205 | 31,590 | 46,035 | 18,790 | 65,450 | 39,995 | 38,300 | 24,415 |
| 2007 | 63,075 | 32,030 | 48,470 | 19,055 | 66,365 | 42,015 | 39,045 | 23,590 |
| 2008 | 55,840 | 30,460 | 48,280 | 18,120 | 63,115 | 39,960 | 37,560 | 22,430 |
| 2009 | 56,230 | 30,280 | 49,275 | 18,010 | 62,735 | 43,700 | 37,820 | 22,295 |
| 2010 | 56,285 | 30,160 | 48,710 | 19,855 | 62,485 | 41,635 | 37,860 | 22,210 |
| 2011 | 54,655 | 30,070 | 47,250 | 19,795 | 62,295 | 39,830 | 62,600 | 22,140 |
| 2012 | 54,490 | 29,465 | 47,110 | 19,400 | 61,050 | 38,865 | 62,410 | 21,700 |
| 2013 | 55,905 | 28,730 | 51,790 | 18,915 | 59,525 | 39,195 | 64,035 | 21,155 |
| 2014 | 58,365 | 29,045 | 54,070 | 19,120 | 60,180 | 39,560 | 66,850 | 21,390 |
| 2015 | 61,225 | 30,295 | 53,410 | 17,720 | 62,770 | 41,260 | 70,125 | 22,310 |
| 2016 | 63,920 | 31,901 | 57,615 | 18,661 | 66,095 | 43,446 | 73,212 | 23,491 |
| 2017 | 65,646 | 32,762 | - | - | 67,880 | 44,619 | 75,189 | 24,125 |
| 2018 | 66,499 | 33,090 | - | - | 68,559 | 45,065 | 76,166 | 24,366 |
| 2019 | 67,164 | 33,686 | - | - | 69,793 | 45,876 | 76,928 | 24,805 |
| 2020 | - | - | - | - | 62,325 | 40,967 | 66,927 | 22,151 |
| 2021 | - | - | - | - | 67,560 | 44,408 | 74,155 | 24,012 |

**Table 32: Annual Average Daily Traffic at Major and Minor Road of the Comparison Group**

| Year | Comparison Group: AADT (veh/day) | | | | | | | | | |
|---|---|---|---|---|---|---|---|---|---|---|
| | Redwood @ 3500 S | | 5600 W @ 3500 S | | State @ 4500 S | | State @ 3300 S | | 700 E @ 3300 S | |
| | Major | Minor | Major | Minor | Major | Minor | Major | Minor | Major | Minor |
| 2006 | 46,460 | 51,120 | 31,080 | 27,560 | 38,830 | 34,790 | 31,185 | 38,385 | 40,065 | 27,715 |
| 2007 | 47,110 | 51,835 | 31,515 | 27,945 | 39,375 | 35,275 | 31,620 | 38,920 | 40,705 | 28,105 |
| 2008 | 44,755 | 49,865 | 38,060 | 26,885 | 37,445 | 33,935 | 30,075 | 37,445 | 39,365 | 27,035 |
| 2009 | 44,485 | 50,215 | 38,325 | 27,070 | 37,220 | 34,175 | 29,895 | 37,705 | 38,495 | 27,225 |
| 2010 | 44,305 | 28,915 | 38,365 | 27,100 | 37,070 | 34,210 | 29,775 | 37,745 | 37,190 | 27,250 |
| 2011 | 40,335 | 29,190 | 40,400 | 26,315 | 32,695 | 38,705 | 27,425 | 36,650 | 37,300 | 24,045 |
| 2012 | 39,530 | 28,920 | 40,280 | 26,235 | 32,045 | 38,590 | 26,875 | 36,540 | 35,695 | 23,970 |
| 2013 | 30,260 | 29,180 | 41,325 | 26,915 | 31,240 | 39,590 | 26,500 | 37,490 | 35,590 | 24,595 |
| 2014 | 30,590 | 30,465 | 43,145 | 28,100 | 31,585 | 41,335 | 26,790 | 39,135 | 37,190 | 25,675 |
| 2015 | 31,905 | 31,960 | 45,255 | 19,975 | 32,945 | 43,360 | 27,940 | 41,055 | 37,750 | 26,935 |
| 2016 | 33,597 | 33,364 | 47,248 | 20,853 | 34,690 | 45,267 | 29,422 | 42,861 | 39,638 | 28,120 |
| 2017 | 34,504 | 34,265 | 48,524 | 21,416 | 35,627 | 46,489 | 30,216 | 44,018 | 40,550 | 21,723 |
| 2018 | 34,849 | 34,710 | 49,155 | 21,694 | 35,983 | 47,093 | 30,518 | 44,590 | 39,658 | 22,005 |
| 2019 | 35,476 | 35,057 | 49,647 | 21,911 | 36,631 | 47,564 | 31,067 | 45,036 | 39,380 | 22,225 |
| 2020 | 31,680 | 30,500 | 43,193 | 19,063 | 32,711 | 41,381 | 27,743 | 39,181 | 32,528 | 19,336 |
| 2021 | 34,341 | 33,794 | 47,858 | 21,122 | 35,459 | 45,850 | 30,073 | 43,413 | 37,570 | 21,424 |

Table 31 and Table 32 presents AADT for major and minor roads for treatment sites and comparison group sites from 2006 to 2021. The AADT trends for major and minor roads at both sites are illustrated Figure 38 and Figure 39, respectively. It shows AADT over time at both sites, representing major-road and the minor-road traffic on the cross street. For the treatment sites, the vertical bar (yellow in color) marks the year the CFI was implemented; data left of the line are the before period, and data right of the line are the after period.


**Figure 38: Plot of annual average daily traffic at major and minor road of the treatment sites**


**Figure 39: Plot of annual average daily traffic at major and minor road of the comparison group**

The treatment sites in Figure 38 illustrate that major-road AADT typically stays flat or declines before CFI construction and often dips during the implementation year, but afterward it consistently rebounds and increases, usually exceeding pre-CFI levels. Minor-road AADT remains stable throughout, showing only small fluctuations and minimal impact from the CFI implementation. The comparison group sites in Figure 39 show that the major roads generally carry higher AADT than minor roads, which remain mostly stable with only small fluctuations over time. Both road types show smooth, gradual changes rather than abrupt shifts, though a few sites—such as State @ 4500 S and State @ 3300 S—exhibit slightly higher minor-road AADT, indicating more balanced traffic or stronger cross-street demand. Overall, traffic volumes vary moderately across years, with occasional localized fluctuations on minor roads.

To collect crash data for intersections, an R script was developed to automate the extraction process by using the exact geographic coordinates of CFI and comparison-group center points, the crash year, and the defined buffer size to accurately identify all relevant crashes within those areas. To isolate intersection-related crashes, those occurring on the mainline freeway, expressway, or interstate segments in the vicinity of the intersection were excluded, and a specific intersection influence area was defined. This influence area was defined as 250 ft (typically the distance from the intersection to the beginning of turn lanes). For the before-construction period of CFI sites, the influence area was based on the geometry of the intersection that existed prior to the CFI. For the after-construction period, an additional 100-ft buffer was applied around each crossover intersection, in addition to the main intersection influence area, to capture crashes occurring near the crossovers, as illustrated in Figure 40 (Zlatkovic and Kergaye 2018; Abdelrahman et al. 2020; Zlatkovic 2019).

Figure 40 and Figure 41 present representative examples of each intersection type: a CFI and a comparison-group intersection. Each image illustrates the buffer circle with its center point, the year of crash data collection, the buffer size and its coverage, and crash point markers that are color-coded according to crash severity for visual clarity. Crash severity classifications include all crashes categorized as fatal (K), suspected serious injury (A), suspected minor injury (B), possible injury (C), and property-damage-only (O) within the defined buffer zones surrounding each intersection.


**Figure 40: Bangerter @ 3100 S CFI (top) and two crossovers (bottom)**


**Figure 41: Redwood @ 3500 S comparison-group intersection**

Table 33 and Table 34 present crashes with their severity type for each year for treatment sites and comparison group sites from 2006 to 2021. Figure 42 and Figure 43 illustrate the annual trends in fatal-and-injury (FI), property-damage-only (PDO), and total crashes for treatment sites and comparison group sites from 2006 to 2021. For the treatment sites, the vertical yellow bar marks the year the continuous flow intersection (CFI) was implemented; data left of the line are the before period, and data right of the line are the after period. Over all years, PDO crashes consistently occurred more frequently than FI crashes at both CFI treatment and comparison sites.

Across the CFI sites (see Figure 42), total, PDO, and FI crashes fluctuate year to year, but a clear before–after pattern emerges around the implementation year. Before the CFI, total and PDO crashes were generally higher or trending upward, with several sites showing noticeable peaks. FI crashes also vary but tend to be more elevated in the pre-CFI period. After the CFI is installed, most locations show a stabilization or reduction in total crashes and PDO crashes, along with fewer spikes in FI crashes. Overall, crash patterns become more stable and generally lower following CFI implementation, indicating improved traffic operations and safety performance.

Overall, the comparison-group sites (see Figure 43) show typical long-term crash variation rather than any major shifts. Total and PDO crashes generally cycle up and down over the years, with periods of decline followed by gradual increases, but without a consistent trend in one direction. FI crashes remain much lower and relatively steady, showing only modest fluctuations compared with the larger swings in total and PDO crashes. Taken together, these sites reflect normal background crash patterns, with gradual changes over time rather than sharp or intervention-driven shifts.

**Table 33: Crashes with their Severity Type at the Treatment Sites**

| Year | Treatment Sites: FI, PDO and Total Crashes, Crash/Year | | | | | | | | | | | |
|---|---|---|---|---|---|---|---|---|---|---|---|---|
| | Bangerter @ 3100 S | | | Bangerter @ 4100 S | | | Bangerter @ 4700 S | | | Bangerter @ 5400 S | | |
| | FI | PDO | Total | FI | PDO | Total | FI | PDO | Total | FI | PDO | Total |
| 2006 | 4 | 4 | 8 | 8 | 10 | 18 | 8 | 21 | 29 | 15 | 44 | 59 |
| 2007 | 7 | 7 | 14 | 14 | 22 | 36 | 18 | 34 | 52 | 12 | 64 | 76 |
| 2008 | 4 | 5 | 9 | 11 | 21 | 32 | 12 | 39 | 51 | 25 | 64 | 89 |
| 2009 | 9 | 8 | 17 | 9 | 16 | 25 | 16 | 29 | 45 | 20 | 40 | 60 |
| 2010 | 2 | 4 | 6 | 4 | 14 | 18 | 10 | 39 | 49 | 12 | 77 | 89 |
| 2011 | 7 | 9 | 16 | 10 | 22 | 32 | 8 | 20 | 28 | 17 | 62 | 79 |
| 2012 | 3 | 7 | 10 | 11 | 31 | 42 | 11 | 18 | 29 | 19 | 50 | 69 |
| 2013 | 6 | 8 | 14 | 16 | 27 | 43 | 7 | 42 | 49 | 20 | 54 | 74 |
| 2014 | 5 | 15 | 20 | 9 | 29 | 38 | 4 | 28 | 32 | 13 | 46 | 59 |
| 2015 | 16 | 15 | 31 | 14 | 24 | 38 | 13 | 38 | 51 | 15 | 46 | 61 |
| 2016 | 4 | 18 | 22 | 17 | 38 | 55 | 8 | 20 | 28 | 16 | 50 | 66 |
| 2017 | 6 | 15 | 21 | 8 | 32 | 40 | 10 | 22 | 32 | 15 | 28 | 43 |
| 2018 | 5 | 20 | 25 | 13 | 52 | 65 | 15 | 39 | 54 | - | - | - |
| 2019 | 8 | 20 | 28 | 13 | 44 | 57 | 22 | 31 | 53 | - | - | - |
| 2020 | 11 | 12 | 23 | 12 | 27 | 39 | 15 | 24 | 39 | - | - | - |
| 2021 | 4 | 10 | 14 | 2 | 32 | 34 | 11 | 36 | 47 | - | - | - |
| Year | Bangerter @ 6200 S | | | Bangerter @ 7000 S | | | Redwood @ 5400 S | | | Redwood @ 6200 S | | |
| | FI | PDO | Total | FI | PDO | Total | FI | PDO | Total | FI | PDO | Total |
| 2006 | 7 | 17 | 24 | 5 | 3 | 8 | 15 | 41 | 56 | 12 | 30 | 42 |
| 2007 | 5 | 24 | 29 | 10 | 14 | 24 | 13 | 39 | 52 | 18 | 42 | 60 |
| 2008 | 12 | 20 | 32 | 7 | 22 | 29 | 9 | 43 | 52 | 15 | 36 | 51 |
| 2009 | 8 | 26 | 34 | 8 | 26 | 34 | 17 | 36 | 53 | 14 | 41 | 55 |
| 2010 | 4 | 27 | 31 | 9 | 21 | 30 | 10 | 37 | 47 | 10 | 34 | 44 |
| 2011 | 16 | 33 | 49 | 9 | 21 | 30 | 19 | 43 | 62 | 6 | 20 | 26 |
| 2012 | 14 | 42 | 56 | 13 | 21 | 34 | 12 | 38 | 50 | 10 | 30 | 40 |
| 2013 | 11 | 37 | 48 | 14 | 30 | 44 | 16 | 32 | 48 | 2 | 27 | 29 |
| 2014 | 8 | 23 | 31 | 18 | 31 | 49 | 14 | 39 | 53 | 5 | 18 | 23 |
| 2015 | 7 | 28 | 35 | 13 | 20 | 33 | 16 | 49 | 65 | 7 | 36 | 43 |
| 2016 | 17 | 42 | 59 | 18 | 25 | 43 | 14 | 41 | 55 | 10 | 29 | 39 |
| 2017 | 17 | 29 | 46 | - | - | - | 19 | 45 | 64 | 15 | 23 | 38 |
| 2018 | 14 | 41 | 55 | - | - | - | 14 | 42 | 56 | 9 | 25 | 34 |
| 2019 | 14 | 51 | 65 | - | - | - | 10 | 48 | 58 | 9 | 18 | 27 |
| 2020 | - | - | - | - | - | - | 13 | 35 | 48 | 15 | 37 | 52 |
| 2021 | - | - | - | - | - | - | 17 | 26 | 43 | 10 | 23 | 33 |


**Figure 42: Plot of crashes with their severity type at the treatment sites**

## Table 34: Crashes with their Severity Type at the Comparison Group

| Year | Comparison Group: FI, PDO and Total Crashes, Crash/Year | | | | | | | | | | | | | | |
|---|---|---|---|---|---|---|---|---|---|---|---|---|---|---|---|
| | Redwood @ 3500 S | | | 5600 W @ 3500 S | | | State @ 4500 S | | | State @ 3300 S | | | 700 E @ 3300 S | | |
| | FI | PDO | Total | FI | PDO | Total | FI | PDO | Total | FI | PDO | Total | FI | PDO | Total |
| 2006 | 8 | 32 | 40 | 23 | 30 | 53 | 12 | 47 | 59 | 22 | 37 | 59 | 15 | 21 | 36 |
| 2007 | 15 | 31 | 46 | 18 | 40 | 58 | 14 | 41 | 55 | 32 | 43 | 75 | 19 | 36 | 55 |
| 2008 | 10 | 17 | 27 | 17 | 20 | 37 | 12 | 29 | 41 | 18 | 21 | 39 | 6 | 18 | 24 |
| 2009 | 16 | 21 | 37 | 14 | 16 | 30 | 10 | 21 | 31 | 12 | 23 | 35 | 8 | 20 | 28 |
| 2010 | 8 | 8 | 16 | 10 | 18 | 28 | 10 | 20 | 30 | 15 | 16 | 31 | 6 | 16 | 22 |
| 2011 | 11 | 15 | 26 | 9 | 17 | 26 | 18 | 20 | 38 | 20 | 21 | 41 | 17 | 31 | 48 |
| 2012 | 14 | 14 | 28 | 20 | 31 | 51 | 12 | 29 | 41 | 16 | 16 | 32 | 10 | 12 | 22 |
| 2013 | 12 | 18 | 30 | 10 | 16 | 26 | 33 | 51 | 84 | 9 | 20 | 29 | 11 | 23 | 34 |
| 2014 | 26 | 36 | 62 | 19 | 25 | 44 | 21 | 49 | 70 | 23 | 20 | 43 | 7 | 23 | 30 |
| 2015 | 38 | 59 | 97 | 14 | 22 | 36 | 28 | 52 | 80 | 13 | 19 | 32 | 15 | 18 | 33 |
| 2016 | 36 | 53 | 89 | 19 | 31 | 50 | 12 | 48 | 60 | 15 | 22 | 37 | 11 | 27 | 38 |
| 2017 | 34 | 62 | 96 | 17 | 47 | 64 | 25 | 48 | 73 | 8 | 24 | 32 | 8 | 23 | 31 |
| 2018 | 17 | 46 | 63 | 16 | 41 | 57 | 12 | 42 | 54 | 12 | 19 | 31 | 6 | 17 | 23 |
| 2019 | 32 | 58 | 90 | 11 | 40 | 51 | 14 | 38 | 52 | 19 | 34 | 53 | 14 | 23 | 37 |
| 2020 | 30 | 45 | 75 | 6 | 33 | 39 | 12 | 25 | 37 | 17 | 25 | 42 | 11 | 33 | 44 |
| 2021 | 36 | 68 | 104 | 5 | 19 | 24 | 18 | 39 | 57 | 18 | 22 | 40 | 10 | 32 | 42 |


**Figure 43: Plots of crashes with their severity type at the comparison group**

## 5.2 Safety Performance Functions (SPF)

The safety performance function (SPF) is a statistical model that predicts the expected number of crashes at a site based on exposure (e.g., AADT) and roadway characteristics. In this study, SPFs from the Highway Safety Manual (HSM) (American Association of State Highway and Transportation Officials [AASHTO] 2010) for signalized intersections are used as the base models.

**Multiple-Vehicle Crashes**

The SPF for total multiple-vehicle crashes is expressed as:

$$N_{bimv} = exp\ (a + b\ ln(AADT_{maj}) + c\ ln(AADT_{min})) \qquad (26)$$

where $N_{bimv}$ is the predicted crash frequency for total multiple-vehicle crashes (crashes/year), $AADT_{maj}$ is the AADT on the major intersection approach (veh/day), $AADT_{min}$ is the AADT on the minor intersection approach (veh/day), and *a, b,* and *c* are regression coefficients.

Equation 26 is applied to estimate $N_{bimv}$ using the coefficients for total crashes provided in Table 35. The total predicted crashes are then divided into severity components: $N_{bimv(FI)}$ for FI crashes, and $N_{bimv(PDO)}$ for PDO crashes. Equation 26 is again used to obtain the preliminary estimates $N'_{bimv(FI)}$and $N'_{bimv(PDO)}$for Equation 27, using the calibrated regression coefficients for FI crashes and PDO crashes, respectively, from Table 35. Finally, adjustments are made to ensure that the sum of $N_{bimv(FI)}$and $N_{bimv(PDO)}$equals $N_{bimv(total)}$, as expressed in Equation 28.

$$N_{bimv(FI)} = N_{bimv(total)} \left( \frac{N'_{bimv(FI)}}{N'_{bimv(FI)} + N'_{bimv(PDO)}} \right) \qquad (27)$$

$$N_{bimv(PDO)} = N_{bimv(total)} - N_{bimv\ (FI)} \qquad (28)$$

Table 35 presents the coefficients *a, b, c*, and the SPF overdispersion parameter *k* used in Equations 26, 26, and 28 for multiple-vehicle collisions at 4SG intersections.

**Single-Vehicle Crashes**

SPFs for single-vehicle crashes are applied in the same form as Equation 26, but with different coefficients. The SPF is given in Equation 29, while the regression coefficients are provided in Table 3.

**Table 35: SPF Coefficients for Multiple-Vehicle Crashes at Four-Leg Signalized Intersections (American Association of State Highway and Transportation Officials [AASHTO] 2010)**

| Crash Type | Intercept (a) | $AADT_{maj}$ (b) | $AADT_{min}$ (c) | Overdispersion (k) |
|---|---|---|---|---|
| Total crashes | -10.99 | 1.07 | 0.23 | 0.39 |
| Fatal-and-injury crashes | -13.14 | 1.18 | 0.22 | 0.33 |
| Property-damage-only crashes | -11.02 | 1.02 | 0.24 | 0.44 |

$N_{biSV} = exp\ (a + b\ ln\ (AADT_{maj}) + c\ ln\ (AADT_{min}))$ (29)

Equation 29 is first applied to determine $N_{biSV(total)}$ using the coefficients for total crashes in Table 36. The predicted $N_{biSV(total)}$ is then divided into components by severity level: $N_{biSV(FI)}$ for FI crashes, and $N_{biSV(PDO)}$ for PDO crashes. Preliminary values of $N_{biSV(FI)}$ and $N_{biSV(PDO)}$, designated as $N'_{biSV(FI)}$ and $N'_{biSV(PDO)}$ in Equation 30, are determined using Equation 31 with the coefficients for FI and PDO crashes, respectively, from Table 36. Adjustments are then made to ensure that $N_{biSV(FI)}$ and $N_{biSV(PDO)}$ sum to $N_{biSV(total)}$, as in Equation 31.

$$N_{biSV(FI)} = N_{biSV(total)} \left( \frac{N'_{biSV(FI)}}{N'_{biSV(FI)} + N'_{biSV(PDO)}} \right) \qquad (30)$$

$$N_{biSV(PDO)} = N_{biSV(total)} - N_{biSV\,(FI)} \qquad (31)$$

**Table 36: SPF Coefficients for Single-Vehicle Crashes at Four-Leg Signalized Intersections (AASHTO 2010)**

| Crash Type | Intercept (a) | $AADT_{maj}$ (b) | $AADT_{min}$ (c) | Overdispersion (k) |
|---|---|---|---|---|
| Total crashes | -10.21 | 0.68 | 0.27 | 0.36 |
| Fatal-and-injury crashes | -9.25 | 0.43 | 0.29 | 0.09 |
| Property-damage-only crashes | -11.34 | 0.78 | 0.25 | 0.44 |

### Pedestrian and Bicycle Crashes

The HSM also provides SPFs for vehicle-pedestrian and vehicle-bicycle collisions. However, pedestrian and bicycle volumes at intersections are not available in this study. A conservative value of 4% is justified because Utah crash data from 2010–2021 indicate that pedestrian and bicycle crashes constitute approximately 3.37% of all multiple-vehicle crashes, and rounding upward accounts for interannual variability while reducing the risk of systematic underestimation in the analysis (Utah Department of Public Safety, Highway Safety Office 2025). For that reason, it is assumed that vehicle-pedestrian and vehicle-bicycle crashes combined are approximately 4% of the multiple-vehicle crashes:

$$N_{bi(ped/bike)} = 0.04\ N_{bimv} \qquad (32)$$

### Crash Modification Factors (CMFs)

CMFs are used to adjust the SPF estimate of predicted average crash frequency for the effect of individual geometric design and traffic control features. The CMFs for signalized intersections from the HSM include CMFs for exclusive left-turn lanes ($CMF_{LT}$), exclusive right-turn lanes ($CMF_{RT}$), and left-turn phasing ($CMF_{LTphase}$). $CMF_{LT}$ and $CMF_{RT}$ are determined based on the intersection type (4SG) and the number of approaches with left- or right-turn lanes. $CMF_{LTphase}$ is determined separately for protected, permitted, or protected/permitted left-turn signal phasing for each intersection approach, and then the obtained values are multiplied to determine $CMF_{LTphase}$ for the entire intersection.

For the local conditions considered in this study, intersections are assumed to have lighting ($CMF_{Lighting}$ = 0.91), but red-light cameras are not installed ($CMF_{Red\text{-}light\ camera}$ = 1.0) and right turns on red are not permitted ($CMF_{Right\text{-}turn\text{-}on\text{-}red}$ = 1.0). Accordingly, the combined crash modification factor for the intersection ($CMF_{comb}$) can be expressed as:

$$CMF_{comb} = CMF_{LT} \times CMF_{RT} \times CMF_{LTphase} \times CMF_{Lighting} \qquad (33)$$

In this study, intersection left-turn signal phasing was observed to change during the different year. These changes were accounted for by calculating the combined CMF values for the respective periods.

**Table 37 CMFs for Geometry and Signal Phasing at Signalized Intersections (AASHTO 2010)**

| **$CMF_{LT}$ for installation of left-turn lanes** | | | | |
|---|---|---|---|---|
| # approaches | One | Two | Three | Four |
| CMF values | 0.9 | 0.81 | 0.73 | 0.66 |
| **$CMF_{RT}$ for installation of right-turn lanes** | | | | |
| # approaches | One | Two | Three | Four |
| CMF values | 0.96 | 0.92 | 0.88 | 0.85 |
| **$CMF_{LTphase}$ for type of left-turn signal phasing** | | | | |
| Type | Protected LT | Permitted LT | Protected/permitted LT | |
| CMF values | 0.94 | 1 | 0.99 | |

The number of predicted crashes for an entire intersection can then be determined with:

$$N'_{pred} = CMF_{comb}\ (N_{bimv} + N_{bisv} + N_{bi(ped/bike)}) \qquad (34)$$

This equation is used for total FI and PDO crashes.

## Calibration for Local Conditions

### SPF Calibration for Local Conditions for Signalized Intersections

The local calibration factor is computed as:

$$C_{UT} = \frac{\sum_{2006}^{2021} N_{total\ Observed}}{\sum_{2006}^{2021} N'_{pred}} \qquad (35)$$

The calibration factors $C_{UT}$ for local conditions were estimated as 6.434 for FI, 6.153 for PDO, and 6.248 for total crashes. These values account for region-specific roadway, traffic, and environmental characteristics that influence crash frequency, ensuring that the model predictions align closely with observed data. The values exceed unity because the HSM predictive models for urban signalized intersections were developed using a broad range of intersection types, including lower-volume facilities, whereas the dataset used in this study consists solely of major intersections. Major intersections generally experience higher traffic volumes and greater conflict exposure, resulting in higher observed crash frequencies than those predicted by the base HSM models. Consequently, the calibration factors adjust the HSM predictions to reflect the intersection types and exposure levels represented in the study sample, improving model applicability under local conditions and enhancing the regional validity of the resulting CMFs for safety analysis and planning.

The calibrated form of the predicted crashes becomes:

$$N''_{pred} = C_{UT}\, CMF_{comb}\, (N_{bimv} + N_{bisv} + N_{bi(ped/bike)}) \qquad (36)$$

To determine the local calibration factor $C_{UT}$, an analysis was performed using crash data for five four-leg signalized intersections over a 15-year period (2006–2021). These intersections represent the comparison group for the EB analysis described in the next section. From the comparison sites, the yearly modification factor $a_y$ is calculated as:

$$a_y = \frac{\sum_{Year} N_{observed}}{\sum_{Year} N''_{pred}} \qquad (37)$$

The yearly modification factor ($a_y$) is defined as the ratio of observed to predicted crashes for a given year, aggregated across all sites. It captures year-to-year variations in crash frequency that may result from changes in external factors such as traffic volumes, enforcement levels, or weather conditions. By quantifying these fluctuations, $a_y$ serves as a temporal adjustment factor that refines the predicted crash estimates for treatment sites, ensuring they align more closely with observed trends over time. This enhances the accuracy of the safety-effectiveness evaluation.

**Table 38: Annual Crash-Rate Modification Factors by Year**

| Year | $a_y$ for FI | $a_y$ for PDO | $a_y$ for Total |
|---|---|---|---|
| 2006 | 0.95 | 1.06 | 1.02 |
| 2007 | 1.14 | 1.19 | 1.17 |
| 2008 | 0.74 | 0.67 | 0.69 |
| 2009 | 0.71 | 0.64 | 0.67 |
| 2010 | 0.6 | 0.52 | 0.55 |
| 2011 | 0.98 | 0.73 | 0.81 |
| 2012 | 0.96 | 0.73 | 0.81 |
| 2013 | 1.06 | 0.96 | 1 |
| 2014 | 1.31 | 1.11 | 1.18 |
| 2015 | 1.46 | 1.22 | 1.3 |
| 2016 | 1.13 | 1.18 | 1.16 |
| 2017 | 1.09 | 1.31 | 1.23 |
| 2018 | 0.74 | 1.05 | 0.94 |
| 2019 | 1.05 | 1.21 | 1.15 |
| 2020 | 1.06 | 1.2 | 1.15 |
| 2021 | 1.11 | 1.23 | 1.19 |

Table 38 presents the yearly modification factors ($a_y$) for FI, PDO, and total crashes at comparison sites. These factors adjust the predicted crash frequencies at treatment locations by accounting for background crash trends unrelated to the intervention. The $a_y$ values fluctuate over time, indicating variability in crash patterns across years. Higher ratios in 2007 and 2015–2017 suggest years with relatively higher crash frequencies, while lower ratios between 2008 and 2012, and again in 2018–2020, reflect reduced crash occurrence. This temporal adjustment ensures that the evaluation more accurately isolates the safety effects of the treatment from general statewide crash trends.

Using this yearly modification factor $a_y$, the predicted number of crashes for treatment sites is computed as:

$$N_{pred} = a_y \cdot C_{UT} \cdot CMF_{comb} \cdot N''_{pred} \qquad (38)$$

The predicted number of FI, PDO and total crashes at the treatment sites using Equation 28 are given in the Table 39, Table 40, and Table 41 respectively.

**Table 39: Predicted Number of FI Crashes at Treatment Sites**

| Year | FI: Predicted Number of Crashes, Crash/Year ($N_{pred}$) | | | | | | | |
|---|---|---|---|---|---|---|---|---|
| | Bangerter @ 3100 S | Bangerter @ 4100 S | Bangerter @ 4700 S | Bangerter @ 5400 S | Bangerter @ 6200 S | Bangerter @ 7000 S | Redwood @ 5400 S | Redwood @ 6200 S |
| 2006 | 17.9 | 20.6 | 21.7 | 19.6 | 23.2 | 14.6 | 28.5 | 14.1 |
| 2007 | 21.7 | 25.2 | 26.3 | 24.0 | 28.4 | 18.7 | 35.2 | 17.2 |
| 2008 | 13.4 | 15.5 | 16.2 | 14.8 | 15.9 | 12.0 | 21.4 | 10.6 |
| 2009 | 12.9 | 15.0 | 15.7 | 14.6 | 15.3 | 11.8 | 20.7 | 10.2 |
| 2010 | 11.0 | 12.8 | 13.2 | 12.4 | 13.0 | 10.1 | 17.4 | 8.7 |
| 2011 | 17.1 | 16.0 | 20.5 | 19.5 | 20.3 | 15.7 | 25.1 | 22.7 |
| 2012 | 15.2 | 15.6 | 20.1 | 19.1 | 19.9 | 15.4 | 24.1 | 22.2 |
| 2013 | 17.2 | 17.6 | 23.1 | 21.6 | 22.5 | 18.8 | 25.9 | 25.2 |
| 2014 | 22.3 | 22.8 | 30.0 | 28.0 | 29.1 | 24.4 | 32.3 | 32.6 |
| 2015 | 26.4 | 27.0 | 35.7 | 35.3 | 34.6 | 26.3 | 38.1 | 38.7 |
| 2016 | 21.9 | 22.4 | 29.5 | 29.3 | 28.7 | 22.6 | 31.9 | 32.2 |
| 2017 | 22.1 | 22.5 | 29.7 | 29.5 | 28.9 | - | 32.1 | 32.4 |
| 2018 | 15.3 | 15.6 | 20.6 | - | 20.0 | - | 22.2 | 22.5 |
| 2019 | 21.8 | 22.2 | 29.3 | - | 28.5 | - | 31.9 | 32.0 |
| 2020 | 18.4 | 18.8 | 24.6 | - | - | - | 27.8 | 27.0 |
| 2021 | 23.9 | 22.4 | 29.5 | - | - | - | 32.3 | 32.2 |

**Table 40: Predicted Number of PDO Crashes at Treatment Sites**

| Year | PDO: Predicted Number of Crashes, Crash/Year | | | | | | | |
|---|---|---|---|---|---|---|---|---|
| | Bangerter @ 3100 S | Bangerter @ 4100 S | Bangerter @ 4700 S | Bangerter @ 5400 S | Bangerter @ 6200 S | Bangerter @ 7000 S | Redwood @ 5400 S | Redwood @ 6200 S |
| 2006 | 35.4 | 40.9 | 42.5 | 39.1 | 44.9 | 29.4 | 55.0 | 29.2 |
| 2007 | 40.0 | 46.8 | 48.1 | 44.7 | 51.3 | 34.8 | 63.3 | 33.2 |
| 2008 | 21.2 | 24.8 | 25.5 | 23.7 | 25.0 | 19.1 | 33.1 | 17.6 |
| 2009 | 20.6 | 24.1 | 24.9 | 23.6 | 24.3 | 18.8 | 32.5 | 17.1 |
| 2010 | 16.6 | 19.4 | 19.8 | 19.0 | 19.5 | 15.3 | 25.8 | 13.8 |
| 2011 | 22.5 | 21.7 | 26.7 | 26.1 | 26.5 | 20.8 | 32.3 | 28.9 |
| 2012 | 20.4 | 21.6 | 26.7 | 25.9 | 26.4 | 20.7 | 31.6 | 28.8 |
| 2013 | 27.4 | 29.1 | 36.5 | 34.9 | 35.6 | 29.8 | 40.8 | 38.8 |
| 2014 | 33.1 | 35.0 | 44.3 | 42.1 | 42.9 | 35.9 | 47.6 | 46.7 |
| 2015 | 38.7 | 41.0 | 51.9 | 52.1 | 50.2 | 38.6 | 55.4 | 54.7 |
| 2016 | 39.7 | 41.9 | 53.1 | 53.3 | 51.4 | 40.8 | 57.2 | 56.1 |
| 2017 | 45.5 | 48.0 | 60.9 | 61.1 | 59.0 | - | 65.7 | 64.4 |
| 2018 | 37.2 | 39.2 | 49.8 | - | 48.2 | - | 53.5 | 52.7 |
| 2019 | 43.4 | 45.8 | 58.0 | - | 56.3 | - | 63.0 | 61.5 |
| 2020 | 36.2 | 38.3 | 48.1 | - | - | - | 54.0 | 51.3 |
| 2021 | 45.3 | 44.5 | 56.2 | - | - | - | 61.4 | 59.6 |

**Table 41: Predicted Number of Total Crashes at Treatment Sites**

| Year | Total: Predicted Number of Crashes, Crash/Year | | | | | | | |
|---|---|---|---|---|---|---|---|---|
| | Bangerter @ 3100 S | Bangerter @ 4100 S | Bangerter @ 4700 S | Bangerter @ 5400 S | Bangerter @ 6200 S | Bangerter @ 7000 S | Redwood @ 5400 S | Redwood @ 6200 S |
| 2006 | 53.3 | 61.5 | 64.2 | 58.7 | 68.2 | 44.0 | 83.5 | 43.4 |
| 2007 | 61.7 | 72.0 | 74.3 | 68.7 | 79.7 | 53.5 | 98.5 | 50.4 |
| 2008 | 34.6 | 40.3 | 41.7 | 38.5 | 40.9 | 31.1 | 54.5 | 28.2 |
| 2009 | 33.5 | 39.1 | 40.6 | 38.1 | 39.7 | 30.6 | 53.3 | 27.4 |
| 2010 | 27.6 | 32.1 | 33.0 | 31.3 | 32.6 | 25.4 | 43.1 | 22.5 |
| 2011 | 39.6 | 37.7 | 47.2 | 45.6 | 46.9 | 36.5 | 57.4 | 51.6 |
| 2012 | 35.6 | 37.2 | 46.8 | 45.0 | 46.3 | 36.0 | 55.6 | 51.0 |
| 2013 | 44.7 | 46.7 | 59.5 | 56.6 | 58.1 | 48.7 | 66.7 | 64.0 |
| 2014 | 55.3 | 57.9 | 74.3 | 70.1 | 72.0 | 60.3 | 79.9 | 79.3 |
| 2015 | 65.2 | 68.0 | 87.6 | 87.4 | 84.8 | 64.8 | 93.5 | 93.4 |
| 2016 | 61.6 | 64.3 | 82.6 | 82.6 | 80.1 | 63.4 | 89.1 | 88.3 |
| 2017 | 67.5 | 70.5 | 90.6 | 90.6 | 87.9 | - | 97.8 | 96.8 |
| 2018 | 52.5 | 54.8 | 70.4 | - | 68.3 | - | 75.8 | 75.2 |
| 2019 | 65.2 | 68.0 | 87.4 | - | 84.8 | - | 94.9 | 93.5 |
| 2020 | 54.6 | 57.0 | 72.8 | - | - | - | 81.7 | 78.3 |
| 2021 | 69.3 | 66.9 | 85.8 | - | - | - | 93.7 | 91.9 |

## 5.3 Empirical Bayes Before- After Analysis

This study applies a robust data-driven methodology to assess the safety effectiveness of CFIs in Utah using the EB before–after evaluation approach. The EB method is a well-established statistical technique in roadway safety research that addresses key biases such as regression-to-the-mean and site selection effects. By combining observed crash data with expected crash frequencies derived from SPFs, the method offers a more accurate estimate of the treatment's safety impact. The following steps are needed to conduct an EB before-after evaluation:

***Predicted Crashes in the After Period (Had Treatment Not Been Applied)***

Let $\hat{\pi}_j$ represent the predicted number of crashes in the after period for site $j$, had the treatment not been applied. Then:

$$\hat{\pi}_j = C_j . M_j \tag{39}$$

Where: $C_j = \frac{\sum(predicted\ crashes\ in\ after\ period\ for\ site\ j)}{\sum(predicted\ crashes\ in\ before\ for\ site\ j)} = \frac{\sum N_{pred}(treatment\ sites,\ \ after\ period)}{\sum N_{pred}(treatment\ sites,\ \ before\ period)}$

and $M_j = w.\ P_j + (1 - w).\ K_j$ *with* $K_j$ is the total observed crashes in the before period for site $j$, $P_j$ is the total predicted crashes in the before period for site $j$, *and* $w = 1/\ (1 + k\,P_j)$ the weight based on the overdispersion parameter $k$.

The total predicted crash across all sites is:

$$\hat{\pi}_j = \sum_j \hat{\pi}_J \tag{40}$$

The remaining steps for variance of predicted crashes, observed crashes in the “after” period, estimate of CMF for treatment, and crash reduction estimate are the same as those used in the previous section of the EB before–after for the DDI.

## 5.4 Crash Reductions and CMF Estimates

From Table 42, the EB analysis results indicate notable reductions in both FI and PDO crashes following implementation of the studied treatment. The predicted number of FI crashes ($\hat{\pi}$) was 1,240.39 compared with 862 observed crashes ($\hat{\lambda}$), resulting in an estimated CMF ($\hat{\theta}$) of 0.69, which corresponds to a 30.71% ± 4.41% reduction. Similarly, PDO crashes were predicted at 2,903.58, but only 2,274 were observed, yielding a CMF of 0.78 and a 21.78% ± 3.16% reduction. The total crash CMF was 0.76, translating to an overall crash reduction of 24.47% ± 2.59%.

The corresponding crash-reduction counts (δ) were 378.39, 629.58, and 1,012.45 for FI, PDO, and total crashes, respectively. The low variances and standard deviations ($\sigma\{\hat{\theta}\}$ = 0.03–0.04) indicate that these estimates are statistically robust and reliable. Collectively, these findings demonstrate that the treatment substantially improves roadway safety by reducing both the frequency and severity of crashes. This consistent crash reduction across severity levels reinforces the intervention’s effectiveness and supports its broader application for safety enhancement on similar roadway facilities.

**Table 42: Crash Prediction and Reduction Parameters**

| Parameters | FI Crashes | PDO Crashes | Total Crashes |
|---|---|---|---|
| $\hat{\pi}$ (Predicted crashes) | 1,240.39 | 2,903.58 | 4,148.45 |
| VAR ($\hat{\pi}$) | 4,471.85 | 10,096.13 | 14,813.67 |
| $\hat{\lambda}$ (Observed crashes) | 862 | 2274 | 3136 |
| VAR ($\hat{\lambda}$) | 862 | 2274 | 3136 |
| $\hat{\theta}$ (Estimated CMF) | **0.69** | **0.78** | **0.76** |
| Crash Reduction | 30.71% ± 4.41% | 21.78% ± 3.16% | 24.47% ± 2.59% |
| VAR ($\hat{\theta}$) | 0.002 | 0.001 | 0.001 |
| $\sigma(\hat{\theta})$ | 0.04 | 0.03 | 0.03 |
| $\delta$ (Crash reduction count) | 378.39 | 629.58 | 1,012.45 |
| VAR($\delta$) | 5,333.85 | 12,370.13 | 17,949.67 |

## 5.5 Comparison with Previous CFI Studies

The results in Table 43 indicate that the estimated safety effects vary across studies, reflecting differences in study design, data, and locations. Most prior studies report CMFs close to or below 1.0 for total crashes, suggesting modest reductions in crashes following treatment, although some studies observed increases for specific crash types. In contrast, this study shows a more pronounced reduction in crashes, with CMFs of 0.69 for FI crashes, 0.78 for PDO crashes, and 0.76 for total crashes, indicating substantial safety benefits.

**Table 43: Comparison of Crash Modification Factors (CMFs) Across Studies**

| Author(s) & Reference | State / Location | CMF – FI Crashes | CMF – PDO Crashes | CMF – Total Crashes | Study Method |
|---|---|---|---|---|---|
| (Zlatkovic and Kergaye 2018; Zlatkovic 2019) | UT | – | – | 0.877 | Empirical Bayes before–after |
| (Abdelrahman et al. 2020; Abdelrahman 2020) | UT, CO, LA, OH | 1.22 | 1.07 | 1.11 | Before–after with comparison group + cross-sectional model |
| (Chris Cunningham et al. 2022) | UT, TX, CO, GA, MD, OH, MS, LA | 0.861 | 0.882 | 0.878 | Empirical Bayes |
| (LaDOTD 2007; Hughes et al. 2010) | LA | 0.81 | – | 0.76 | Simple before–after |
| This Study | **UT** | **0.69** | **0.78** | **0.76** | Empirical Bayes before–after |

## 5.6 Conclusion

This study provides a comprehensive safety evaluation of CFIs using an empirical Bayes (EB) before–after methodology based on locally calibrated SPFs. By combining 16 years of crash and AADT data from eight CFI treatment sites and five conventional signalized comparison sites, the analysis isolates the safety effects of CFI implementation from background trends in traffic volumes and crash occurrence. The use of HSM-based SPFs, adjusted with region-specific calibration factors and crash modification factors (CMFs) for geometry, signal phasing, and lighting, ensured that predictions captured local operating conditions and design practices.

The results show that CFIs in Utah are associated with substantial and statistically significant reductions in both the frequency and severity of crashes. After CFI implementation, fatal-and-injury (FI) crashes decreased by approximately 30.7% (CMF = 0.69), property-damage-only (PDO) crashes by 21.8% (CMF = 0.78), and total crashes by 24.5% (CMF = 0.76) compared with the expected values had the intersections remained in their conventional configuration. In absolute terms, this corresponds to an estimated reduction of about 378 FI crashes and 630 PDO crashes over the study period.

Several limitations should be acknowledged. The analysis is based on a relatively small sample of CFI sites within a single state, and pedestrian and bicycle exposure had to be approximated rather than directly measured. In addition, geometric and operational details (such as driveway density or enforcement levels) could not be modeled explicitly at each site. These factors suggest that while the results are robust for the studied context, caution is warranted when transferring the CMFs directly to substantially different environments. Overall, this study adds to the growing evidence that CFIs, when thoughtfully implemented, can deliver meaningful and sustained safety benefits alongside their operational and environmental advantages.

# 6. CONCLUSIONS AND RECOMMENDATIONS

This report presents a comprehensive, dual-framework evaluation of the operational and safety performance of DDIs and CFIs under Utah-specific conditions. Recognizing the limitations of traditional, siloed assessment methods, this research successfully integrated crash-based empirical evaluations with safety-integrated microscopic traffic simulations. By analyzing 16 years of historical crash and traffic data (2006–2021) and developing highly calibrated PTV VISSIM models, the study provides a robust, data-driven foundation for assessing these innovative geometric designs.

The simulation-based framework demonstrated that microscopic modeling, when calibrated with both operational metrics and surrogate safety measures, can reliably predict crash frequencies. The developed PTV VISSIM models successfully replicated field conditions, achieving GEH statistics below 5 and average speed percent errors under 2% for both calibration and independent validation datasets. By extracting TTC and MaxD from SSAM and applying a bivariate POT-EVT approach, the methodology successfully translated simulated vehicle conflicts into highly accurate annual crash estimates. The validation process further revealed that CFIs exhibited highly stable and predictable traffic flow and conflict characteristics. Conversely, DDIs displayed slightly higher variability in surrogate safety crash estimation, reflecting the heightened complexity of vehicle interactions, weaving maneuvers, and unconventional movement paths inherent to the crossover design.

The EB before–after analysis confirmed that both DDIs and CFIs deliver substantial and statistically significant safety benefits, particularly in mitigating high-severity collisions. By developing locally calibrated SPFs and adjusting for year-to-year statewide crash trends, the evaluation generated highly reliable, Utah-specific crash modification factors (CMFs). For DDIs, the analysis showed a 47.8% reduction in fatal-and-injury (FI) crashes (a CMF of 0.522) and a 28.1% reduction in property-damage-only (PDO) crashes (a CMF of 0.719). The notably lower CMF for FI crashes shows the DDI's effectiveness in eliminating severe conflict points, such as opposing left turns. Similarly, CFIs demonstrated a 30.7% reduction in FI crashes (a CMF of 0.69) and a 21.8% reduction in PDO crashes (a CMF of 0.78), corresponding to an overall total crash reduction of 24.5% (a CMF of 0.76). These reductions prove that relocating left-turn movements upstream successfully decreases exposure to severe angle crashes without compromising intersection throughput.

The findings provide transportation agencies with defensible, locally calibrated tools for evidence-based decision-making. The Utah-specific CMFs derived in this study offer a more accurate alternative to national averages for regional safety planning, benefit-cost analyses, and alternative intersection selection. Furthermore, the proven transferability of the safety-integrated microscopic simulation framework empowers engineers to proactively evaluate the safety of proposed geometric designs and signal timing strategies before physical implementation.

While this study establishes a robust baseline for evaluating DDIs and CFIs, future work should address existing limitations and expand the analytical framework to accommodate evolving traffic dynamics. Future analyses should incorporate a broader diversity of intersection geometries, such as varying crossover angles, ramp terminal spacing, and rural versus urban settings, while isolating CMFs for specific manners of collision to provide more granular design guidance. Since simulation accuracy is highly dependent on predefined driver behavior parameters, future studies should also integrate high-resolution vehicle trajectory data and computer vision algorithms to refine microscopic models. Incorporating advanced behavioral frameworks, such as inverse reinforcement learning or game-theoretic models, can better capture complex gap acceptance, lane-changing, and cut-in behaviors at these unconventional junctions. As the vehicle fleet evolves, it will be critical to

evaluate how connected and automated vehicle (CAVs) interact with human-driven vehicles at DDIs and CFIs. Future simulation studies should utilize the established EVT-based framework to model mixed-traffic flow, testing collective action strategies and advanced car-following models to anticipate how CAV integration will impact the operational efficiency and safety of innovative intersection designs. Finally, further investigation is recommended to test the sensitivity of the bivariate EVT model to different conflict thresholds and to explore additional metrics, such as PET or DRAC, to continually improve proactive crash estimation.

# 7. REFERENCES

Abdelrahman, Ahmed. 2020. "Safety Evaluation of Innovative Intersection Designs: Diverging Diamond Interchanges and Displaced Left-Turn Intersections." Master's Thesis, University of Central Florida.

Abdelrahman, Ahmed, Mohamed Abdel-Aty, Jaeyoung Lee, Lishengsa Yue, and Ma'en Mohammad Ali Al-Omari. 2020. "Evaluation of Displaced Left-Turn Intersections." *Transportation Engineering* 1 (June): 100006. https://doi.org/10.1016/j.treng.2020.100006.

Abdelrahman, Ahmed, Mohamed Abdel-Aty, Jinghui Yuan, and Ma'en M. A. Al-Omari. 2021. "Systematic Safety Evaluation of Diverging Diamond Interchanges Based on Nationwide Implementation Data." *Transportation Research Record: Journal of the Transportation Research Board* 2675 (9): 961–71. https://doi.org/10.1177/03611981211004961.

Ahmed, Talha, Asad Ali, Ying Huang, and Pan Lu. 2025. "Evaluating the Impact of Human-Driven and Autonomous Vehicles in Adverse Weather Conditions Using a Verkehr in Städten—SIMulationsmodell (VISSIM) and Surrogate Safety Assessment Model (SSAM)." *Electronics* 14 (10): 2046. https://doi.org/10.3390/electronics14102046.

Ali, Yasir, Md Mazharul Haque, and Fred Mannering. 2023a. "Assessing Traffic Conflict/Crash Relationships with Extreme Value Theory: Recent Developments and Future Directions for Connected and Autonomous Vehicle and Highway Safety Research." *Analytic Methods in Accident Research* 39 (September): 100276. https://doi.org/10.1016/j.amar.2023.100276.

Ali, Yasir, Md Mazharul Haque, and Fred Mannering. 2023b. "Assessing Traffic Conflict/Crash Relationships with Extreme Value Theory: Recent Developments and Future Directions for Connected and Autonomous Vehicle and Highway Safety Research." *Analytic Methods in Accident Research* 39 (September): 100276. https://doi.org/10.1016/j.amar.2023.100276.

Allen, Brian L., B. Tom Shin, and Peter J. Cooper. 1978. *Analysis of Traffic Conflicts and Collisions*. https://onlinepubs.trb.org/Onlinepubs/trr/1978/667/667-009.pdf.

Almoshaogeh, Meshal, Hatem Abou-Senna, Essam Radwan, and Husnain Haider. 2020. "Sustainable Design of Diverging Diamond Interchange: Development of Warrants for Improving Operational Performance." *Sustainability* 12 (14): 5840. https://doi.org/10.3390/su12145840.

American Association of State Highway and Transportation Officials (AASHTO). 2010. *Highway Safety Manual*. Washington, DC, USA.

Archer, Jeffery. 2005. *Indicators for Traffic Safety Assessment and Prediction and Their Application in Micro-Simulation Modelling: A Study of Urban and Suburban Intersections*. Stockholm.

Astarita, Vittorio, Giuseppe Guido, and Alessandro Vitale. 2012. *A New Microsimulation Model for the Evaluation of Traffic Safety Performances*. no. 51.

Badgley, Jonathan, Joshua Fowler, Kendall Mahavier, and Sean Peirce. 2021. *FHWA Research and Technology Evaluation: Innovative Intersection Design*. FHWA-HRT-21-024. https://highways.dot.gov/sites/fhwa.dot.gov/files/FHWA-HRT-21-024.pdf.

Bared, Joe G., Praveen K. Edara, and Ramanujan Jagannathan. 2005. "Design and Operational Performance of Double Crossover Intersection and Diverging Diamond Interchange." *Transportation Research Record: Journal of the Transportation Research Board* 1912 (1): 31–38. https://doi.org/10.1177/0361198105191200104.

Bonneson, James A., Srinivas Geedipally, Michael P. Pratt, et al. 2021. *Safety Prediction Methodology and Analysis Tool for Freeways and Interchanges*. Transportation Research Board. https://doi.org/10.17226/26367.

Chilukuri, Venkata, Smith Siromaskul, Michael Trueblood, and Tom Ryan. 2011. *Diverging Diamond Interchange Performance Evaluation (I-44 and Route 13)*. Nos. OR11-012.

Chlewicki, Gilbert. 2003. "New Interchange and Intersection Designs: The Synchronized Split-Phasing Intersection and the Diverging Diamond Interchange."

Ciuffo, Biagio, and Carlos Lima Azevedo. 2014. "A Sensitivity-Analysis-Based Approach for the Calibration of Traffic Simulation Models." *IEEE Transactions on Intelligent Transportation Systems* 15 (3): 1298–309. https://doi.org/10.1109/TITS.2014.2302674.

Claros, Boris, Praveen Edara, and Carlos Sun. 2016. "Site-Specific Safety Analysis of Diverging Diamond Interchange Ramp Terminals." *Transportation Research Record: Journal of the Transportation Research Board* 2556 (1): 20–28. https://doi.org/10.3141/2556-03.

Claros, Boris, Praveen Edara, and Carlos Sun. 2017a. "Safety Effect of Diverging Diamond Interchanges on Adjacent Roadway Facilities." *Transportation Research Record: Journal of the Transportation Research Board* 2618 (1): 78–90. https://doi.org/10.3141/2618-08.

Claros, Boris, Praveen Edara, and Carlos Sun. 2017b. "When Driving on the Left Side Is Safe: Safety of the Diverging Diamond Interchange Ramp Terminals." *Accident Analysis & Prevention* 100 (March): 133–42. https://doi.org/10.1016/j.aap.2017.01.014.

Claros, Boris R., Praveen Edara, Carlos Sun, and Henry Brown. 2015. "Safety Evaluation of Diverging Diamond Interchanges in Missouri." *Transportation Research Record: Journal of the Transportation Research Board* 2486 (1): 1–10. https://doi.org/10.3141/2486-01.

Cunningham, Chris, Taehun Lee, Taha Saleem, and Raghavan Srinivasan. 2022. "Development of a Crash Modification Factor for Conversion of a Conventional Signalized Intersection to a CFI." August 29.

Cunningham, Christopher, Thomas Chase, Yulin Deng, et al. 2021. *Diverging Diamond Interchange Informational Guide, Second Edition*. Transportation Research Board. https://doi.org/10.17226/26027.

Dhatrak, Amit, Praveen Edara, and Joe G. Bared. 2010. "Performance Analysis of Parallel Flow Intersection and Displaced Left-Turn Intersection Designs." *Transportation Research Record: Journal of the Transportation Research Board* 2171 (1): 33–43. https://doi.org/10.3141/2171-04.

Dowling, Richard, Alexander Skabardonis, and Vassili Alexiadis. 2004. *Traffic Analysis Toolbox Volume III: Guidelines for Applying Traffic Microsimulation Modeling Software*. FHWA-HRT-04-040. https://highways.dot.gov/sites/fhwa.dot.gov/files/FHWA-HRT-04-040.pdf.

Esawey, Mohamed El, and Tarek Sayed. 2007. “Comparison of Two Unconventional Intersection Schemes: Crossover Displaced Left-Turn and Upstream Signalized Crossover Intersections.” *Transportation Research Record: Journal of the Transportation Research Board* 2023 (1): 10–19. https://doi.org/10.3141/2023-02.

FHWA. 2025. *CMF Clearinghouse*. Webpage. U.S. Department of Transportation. https://cmfclearinghouse.fhwa.dot.gov/.

Gettman, Douglas, and Larry Head. 2003. “Surrogate Safety Measures from Traffic Simulation Models.” *Transportation Research Record: Journal of the Transportation Research Board* 1840 (1): 104–15. https://doi.org/10.3141/1840-12.

Haq, Muhammad Tahmidul, Amirarsalan Mehrara Molan, and Khaled Ksaibati. 2022. "Proposing the Super DDI Design to Improve the Performance of Failing Service Interchanges in Denver Metro, Colorado" (MPC-22-461).

Hayward, John C. 1972. "NEAR-MISS DETERMINATION THROUGH USE OF A SCALE OF DANGER."

Hughes, Warren, Ram Jagannathan, Dibu Sengupta, and Joe Hummer. 2010. *Alternative Intersections/Interchange: Informational Report (AIIR)*. FHWA-HRT-09-060. https://www.fhwa.dot.gov/publications/research/safety/09060/09060.pdf.

Hummer, Joseph E., Christopher M. Cunningham, Raghavan Srinivasan, et al. 2016. “Safety Evaluation of Seven of the Earliest Diverging Diamond Interchanges Installed in the United States.” *Transportation Research Record: Journal of the Transportation Research Board* 2583 (1): 25–33. https://doi.org/10.3141/2583-04.

Hunter, Michael, Angshuman Guin, James Anderson, and Sung Jun Park. 2019. “Operating Performance of Diverging Diamond Interchanges.” *Transportation Research Record: Journal of the Transportation Research Board* 2673 (11): 801–12. https://doi.org/10.1177/0361198119855341.

LaDOTD. 2007. *Continous Flow Intersection (CFI) Report US 61(Airline Highway) @LA 3246 (Siegen Lane)*.

Liu, Huasheng, Haoran Deng, Jin Li, Sha Yang, Kui Dong, and Yuqi Zhao. 2025. “Calibration Method for Microscopic Traffic Simulation Considering Lane Difference.” *SIMULATION* 101 (6): 625–44. https://doi.org/10.1177/00375497241268740.

Lloyd, Holly, and Ziqi Song. 2017. "A COMPREHENSIVE SAFETY ASSESSMENT METHODOLOGY FOR INNOVATIVE GEOMETRIC DESIGNS." Final UT-17.07.

Mary Eileen Yahl. 2013. “Safety Effects of Continuous Flow Intersections.” Masters Thesis, North Carolina State University.

Minderhoud, Michiel M., and Piet H. L. Bovy. 2001. “Extended Time-to-Collision Measures for Road Traffic Safety Assessment.” *Accident Analysis & Prevention* 33 (1): 89–97. https://doi.org/10.1016/S0001-4575(00)00019-1.

MoDOT. 2010. *Missouri's Experience with a Diverging Diamond Interchange - Lessons Learned*. OR 10-021. Missouri Department of Transportation. https://rosap.ntl.bts.gov/view/dot/18089.

Nye, Timothy S., Christopher M. Cunningham, and Elizabeth Byrom. 2019. "National-Level Safety Evaluation of Diverging Diamond Interchanges." *Transportation Research Record: Journal of the Transportation Research Board* 2673 (7): 696–708. https://doi.org/10.1177/0361198119849589.

Park, Byungkyu (Brian), and J. D. Schneeberger. 2003. "Microscopic Simulation Model Calibration and Validation: Case Study of VISSIM Simulation Model for a Coordinated Actuated Signal System." *Transportation Research Record: Journal of the Transportation Research Board* 1856 (1): 185–92. https://doi.org/10.3141/1856-20.

Park, Sangjun, and Hesham Rakha. 2010. "Continuous Flow Intersections: A Safety and Environmental Perspective." *13th International IEEE Conference on Intelligent Transportation Systems*, September, 85–90. https://doi.org/10.1109/ITSC.2010.5625038.

Qi, Yan, Jacqueline Walls, Md Abdur Rab, and Ryan N. Fries. 2018. *Safety Evaluation of Diverging Diamond Interchanges Design for Intersections in Minnesota*.

Qu, Wenrui, Qiao Sun, Qun Zhao, Tao Tao, and Yi Qi. 2020. "Statistical Analysis of Safety Performance of Displaced Left-Turn Intersections: Case Studies in San Marcos, Texas." *International Journal of Environmental Research and Public Health* 17 (18): 6446. https://doi.org/10.3390/ijerph17186446.

Schroeder, Bastian, Chris Cunningham, Brian Ray, et al. 2014. *Diverging Diamond Interchange Informational Guide*. Technical Report Informational Report FHWA-SA-14-067.

Songchitruksa, Praprut, and Andrew P. Tarko. 2006. "The Extreme Value Theory Approach to Safety Estimation." *Accident Analysis & Prevention* 38 (4): 811–22. https://doi.org/10.1016/j.aap.2006.02.003.

Steyn, Hermanus, Zachary Bugg, Brian Ray, et al. 2014. *Displaced Left Turn Informational Guide*. Technical Report FHWA-SA-14-068.

Tarko, Andrew P. 2018. "Surrogate Measures of Safety." In *Safe Mobility: Challenges, Methodology and Solutions*, edited by Dominique Lord and Simon Washington. Emerald Publishing Limited. https://doi.org/10.1108/S2044-994120180000011019.

UDOT. 2025. *Traffic Statistics*. Webpage. Utah Department of Transportation. https://www.udot.utah.gov/connect/business/traffic-data/traffic-statistics/.

Utah Department of Public Safety – Highway Safety Office. 2026. *Crash Data and Statistics*. Released. https://highwaysafety.utah.gov/crash-data-and-statistics/.

Utah Department of Public Safety, Highway Safety Office. 2025. *Utah Crash Summary: Crash Statistics Dashboard*. Webpage. https://udps.numetric.net/utah-crash-summary#/.

Vaughan, Christopher, Chaithra Jagadish, Shreyas Bharadwaj, et al. 2015. "Long-Term Monitoring of Wrong-Way Maneuvers at Diverging Diamond Interchanges." *Transportation Research Record: Journal of the Transportation Research Board* 2484 (1): 129–39. https://doi.org/10.3141/2484-14.

Wolfgram, Joshua. 2018. "A Safety and Emissions Analysis of Continuous Flow Intersections." *Department of Civil and Environmental Engineering, University of Massachusetts Amherst*, February.

Zheng, Lai, Karim Ismail, and Xianghai Meng. 2014. "Freeway Safety Estimation Using Extreme Value Theory Approaches: A Comparative Study." *Accident Analysis & Prevention* 62 (January): 32–41. https://doi.org/10.1016/j.aap.2013.09.006.

Zheng, Lai, Karim Ismail, Tarek Sayed, and Tazeen Fatema. 2018. "Bivariate Extreme Value Modeling for Road Safety Estimation." *Accident Analysis & Prevention* 120 (November): 83–91. https://doi.org/10.1016/j.aap.2018.08.004.

Zlatkovic, Milan. 2015. "DEVELOPMENT OF PERFORMANCE MATRICES FOR EVALUATING INNOVATIVE INTERSECTIONS AND INTERCHANGES." Final Report UT-15.13.

Zlatkovic, Milan. 2019. "Development of Performance Matrices for Evaluating Innovative Intersections and Interchanges" (MPC-19-391).

Zlatkovic, Milan, and Cameron Kergaye. 2018. "Development of Crash Modification Factors for Continuous Flow Intersections." *Put i Saobraćaj* 64 (3): 5–11. https://doi.org/10.31075/PIS.64.03.01.

# 8. APPENDICES

**Appendix A: Summary of Traffic Volume Conversion for DDI (2016 & 2019) all Approaches**

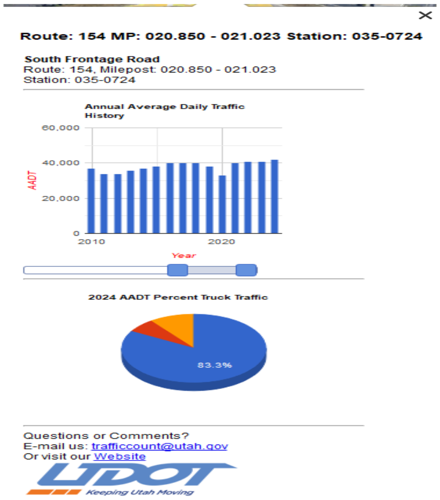


AADT 2024- 42,000
AADT 2016- 40,000
AADT 2019- 38,000

| Intersection | Approach | Movement | 2024 Volume Count | Estimated 2016 Volume | VISSIM Input |
|---|---|---|---|---|---|
| DDI | EB | Left | 106 | 100 | 100 |
| DDI | EB | Right | 120 | 114 | 114 |
| DDI | WB | Left | 955 | 907 | 907 |
| DDI | WB | Right | 165 | 156 | 156 |
| DDI | NB | Left | 169 | 160 | 160 |
| DDI | NB | Through | 372 | 353 | 353 |
| DDI | NB | Right | 796 | 756 | 756 |
| DDI | SB | Left | 479 | 455 | 455 |
| DDI | SB | Through | 1,146 | 1,088 | 1,088 |
| DDI | SB | Right | 8 | 7 | 7 |
| DDI | EB | Left | 106 | 95 | 95 |
| DDI | EB | Right | 120 | 108 | 108 |
| DDI | WB | Left | 955 | 859 | 859 |
| DDI | WB | Right | 165 | 148 | 148 |
| DDI | NB | Left | 169 | 152 | 152 |
| DDI | NB | Through | 372 | 334 | 334 |
| DDI | NB | Right | 796 | 716 | 716 |
| DDI | SB | Left | 479 | 431 | 431 |
| DDI | SB | Through | 1,146 | 1,031 | 1,031 |
| DDI | SB | Right | 8 | 7 | 7 |

**Appendix B:Summary of Traffic Volume Conversion for CFI (2016 & 2019) all Approaches**

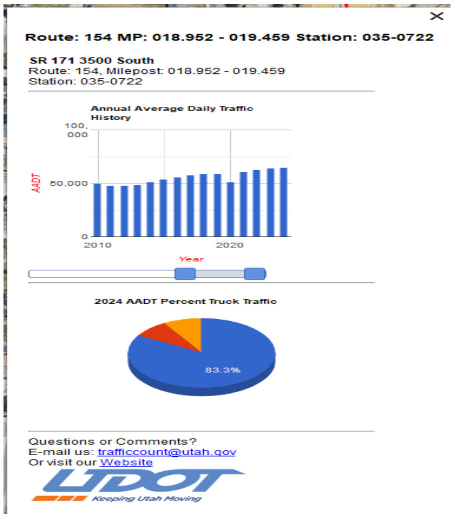


AADT 2024-65000
AADT 2016- 56000
AADT 2019- 59000

| Intersection | Approach | Movement | 2024 Volume Count | Estimated 2016 Volume | VISSIM Input |
|---|---|---|---|---|---|
| CFI | EB | Left | 111 | 95 | 95 |
| CFI | EB | Right | 89 | 76 | 76 |
| CFI | EB | Through | 367 | 315 | 315 |
| CFI | WB | Left | 187 | 160 | 160 |
| CFI | WB | Right | 13 | 11 | 11 |
| CFI | WB | Through | 361 | 310 | 310 |
| CFI | SB | Left | 25 | 21 | 21 |
| CFI | SB | Right | 1 | 1 | 1 |
| CFI | SB | Through | 1,623 | 1,395 | 1,395 |
| CFI | NB | Left | 91 | 78 | 78 |
| CFI | NB | Right | 1 | 1 | 1 |
| CFI | NB | Through | 609 | 523 | 523 |
| CFI | EB | Left | 111 | 99 | 99 |
| CFI | EB | Right | 89 | 80 | 80 |
| CFI | EB | Through | 367 | 330 | 330 |
| CFI | WB | Left | 187 | 168 | 168 |
| CFI | WB | Right | 13 | 12 | 12 |
| CFI | WB | Through | 361 | 324 | 324 |
| CFI | SB | Left | 25 | 22 | 22 |
| CFI | SB | Right | 1 | 1 | 1 |
| CFI | SB | Through | 1,623 | 1,460 | 1,460 |
| CFI | NB | Left | 91 | 81 | 81 |
| CFI | NB | Right | 1 | 1 | 1 |
| CFI | NB | Through | 609 | 548 | 548 |

# Appendix C: Signal Timing Plans for DDI

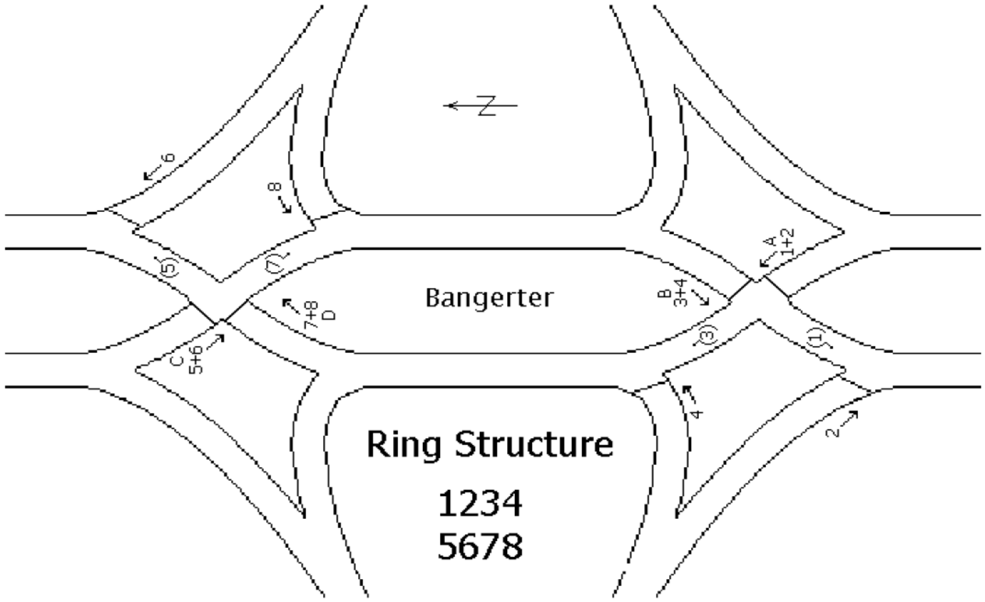


Bangerter & SR-201

**Figure 44: Ring-barrier structure**

```
COORDINATOR PATTERN [ 12]
USE SPLIT PATTERN. 12 SPLIT SUM ....126s
TS2 (PAT-OFF)..   3-3
CYCLE.........  100s STD (COS)......123
OFFSET VAL.....   10s
ACTUATED COORD...  NO TIMING PLAN....  1
ACT WALK REST....  NO SEQUENCE........ 1
PHASE RESRVCE....  NO ACTION PLAN.... 12
SPLIT PREFERENCE PHASES
 PHASE[s]  1   2   3   4   5   6   7   8
SPT[ 12]   7  20   7  66   7  46   7  40
PREF 1...  0   0   0   0   0   0   0   0
PREF 2...  0   0   0   0   0   0   0   0
```

```
SPLT EXT...0s. 0s  0s  0s
VEH PERM.  0s  0s  0s  DISP
RING DISP  -  19s  0s  0s (RING 2-4)
 PHASE[s]  9  10  11  12  13  14  15  16
SPT[ 12]   0   0   0   0   0   0   0   0
PREF 1...  0   0   0   0   0   0   0   0
PREF 2...  0   0   0   0   0   0   0   0

SPLIT DEMAND PTRN.  0   0 XART PTRN.   0
PHASE..  1 2 3 4 5 6 7 8 9 0 1 2 3 4 5 6
COORD... . . . X . X . . . . . . . . . .
VE RCALL . . . . . . . . . . . . . . . .
PD RCALL . . . . . . . . . . . . . . . .
MX RCALL . . . . . . . . . . . . . . . .
OMIT.... . . . . . . . . X X X X X X X X
SF OUT.. . . . . . . . . (1-8)
```

**Figure 45: Signal timing plan showing coordination pattern**

## Appendix D: Signal timing plans for CFI

| | | | | | |
|---|---|---|---|---|---|
| 10 | 2 | 3 | 4 | 9 | |
| 12 | 5 | 6 | 7 | 8 | 11 |
| 13 | 14 | | | | |

**Figure 46: Ring-barrier structure**

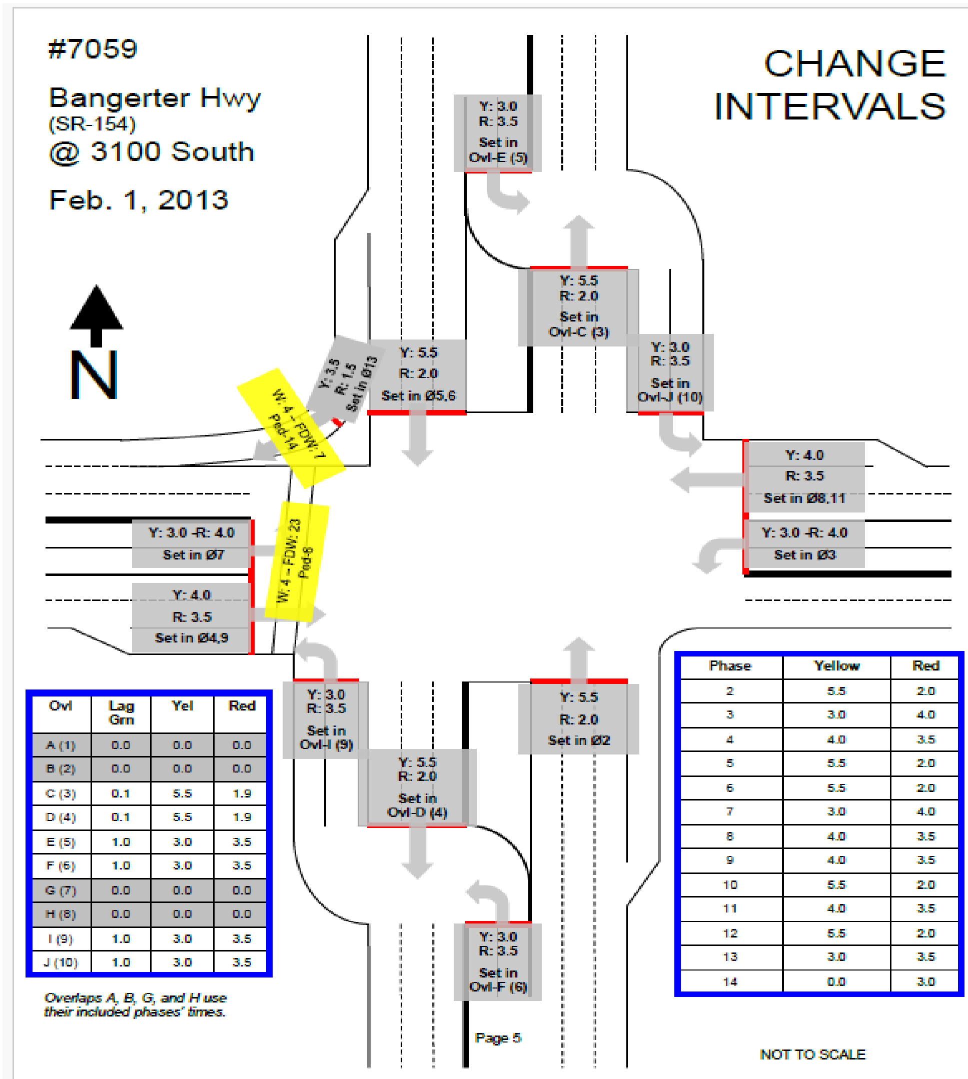


**Figure 47: Signal timing change intervals and phase configuration**

## Appendix E: Sample Crash Dataset (2010-2022)

| Crash Tim | Fatal Cras | Fatal Roac | Near-Schc | No injury/ | RoadView | Roadway [ | Suspectec | Urban/Rur | V1 & V2 M | Week of Y | Month Nu | Age Group | Age Text | Alcohol Su | Drug Susp | Age | Air Bag | Alcohol D | Alcohol D | Alcohol D | Bac |
|---|---|---|---|---|---|---|---|---|---|---|---|---|---|---|---|---|---|---|---|---|---|
| 5:45:00 | | | FALSE | 1 | http://168 | 1 | | Urban | | 1 | 1 | 20 to 29 | 25 | No | No | 25 | Not Deplo | None | Not Given | Not Applic | - |
| 8:20:00 | | | TRUE | 1 | http://168 | 1 | | Urban | | 1 | 1 | 30 to 39 | 32 | No | No | 32 | Not Deplo | None | Not Given | Not Applic | - |
| 7:50:00 | | | FALSE | | http://168 | 1 | | Urban | | 1 | 1 | ["10 to 19 | ["15","43" | ["No","No | ["No","No | [15,43] | ["Not Dep | ["None"," | ["Not Give | ["Not Appl | - |
| 8:23:00 | | | FALSE | | http://168.178.125.102/UtahR | | | Urban | | 1 | 1 | ["10 to 19 | ["11","11" | ["No","No | ["No","No | [11,11,14 | ["No Air Ba | ["None"," | ["Not Give | ["Not Appl | - |
| 7:46:00 | | | FALSE | 1 | http://168.178.125.102/UtahR | | | Urban | | 1 | 1 | ["0 to 9"," | ["0","21"," | ["No","No | ["No","No | [0,21,45] | ["Not Dep | ["None"," | ["Not Give | ["Not Appl | - |
| 8:21:00 | | | FALSE | 1 | http://168.178.125.102/UtahR | | | Rural | | 2 | 1 | 70 to 79 | 76 | No | No | 76 | Deployed | None | Not Given | Not Applic | N/A |
| 8:15:00 | | | FALSE | | http://168 | 1 | | Urban | | 1 | 1 | 40 to 49 | 44 | No | No | 44 | Not Deplo | None | Not Given | Not Applic | N/A |
| 9:27:00 | | | FALSE | 1 | http://168 | 1 | | Urban | | 1 | 1 | 20 to 29 | 22 | No | No | 22 | Not Deplo | None | Not Given | Not Applic | - |
| 8:30:00 | | | FALSE | | http://168.178.125.102/UtahR | | | Urban | | 1 | 1 | ["10 to 19 | ["16","16" | ["No","No | ["No","No | [16,16] | ["Not Dep | ["None"," | ["Not Give | ["Not Appl | N/A |
| 4:56:00 | | | FALSE | 1 | http://168 | 1 | | Urban | Straight Al | 1 | 1 | ["20 to 29 | ["25","27" | ["No","No | ["No","No | [25,27,28 | ["Not Dep | ["None"," | ["Not Give | ["Not Appl | ["-","-"] |
| 17:56:00 | | | FALSE | | http://168 | 1 | | Urban | | 1 | 1 | ["20 to 29 | ["26","27" | ["No","No | ["No","No | [26,27] | ["Not Dep | ["None"," | ["Not Give | ["Not Appl | - |
| 15:20:00 | | | FALSE | | http://168 | 1 | | Rural | | 1 | 1 | ["0 to 9"," | ["35","8"] | ["No","No | ["No","No | [8,35] | ["No Air Ba | ["None"," | ["Not Give | ["Not Appl | - |
| 2:52:00 | | | FALSE | 1 | http://168 | 1 | | Rural | | 1 | 1 | 20 to 29 | 23 | No | No | 23 | Not Deplo | Alcohol | Alcohol | Alcohol-Pos | |
| 18:31:00 | | | FALSE | | http://168.178.125.102/UtahR | | | Rural | Making U- | 2 | 1 | ["0 to 9"," | ["1","17"," | ["No","No | ["No","No | [1,17,24,2 | ["Deploye | ["None"," | ["Not Give | ["Not Appl | ["-","-"] |
| 15:50:00 | | | FALSE | 1 | http://168.178.125.102/UtahR | | | Urban | | 1 | 1 | ["20 to 29 | ["22","24" | ["No","No | ["No","No | [22,24,25 | ["Deploye | ["None"," | ["Not Give | ["Not Appl | - |
| 18:30:00 | | | FALSE | 1 | http://168.178.125.102/UtahR | | | Rural | | 2 | 1 | 20 to 29 | 21 | No | No | 21 | Not Deplo | None | Not Given | Not Applicable/No T | |
| 18:15:00 | | | FALSE | 1 | http://168.178.125.102/UtahR | | | Rural | | 1 | 1 | ["40 to 49 | ["41","65" | ["No","No | ["No","No | [41,65,68 | ["Not Dep | ["None"," | ["Not Give | ["Not Appl | - |
| 17:50:00 | | | FALSE | 1 | http://168.178.125.102/UtahR | | | Urban | Straight Al | 2 | 1 | ["20 to 29 | ["21","40" | ["No","No | ["No","No | [21,40] | ["No Air Ba | ["None"," | ["Not Give | ["Not Applicable/No | |
| 22:30:00 | | | FALSE | 1 | http://168 | 1 | | Rural | | 1 | 1 | 10 to 19 | 18 | No | No | 18 | Deployed | None | Not Given | Not Applicable/No T | |
| 21:10:00 | | | FALSE | 1 | http://168.178.125.102/UtahR | | | Urban | | 2 | 1 | 10 to 19 | 19 | No | No | 19 | Not Deplo | None | Not Given | Not Applic | - |
| 1:45:00 | | | FALSE | 1 | http://168.178.125.102/UtahR | | | Rural | | 1 | 1 | 20 to 29 | 24 | No | No | 24 | Not Deplo | None | Not Given | Not Applic | - |
| 8:12:00 | | | FALSE | | http://168 | 1 | | Rural | | 2 | 1 | ["20 to 29 | ["22","31" | ["No","No | ["No","No | [22,31] | ["Deploye | ["None"," | ["Not Give | ["Not Applicable/No | |
| 11:06:00 | | | FALSE | 1 | http://168.178.125.102/UtahR | | | Urban | | 1 | 1 | ["10 to 19 | ["18","20" | ["No","No | ["No","No | [18,20] | ["Not Dep | ["None"," | ["Not Give | ["Not Applicable/No | |
| 17:59:00 | | | FALSE | 1 | http://168.178.125.102/UtahR | | | Urban | Changing | 1 | 1 | ["20 to 29 | ["21","22" | ["No","No | ["No","No | [21,22,26 | ["Not Dep | ["None"," | ["Not Give | ["Not Appl | ["-","-","-" |
| 16:15:00 | | | FALSE | 1 | http://168.178.125.102/UtahR | | | Urban | Entering T | 2 | 1 | ["30 to 39 | ["35","65" | ["No","No | ["No","No | [35,65] | ["Not Dep | ["None"," | ["Not Give | ["Not Applicable/No | |
| 17:35:00 | | | FALSE | 1 | http://168.178.125.102/UtahR | | | Urban | Slowing in | 2 | 1 | ["10 to 19 | ["15","18" | ["No","No | ["No","No | [15,18,19 | ["Not Dep | ["None"," | ["Not Give | ["Not Applicable/No | |
| 15:43:00 | | | FALSE | 1 | http://168.178.125.102/UtahR | | | Urban | Straight Al | 2 | 1 | ["20 to 29 | ["25","66" | ["No","No | ["No","No | [25,66] | ["Deploye | ["None"," | ["Not Give | ["Not Applicable/No | |
| 2:28:00 | | | FALSE | 1 | http://168.178.125.102/UtahR | | | Rural | | 1 | 1 | 40 to 49 | 47 | No | No | 47 | Not Deplo | None | Not Given | Not Applic | - |
| 21:19:00 | | | FALSE | 1 | http://168.178.125.102/UtahR | | | Urban | Straight Al | 2 | 1 | ["20 to 29 | ["20","20" | ["No","No | ["No","No | [20,20] | ["Not Dep | ["None"," | ["Not Give | ["Not Applicable/No | |
| 7:45:00 | | | FALSE | 1 | http://168.178.125.102/UtahR | | | Urban | Turning Le | 2 | 1 | ["10 to 19 | ["17","51" | ["No","No | ["No","No | [17,51] | ["Not Dep | ["None"," | ["Not Give | ["Not Appl | ["***","** |
| 11:08:00 | | | FALSE | 1 | http://168.178.125.102/UtahR | | | Urban | Straight Al | 2 | 1 | ["40 to 49 | ["44","57" | ["No","No | ["No","No | [44,57] | ["Deploym | ["None"," | ["Not Give | ["Not Appl | ["***","** |
| 14:35:00 | | | FALSE | | http://168.178.125.102/UtahR | | | Urban | Straight Al | 2 | 1 | ["10 to 19 | ["18","19" | ["No","No | ["No","No | [18,19,25 | ["Not Dep | ["None"," | ["Not Give | ["Not Appl | ["***","** |
| 18:06:00 | | | FALSE | 1 | http://168.178.125.102/UtahR | | | Urban | Straight Al | 2 | 1 | ["20 to 29 | ["24","28" | ["No","No | ["No","No | [24,28,46 | ["Not Dep | ["None"," | ["Not Give | ["Not Appl | ["-","-","-" |
| 17:47:00 | | | FALSE | 1 | http://168.178.125.102/UtahR | | | Urban | Straight Al | 2 | 1 | ["10 to 19 | ["18","21" | ["No","No | ["No","No | [18,21,37 | ["Deploye | ["None"," | ["Not Give | ["Not Appl | ["-","-","-" |
| 17:51:00 | | | FALSE | | http://168.178.125.102/UtahR | | | Urban | Straight Al | 2 | 1 | ["20 to 29 | ["28","34" | ["No","No | ["No","No | [28,34] | ["Not Dep | ["None"," | ["Not Give | ["Not Appl | ["-","-"] |
| 17:41:00 | | | FALSE | 1 | http://168.178.125.102/UtahR | | | Urban | Changing | 2 | 1 | ["30 to 39 | ["34","49" | ["No","No | ["No","No | [34,49] | ["Not Dep | ["None"," | ["Not Give | ["Not Appl | ["-","-"] |
| 23:06:00 | | | FALSE | | http://168 | 1 | | Urban | | 2 | 1 | 30 to 39 | 34 | No | No | 34 | Not Deplo | None | Not Given | Not Applic | - |

**Figure 48: Sample of crash dataset used in the study**

## Appendix F: Peak Hour Percentage Calculation

**Table 44:DDI Peak Hour Percentage (Weekdays)**

| Date | Total Traffic | Peak Hour Traffic | Percent |
|---|---|---|---|
| 1/17/2024 | 8,4496 | 7,164 | 8.47 |
| 2/14/2024 | 10,6533 | 8,741 | 8.20 |
| 3/14/2024 | 98,588 | 7,858 | 7.97 |
| 4/17/2024 | 108,772 | 8,724 | 8.02 |
| 5/15/2024 | 111,093 | 8,706 | 7.83 |
| 6/18/2024 | 102,667 | 8,555 | 8.33 |
| 7/17/2024 | 116,594 | 8,887 | 7.62 |
| 8/14/2024 | 126,806 | 8,403 | 6.62 |
| 9/18/2024 | 128,175 | 8,761 | 6.83 |
| 10/16/2024 | 126,158 | 8,653 | 6.85 |
| 11/15/2024 | 121,405 | 8,024 | 6.60 |
| 12/17/2024 | 125,120 | 9,034 | 7.22 |
| Average | | | 7.55 |
| Percent | | | 0.0755 |

**Table 45:DDI Peak Hour Percentage (Weekends)**

| Date | Total Traffic | Peak Hour Traffic | Percent |
|---|---|---|---|
| 1/14/2024 | 40,393 | 2,926 | 7.24 |
| 2/18/2024 | 44,213 | 2,913 | 6.58 |
| 3/17/2024 | 48,154 | 3,273 | 6.79 |
| 4/14/2024 | 48,881 | 3,353 | 6.85 |
| 5/12/2024 | 54,231 | 3,465 | 6.38 |
| 6/16/2024 | 28,960 | 2,690 | 9.28 |
| 7/14/2024 | 53,409 | 3,326 | 6.22 |
| 8/18/2024 | 57,513 | 3,844 | 6.68 |
| 9/15/2024 | 59,206 | 3,925 | 6.62 |
| 10/13/2024 | 68,973 | 3,755 | 5.44 |
| 11/17/2024 | 52,928 | 3,760 | 7.10 |
| 12/15/2024 | 55,048 | 3,952 | 7.17 |
| Average | | | 6.86 |
| Percent | | | 0.0686 |

**Table 46:CFI Peak Hour Percentage (Weekdays)**

| **Date** | **Total Traffic** | **Peak Hour Traffic** | **Percent** |
|---|---|---|---|
| 1/17/2024 | 17,044 | 1,249 | 7.32 |
| 2/14/2024 | 20,171 | 1,629 | 8.07 |
| 3/14/2024 | 19,234 | 1,378 | 7.16 |
| 4/17/2024 | 19,607 | 1,402 | 7.15 |
| 5/15/2024 | 20,011 | 1,475 | 7.37 |
| 6/18/2024 | 18,134 | 1,208 | 6.66 |
| 7/17/2024 | 19,360 | 1,367 | 7.06 |
| 8/14/2024 | 19,497 | 1,400 | 7.18 |
| 9/18/2024 | 19,086 | 1,350 | 7.07 |
| 10/16/2024 | 17,928 | 1,124 | 6.26 |
| 11/15/2024 | 19,248 | 1,521 | 7.90 |
| 12/17/2024 | 18,603 | 1,452 | 7.80 |
| Average | | | 7.25 |
| Percent | | | 0.0725 |

**Table 47:CFI Peak Hour Percentage (Weekends)**

| Date | Total Traffic | Peak Hour Traffic | Percent |
|---|---|---|---|
| **1/14/2024** | **13,188** | **1,048** | **7.94** |
| 2/18/2024 | 14,102 | 1,032 | 7.31 |
| 3/17/2024 | 15,810 | 1,152 | 7.28 |
| 4/14/2024 | 15,911 | 1,219 | 7.66 |
| 5/12/2024 | 16,400 | 1,214 | 7.40 |
| 6/16/2024 | 17,458 | 1,184 | 6.78 |
| 7/14/2024 | 15,443 | 1,111 | 7.19 |
| 8/18/2024 | 15,115 | 1,168 | 7.72 |
| 9/15/2024 | 15,501 | 1,154 | 7.44 |
| 10/13/2024 | 15,489 | 1,117 | 7.21 |
| 11/17/2024 | 14,506 | 1,146 | 7.90 |
| 12/15/2024 | 15,400 | 1,340 | 8.70 |
| Average | | | 7.54 |
| Percent | | | 0.0754 |

CTIPS Center for Transformative Infrastructure Preservation and Sustainability

USDOT Region 8 University Transportation Center

NDSU Dept 2880 • P.O. Box 6050
Fargo, ND 58108-6050

(701)231-7767

ndsu.ugpti@ndsu.edu